WEAR SIMULATION OF ELECTRICAL CONTACTS SUBJECTED TO

VIBRATIONS

Except where reference is made to the work of others, the work described in this thesis is my own or was done in collaboration with my advisory committee. This thesis does not include proprietary or classified information.

_____

Darshan U Shinde

Certificate of Approval:

_____	_____
Bart Prorok Assistant Professor Materials Engineering	Pradeep Lall, Chair Thomas Walter Professor Mechanical Engineering
_____	_____
Robert L. Jackson Assistant Professor Mechanical Engineering	Jeffrey C. Suhling Quina Distinguished Professor Mechanical Engineering

_____

Joe F. Pittman
Interim Dean
Graduate School

WEAR SIMULATION OF ELECTRICAL CONTACTS SUBJECTED TO VIBRATIONS

Darshan U Shinde

A Thesis

Submitted to

the Graduate Faculty of

Auburn University

in Partial Fulfillment of the

Requirement for the

Degree of

Master of Science

Auburn, Alabama
August 9, 2008

WEAR SIMULATION OF ELECTRICAL CONTACTS, SUBJECTED TO VIBRATIONS

Darshan Shinde

_____
Signature of Author

_____
Date of Graduation

THESIS ABSTRACT

WEAR SIMULATION OF ELECTRICAL CONTACTS, SUBJECTED TO VIBRATIONS

Darshan Shinde

Master of Science, August 9, 2008
(B.E., Pune University, VIT, 2003)

139 Typed Pages

Directed by Pradeep Lall

Electrical contacts may be subjected to wear because of shock, vibration, and thermo-mechanical stresses resulting in fretting, increase in contact resistance, and eventual failure over the lifetime of the product. Previously, models have been constructed for various applications to simulate wear for dry unidirectional-sliding wear of a square-pin, unidirectional sliding of pin on disk, and wear mechanism maps for steel-on-steel contacts. In this paper, a wear simulation model for fretting of reciprocating curved spring-loaded contacts has been proposed, based on instantaneous estimation of wear rate, which is time-integrated over a larger number of cycles, with continual update of the contact geometry during the simulation process. Arbitrary Lagrangian-Eulerian adaptive meshing has been used to simulate the wear phenomena. Model predictions of wear have been compared to experimental data plots, available from existing literature, to

validate both, the 2D and 3D models. A large number of wear cycles have been simulated for common contact geometries, and the wear accrued computed in conjunction with the wear surface updates. The modeling methodology extends the state-of-art by enabling the continuous wear evolution of the contact surfaces through computation of accrued wear. The proposed methodology is intended for reducing the number of design iterations in deployment and selection of electrical contact systems in consumer and defense electronics. The presented analysis is applicable to wide variety of contact systems found in consumer and defense applications including, RAM memory-card sockets, SD-card sockets, microprocessor, ZIF sockets, and fuzz button contacts.

ACKNOWLEDGEMENTS

I would like express my sincere gratitude to my advisor, Dr. Pradeep Lall, for letting me work on this challenging project. I have benefited both professionally and personally from the many interactions I have had with him. Without his guidance, patience and constant encouragement, completion of the thesis would not have been possible. It has been a real pleasure to work with, and learn from him. I also wish to extend my gratitude to Dr. Robert Jackson, Dr. Barton Prorok and Dr. Jeff Suhling for serving on my thesis committee and examining my thesis. I would like to thank Dr. Suhling for agreeing to be on my committee at a short moment's notice.

I would also like to thank all my friends, especially Chandan, Robert, Bhushan, Shirish, Prashant, Amit, Ganesh, Sandeep and all other colleagues and friends whose names are not mentioned, for their priceless love and support. Finally, many thanks go to my family for their unwavering encouragement and love.

Style manual or journal used Graduate School: Guide to Preparation and Submission of Theses and Dissertations

Computer software used Microsoft Office 2003, Abaqus V6.5, Hypermesh V7.0, Compaq Visual Fortran V6.0

TABLE OF CONTENTS

LIST OF FIGURES

LIST OF TABLES

CHAPTER 1

INTRODUCTION

Microelectronic Technology has evolved at a fast rate, resulting in the shrinking of the size of electronic components. As devices become portable, they also become more susceptible to vibrations during usage and transportation. Electronic components are subjected to vibrations during the operational life of the component. The vibrations are transmitted inside the body of the component. There exist several electrical contacts in a component. When these contacts are subjected to repetitive vibrations, fretting wear occurs. Fretting wear is defined as the repeated cyclical rubbing between two surfaces, which, over a period of time will remove material from one or both surfaces in contact. Fretting wear can reduce the life of components.

Wear is a very complex phenomenon. Based on the failure mechanism wear can be defined in many ways, a few of which are listed below. Wear can be categorized into several categories, adhesive wear, abrasive wear, surface fatigue and corrosion. Adhesive wear occurs when asperities interact, leading to transfer of metal from one surface to another. This occurs at high speeds and temperatures. Scuffing is a severe form of adhesive wear. In Scuffing material is removed from the hotter surface and deposited on the cooler surface. Abrasive wear occurs when a surface is damaged by the introduction of a harder material. This harder material could exist in the form of particles, which enter

the contact system externally or they can be internally generated by oxidation or other chemical processes Surface fatigue is a form of wear which is predominant in rolling contact bearings. These bearings are subjected to repeated intense loadings. Hertzian stress is distributed in such a way, such that the max shearing stress occurs within the surface. As a result of this failure commences below the surface. This finally results in pitting failure.

Hirst [1957] classified wear depending on it's intensity into mild and severe wear. Lancaster [1963] suggested a theory for the transition of wear from mild wear to severe wear. When two surfaces contact resulting in wear, there exists two opposing dynamic processes, the first one being the rate of formation of fresh metal surfaces as a result of wear, the other being the rate of formation of a surface film as a result of the reaction with atmosphere. These surface films are generally oxide films which remain protective as long as they bond to the parent surface and are rapidly renewed. In the absence of these films, surfaces in contact tend to seize, resulting in extremely high friction and surface damage. Scuffing wear is defined as surface damage characterized by the formation of local welds between sliding surfaces. In scuffing there is a tendency for material to be removed from a slower surface and deposited on the faster surface.

Fretting was first recorded by Eden et al. [1911]. Tomlinson [1927] first defined fretting wear as wear which occurs as a result of very small oscillatory displacement between surfaces, consisting of interactions among several forms of wear, initiated by adhesion, amplified by corrosion and having it's major effect by abrasion or fatigue. Fretting occurs when two loaded surfaces in contact undergo relative oscillatory tangential motion, known as slip, as a result of vibrations or cyclic stressing. The

amplitude of relative motion is very small. As fretting proceeds, the area over which slip is occurring usually increases due to the incursion of debris. The amount of debris produced depends on the mechanical properties of the material and it's chemical reactivity. This debris produced by fretting is mainly the oxide of the metal involved. This oxide occupies a greater volume than the volume of metal destroyed. If space is confined, this will lead to seizure of the contact.

1.1 Selection of Wear Mechanism

Table 1: Classification of Wear Mechanisms

No.	**Wear Mechanism**	**Motion**	**Typical Occurrences of the Mechanism**
1.	Fretting Wear	Reciprocating	Electrical Contacts, Fasteners subjected to vibrations
2.	Abrasion	Particle sliding	Abrasive sand papers, files, punches
3.	Scuffing	Sliding with the formation of local welds	Gears
4.	Surface Fatigue	Relative motion with repeated intense loadings	Bearings
5.	Pitting	Relative motion where stresses	Bearings, Gears

		exceed the endurance limit of the material	
6.	Adhesive Wear	Relative motion with interaction of asperities	Bronze Bush wear, wear of shafts
7.	Impact Wear	One body impacts the other	Presses, Punches, hammers, rain erosion
8.	Corrosive Wear	No motion necessary. Deterioration of the material due to reaction with the environment	Metal parts like chains subjected to harsh environments
9.	Cavitation	Collapse of vapor bubbles in liquid due to pressure fluctuations	Water pipes, water pumps

From the above discussion it can be inferred that when relative motion exists between two surfaces, the surfaces can be attacked by a variety of wear modes, they can be damaged in different ways depending on various factors like the thermal and chemical environment at the point of contact and materials of the mating surfaces and surface

properties. In most cases wear can result due to the combination of wear modes described above and it is impossible to predict which mode is dominant. It is possible, however, to select the dominant wear mode based on the type of system, the nature of relative motion between the contacting surfaces and the application. In this work, wear between electrical contacts subjected to vibrations has been simulated. Based on the application and the nature of relative motion, fretting wear is the dominant wear mode. Table 1 shows classification of wear mechanisms with typical examples where the corresponding form of wear is most likely to be found. Once the wear mechanism is identified, a suitable wear model needs to be selected which will accurately represent the wear mechanism.

1.2 Selection of Wear Model

There exist hundreds of wear models in wear literature. A suitable wear model must be selected depending on the wear mechanism which is being simulated. Some wear models are empirical equations involving material properties and working conditions. These models are constructed by manipulating experimental data and they are valid within a tested range. Some of these wear models are listed below. Barwell [1958] suggested a wear model which consists of three empirical equations,

$$W = \frac{\beta}{\alpha}\left(1 - \varepsilon^{-\alpha t}\right) \qquad (1)$$

$$W = \alpha t \qquad (2)$$

$$W = \beta \varepsilon^{\alpha t} \qquad (3)$$

Where V is the Volume loss, β is a constant, α is some characteristic of the initial surfaces, t is the time and ε is natural logarithm.

Rhee [1970] suggested another empirical wear equation where wear was a function of

The load (F), speed (V) and time (t).

$$\Delta W = KF^a V^b t^c \quad (4)$$

Where ΔW is the weight loss of a friction material, and K, a, b, c are empirical constants. Some models were developed to identify the main mechanism of material loss from surfaces. These models were based on explanations consistent with observed wear behavior. Wear maps were developed for specific materials. Lim & Ashby [1987] developed a wear map for steel, Hsu & Shen [1996] developed a wear map for ceramics, Chen & Alpas [2000] developed a wear map for magnesium alloy. These wear maps helped in the selection of the dominant wear mechanism depending on a particular set of operating conditions.

Archard [1961] proposed a wear model to model sliding wear. According to Archard's model, the amount of wear depends on the stress field in the contact and the relative sliding distance between the contacting surfaces.

$$\frac{W}{A*s} = \frac{k}{H} * \frac{F}{A} \quad (5)$$

This equation can be rewritten in terms of wear depth,

$$h = \frac{k}{H} * s * P \quad (6)$$

where W is the wear volume, A is the area of contact, k is the wear coefficient, F is the contact force, H is the hardness of the softer material, s is the sliding distance, h is the wear depth and P is the contact pressure. Measuring wear volume is difficult because wear volume boundaries are established subjectively [Kalin and Vizintin, 2000]. This makes predicting wear depth an important step. Archard's wear coefficient has been

interpreted in various ways. It is the fraction of asperities yielding wear particles, ratio of volume worn to volume deformed, a factor inversely proportional to critical number of load cycles, number of repeated asperity encounters for producing ruptures, as a factor reflecting the inefficiencies associated with the various processes involved in generating wear particles. [Rigney 1994]. Even though Archard's wear model gives little insight into the dominant wear mechanism, it can be used fairly accurately and conveniently to model mild wear. Archard's law is not applicable for any specific mechanism. It is generally used to model Adhesive and Abrasive wear. Quinn [1971] proposed a wear mechanism based on oxidation. This model was based on Archard's wear model. Quinn's model is based on the assumption that a volume of material near the region of contact gets heated up due to sliding force and an oxide film grows on the surface. After the thickness of the oxide film reaches a critical value, it will separate from the surface as wear debris.

$$W = \frac{d * A * A_p * e^{-(Q_p / RT_o)}}{\xi^2 * \rho^2 * V * f^2} \qquad (7)$$

Where A_p is Arrhenius constant, Q_p is the activation energy for oxidation, R is the gas constant, T_0 is the temperature of oxidation.

Suh [1973] proposed the delamination theory to explain the production of flake debris on worn surfaces. According to this model, crystal lattices dislocations under the influence of a sliding force, meet together, form a crack and propagate parallel to the surface to produce flake debris. Cracks become nucleated below the surface and join, resulting in the loosening of thin sheets of metals,

forming wear debris. Challen and Oxley [1979] applied slip line field analysis to describe the deformation of a soft asperity by a hard one and derived equations for wear rate

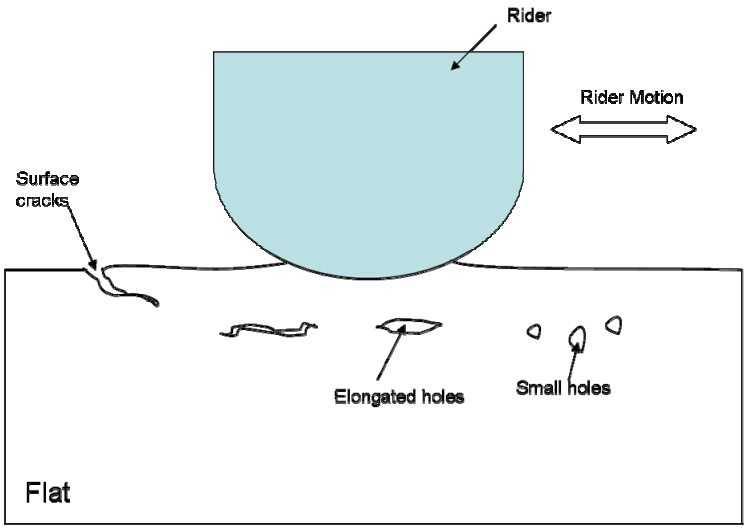

Figure1: Delamination Wear Mechanism derived from Suh [1973]

The most common wear model used to model sliding wear is Archard's wear model. Archard's model has been used by Molinari [2000], Podra [1999], Cantizano [2002], Agelet [1999], Hegadekatte [2005]. In this wear simulation Archard's wear model has been selected to simulate fretting wear occurring in electrical contacts. The Arbitrary Lagrangian-Eulerian (ALE) adaptive meshing technique has been used in this model. ALE was developed to combine the advantages of the Lagrangian and Eulerian descriptions while minimizing their respective drawbacks as far as possible. Archard's wear law is integrated into a Fortran code and used in the Abaqus user subroutine, UMESHMOTION. To take into account damage accumulation caused by surface wear, adaptive meshing is employed. As the surface wears the elements in the components get distorted. This will eventually cause the simulation to fail. Adaptive meshing remeshes the components at a regular frequency to take into account the damage accumulation.

CHAPTER 2

LITERATURE REVIEW

All complex electronic products used today have thousands of electrical contacts. New advances in electronic packaging technology have shrunk the size of electronic components resulting in the reduction in size of electronic devices. This in turn has resulted in the increased density of electrical contacts in electronic devices. These devices are subjected to vibrations during their operation. These vibrations are transmitted inside the electronic components to the contacts. This causes repeated cyclical rubbing between the contact surfaces resulting in fretting wear. This can lead to sudden and premature failure of the component. Experimental techniques and simulations are used to predict wear rates for different contact systems. This has resulted in a better understanding of the wear processes leading to accurate life predictions. Wear is a complex phenomenon. Wear modeling has been a subject of extensive research in the past. There exist several theories and equations that try to explain wear and measure it. Due to its complex nature, there exists no universal law that can explain wear. A thorough study of the literature published on wear is necessary to understand the various methodologies used to predict wear and how various wear models are used in wear simulations to predict wear rates. Wear is a process which occurs when the surfaces of engineering components are loaded together and subjected to sliding or rolling motion [Archard 1980].

There are many major mechanisms that are involved in wear. Burwell [1957] was the first to attempt a classification of these wear mechanisms. Wear mechanisms were classified by Suh [1986] into two groups. The first group consisted of mechanisms which were governed by mechanical behavior of solids. The second group consisted of mechanisms which were governed by the chemical behavior of materials. Solids can cause wear in different ways. The first group was further classified into five subgroups, Fretting Wear, Erosive Wear, Abrasive Wear, Sliding Wear and Fatigue Wear. Fretting Wear occurs when two contacting surfaces undergo small oscillatory motion. Wear particles generated during this process can have a significant effect, due to the high frequency of sliding and small contact area. This type of wear is common in electrical contacts. In case of noble metals, fretting wear may cause the electrical contact resistance to change due to wearout of the surface finish, resulting in exposure of the underlying base metal.

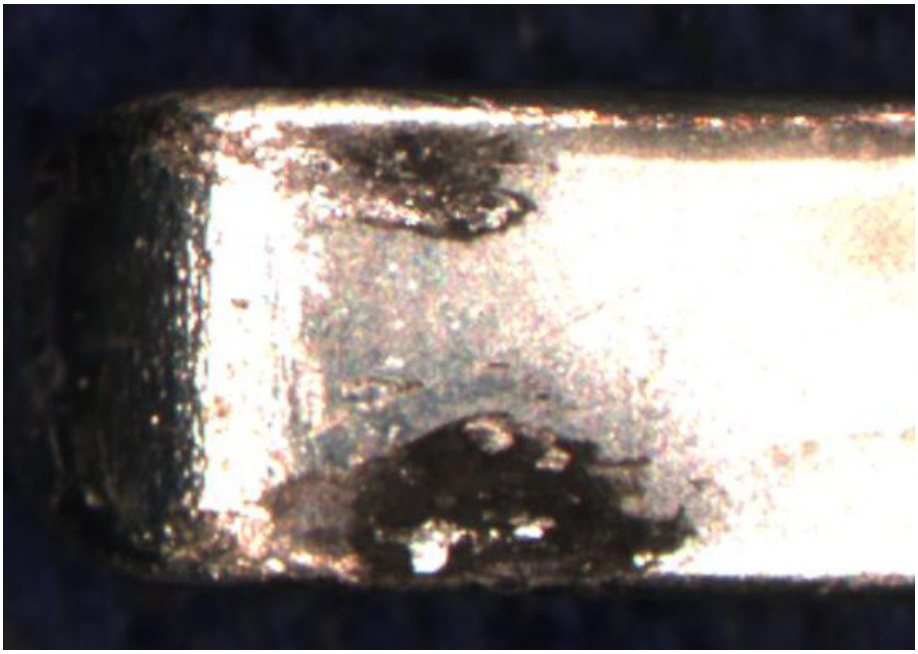

Figure 2: Fretting wear of a tin terminal [Courtesy of Molex]

Erosive wear occurs due to the impingement of solid particles on the wearing surface. Large sub-surface deformation, crack nucleation and propagation take place during this wear. This type of wear is observed in turbines and helicopter blades.

Figure 3: Erosion of a turbine blade subjected to 1500 micron particles [Hamed 2005]

Abrasive wear occurs when hard particles or asperities plow and cut the contacting surfaces during relative motion. This type of wear is observed in earth moving equipment after prolonged use. Sliding wear occurs when two materials slide against each other. It results in plastic deformation, crack nucleation and propagation in the subsurface. This type of wear is observed in journal bearings, gears and cams. Fatigue wear occurs when the surface is subjected to cyclic loading. After several cycles, fatigue cracks appear, which propagate perpendicular to the surface. This type of wear is observed in ball bearings and roller bearings. The second group, Chemical wear was

further classified into four subgroups, Oxidative Wear, Corrosive Wear, Solution Wear and Diffusive Wear. Oxidation Wear occurs when oxide films are formed on the surface during high sliding velocities. As the thickness of the oxide film increases, frictional heating causes it to flow plastically or melt. Corrosive wear occurs when surfaces slide against each other in a corrosive atmosphere. This results in the formation of pits. Solution wear occurs when a solution is formed between the materials in contact decreasing the free energy. This is an atomic level wear process in which new compounds are formed at high temperatures. This type of wear is observed in carbide tools during high speed cutting. Diffusive Wear occurs when there is a diffusion of elements across the interface. It is observed in high speed tool steels.

In most practical cases, materials wear out due to the combination of the above mentioned mechanisms. In spite of this, in order to solve the wear problem, a primary mechanism is identified. Ragnar Holm [1938] stated that when two surfaces were brought together, they touched at their asperities and the area of contact was related to the load divided by the yield pressure of the material. This contact resulted in cold welding of the asperities, particularly if the contact surfaces were clean. The force required to separate these members, resulted in the shearing of asperities. This was the beginning of adhesion theory of friction which was subsequently developed by Bowden and Tabor [1950]. The first quantitative statement of wear was also given by Holm [1946].

$$W = Z\frac{Ps}{H} \qquad (8)$$

W is the wear volume, s is the sliding distance, P is the load, H is the yield pressure of the metal and Z is a dimensionless number. P/H was called the real area of contact.

The serious deficiency in Holm's analysis was, Holm believed that asperity encounters and wear occurred at an atomic level, when in they start at an atomic level but are active at a much larger scale. Wear in electrical contacts usually occurs due to the loss of material from contacting surfaces in the form of particles. Adhesive wear occurs in electrical contacts when bonds formed between touching asperities are stronger than the cohesive strength of the metal. In electrical contacts, the transition from mild to severe wear occurs due to the loss of a protective oxide layer. Most electrical contacts are made up of noble metals. Noble metals are oxide free. Any sliding results in noble metals results in severe wear due to the absence of an oxide film. Many electrical contacts wear by a severe adhesive process called prow formation [Slade 1999]. When two surfaces which are made up of the same material contact, metal transfer occurs if the contacting members are of different sizes. There is a net metal transfer from the part with the larger surface involved in sliding to the smaller surface. As shown in Figure 4, this is observed in a rider-flat contact. As sliding progresses, a lump of severely work hardened metal, the prow, builds up and wears the flat by continuous plastic shearing or cutting. The rider is not affected by wear. Prows get detached from the rider by back transfer to the flat or as loose debris. Theoretically if the rider always contacts virgin metal, prow formation continues indefinitely. When electrical contacts are made of dissimilar contacting metals, prows are formed even when the flat is harder than the rider, provided the hardness of the flat is not greater than the hardness of the rider by a factor of three. The size of the prow formed is inversely related to the hardness. Soft ductile metals like gold form large prows which can be seen by the naked eye.

Cocks [1962] explained the formation of prows with the following steps:

1) Adhesion of metal at the point of contact 2) Plastic deformation of a volume of metal in the flat 3) Development of tensile stresses at the back of this deformed volume of metal 4) Rupture and separation of the deformed metal with transfer to the rider as a chip. 5) Formation of multiple layers of chips on the rider 6) Loss of prow from the rider when it grows large and unstable by back transfer to the flat.

On many electrical contacts, fretting wear occurs, where the rider repeatedly traverses the same path, resulting in rider wear. Prow formation stops after a certain number of cycles. The back transfer prows from the rider accumulate on the flat, increasing its hardness at all places due to work hardening. When the hardness of the flat reaches the hardness of the prows, the rider begins to wear. This rider wear has been modeled in this work.

Burwell and Strang [1952] measured the wear of steels and other metals at slow speeds using cetane as the lubricant. The relationship between wear rate, pressure and load was determined. It was found that wear rate is proportional to the load and independent of pressure, until the point where the surface stress exceeds a value equal to one third the hardness of the material. Krushchov and Babichev [1953] measured the wear of metals when rubbing against emery cloth and concluded that the wear rate of different metals was inversely proportional to their hardness with the exception of heat treated steels. Archard [1956] conducted experiments and found that the wear rate was independent of the apparent area of contact. A pin on ring contact was used during these experiments.

The ring was rotated and a pin was pressed against the circumference of the ring. For low

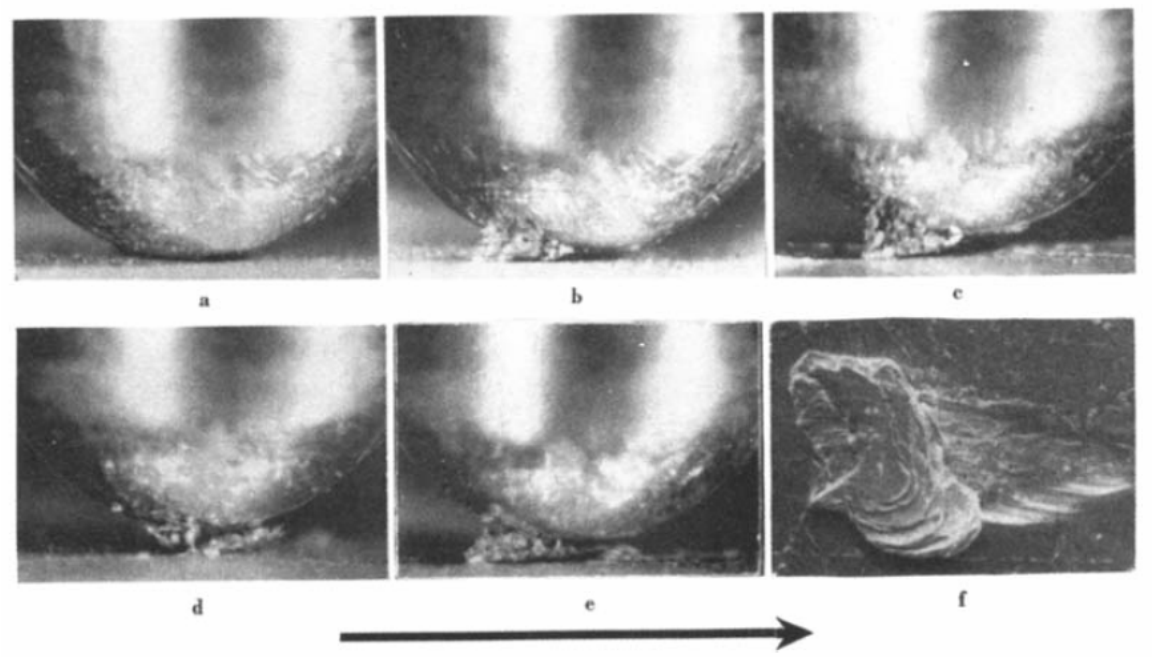

Figure 4: Prow formation mechanism for a rider on a flat. Gold on gold contact.
a) Start of run b) Well developed prow c) and d) Loss of portion of prow by back transfer to flat e) Newly formed prow f) Prow consisting of overlapping thin layers of metal
The Arrow indicates the direction of movement of flat. [Slade 1999]

wear rates, wear was determined by measuring the wear scar on the pin. For higher wear rates, wear was measured by weighing the pin. The apparent area of contact was minimum at the start of the experiment and increased with an increase in the dimension of the wear scar. It was found, for metals, light loads resulted in mild wear. As the load was increased, after a period of mild wear, severe wear was initiated as a patch of heavy damage. This creates the conditions for the continuance of severe wear and the rough patch spreads to cover the entire contacting surface. It was found that mild wear involved the slow removal of the tips of the higher asperities and severe wear involved the welding and plucking of surfaces. Unlike mild wear, severe wear also resulted in subsurface

damage. In severe wear, the crystal structure of the surface layers becomes heavily distorted and these deformations extended below the surface. It was concluded that the transition from mild to severe wear was associated with a change in depth of deformation. Hirst and Lancaster [1956] found, during the early stages of rubbing, wear rate changes but after an initial period of running, the wear rate becomes constant. This occurred when the two contacting surfaces attained their equilibrium condition. At this stage the wear rate became independent of the apparent area of contact. Kapoor and Franklin [2000] have used Archard's wear model to simulate delamination wear. Sarkar [1980] has proposed a wear model that relates the friction coefficient and the volume of the material removed. This model is an extension of Archard's wear model and is given by,

$$\frac{V}{s} = k\frac{F_n}{H}\sqrt{1+3\mu^2} \qquad (9)$$

V is the volume of material removed, s is the sliding distance, k is a dimensionless wear coefficient, F_n is the normal load, H is the hardness and μ is the friction coefficient.

Strömberg [1999] developed a finite element formulation for thermoelastic wear based on Signorini contact and Archard's wear model. de Saracibar & Chiumenti [1999] developed a numerical model for simulating the frictional wear behavior within a fully nonlinear kinematical setting, including large slip and finite deformations. This model was implemented into a finite element program, where the wear was computed using Archard's wear model. Öquist [2001], Ko et al. [2002], McColl et al. [2004], Ding et al. [2004], Gonzalez et al. [2005] and Kónya et al. [2005] developed wear models based on Archard's wear model and implemented them in finite element post processing. Sui et al. [1999] and Hoffmann et al. [2005] implemented re-meshing to update the geometry of

the model after wear. Kim et al. [2005] developed a three dimensional finite element model and a re-meshing technique for simulating wear on a block contacting a rotating ring. Podra & Andersson [1997], Jiang & Arnell [1998] and Dickrell & Sawyer [2004] used the elastic foundation method for the computation of contact pressure. The elastic foundation method for contact pressure computation did not take into consideration the effects of shear deformation or lateral interactions in the contact. In these models, wear was calculated using Archard's wear model. Yan et al. [2002] proposed a computational approach for simulating wear on coatings in a pin on disc contact system.

Agelet [1999] developed a numerical model for the simulation of frictional wear behavior. He used a nonlinear kinematic setting which included large slip and finite deformation. The model uses a fully nonlinear frictional contact formulation. Wear occurring in tools is predicted by using a wear estimate derived from Archard's Law. Hot forging and sheet metal forming are the two processes considered for which wear is calculated. Hot forging dies get worn off due to Abrasive Wear. Hard scale particles embedded in the surface of the work piece cause the die to wear. In sheet metal forming process, abrasive and adhesive wear are the two main mechanisms which cause die failure. During the process, when the sheets are pressed together, the real area of contact is much smaller than the apparent one, due to the presence of asperities and surface roughness. The high pressures involved, causes plastic deformation of these asperities. At the same time the metal sheet slides over the tool surface generating heat due to frictional dissipation. High pressures combined with heat generation leads to welding of the asperities of the two contacting surfaces. The break off of these welded asperities

scratches the tool surface and causes wear. For constant friction coefficient, wear is calculated using the formula,

$$Z = \frac{K_{wear}}{\mu_o H}\alpha \qquad (10)$$

where Z is the wear volume per unit area, K_{wear} is a wear constant which is determined experimentally, μ_o is the constant friction coefficient, H is the hardness of the material and α is the frictional dissipation force per unit length or the slip amount.

A two dimensional model of the roller die was constructed to study the effects of wear on the die. Time integration of the wear rate estimate is carried out which gives an estimate of the accumulated tool wear over a large number of cycles. Cantizano [2002] used a microthermomechanical approach in his model. In this model, depending on the operating conditions, normal force and sliding velocity, the predominant wear mechanism is selected. In order to reproduce the behavior of the contact interface between two rough surfaces, a plastic law for the behavior of the asperities in contact, based on statistical characterization of the surfaces, has been implemented. Steel on steel contact has been modeled. Cantizano calculated wear using three different wear equations depending on the sliding velocity. At moderate sliding velocities, flash temperatures are reached and iron oxide is formed as wear debris. The oxide film formed on the surface is cold and brittle which causes this film to split off. This is called mild oxidation wear. The amount of wear is given by,

$$W = \left(\frac{C^2 A_0 r_0}{Z_c a}\right)\exp\left[-\frac{Q_0}{RT_f}\right]\frac{F}{v} \qquad (11)$$

W is the normalized wear rate, C is a constant, A_0 is the Arrhenius constant for oxidation, r_0 is the radius of the pin, Z_c is the critical thickness of the oxide film, a is the thermal diffusivity, Q_0 is the activation energy for oxidation, R is the molar gas constant, T_f is the flash temperature, F is the normalized load and v is the sliding velocity

As the sliding velocities increase, the interface temperatures increase, resulting in the formation of a thicker, continuous and a more plastic oxide film. This is called severe oxidation wear. The amount of wear is given by,

$$W = \frac{f_m}{v}\left(\alpha q - \frac{K_{ox}\left(T_m^{ox} - T_b\right)}{l_f}\right)\left(\frac{A_r}{A}\right) \qquad (12)$$

f_m is the volume fraction of molten material removed during sliding, α is the heat distribution coefficient, q is the rate of heat input per unit area, K_{ox} is the thermal conductivity of the oxide, T_m^{ox} is the melting temperature of the oxide, T_b is the bulk temperature, l_f is the diffusion distance for flash heating, A_r is the real area of contact, A is the nominal area of contact. At very low sliding speeds, surface heating is negligible.

Wear rate was calculated using Archard's Law,

$$W = k_A F \qquad (13)$$

k_A is the Archard's wear coefficient.

A two dimensional model was constructed for a pin on disk configuration, with the pin modeled as a square pin for the sake of simplicity. Molinari [2000] developed a finite element model to show dry sliding wear in metals. Adaptive meshing was used in the model to remove deformation induced element distortions. While using Adaptive meshing, a Lagrangian formulation was used to move nodes to their new position.

Archard's law was used for damage computation. To model the transition of wear rates with increase in sliding speeds, Archard's law was generalized by allowing the hardness of the material to change with temperature. The change in hardness affects the wear rate when used in Archard's Law.

According to Lancaster [1963] the transition of wear rates was a direct result of the presence of oxide layer. At higher sliding speeds higher contact temperatures exist, which increases the oxidation rate. The protective oxide layer gets regenerated faster, than it is removed by wear. The dependence of hardness on temperature, H(T), takes into account the effects of oxidation. The Newmark algorithm was used to enforce the impenetrability constraint in the contact, which is used to calculate the frictional forces and the contact pressure, used in Archard's Law. Frictional forces are used to calculate heat generated, which change the hardness of the material. During adaptive meshing, a mesh adaptation strategy based on local error indicators for non-linear dynamic problems developed by Radovitzky and Ortiz (1999) has been used. This meshing algorithm automatically generates unstructured tetrahedral meshes. The finite element model was validated against experimental observations of Lancaster [1963]. The contact system used was a 60-40 brass pin set against a rotating steel disk.

Podra [1999] used a finite element model to model wear for a pin-on-disc contact system. The contact problem was solved with the area of contact between the bodies not known in advance, making the analysis non-linear. Special subroutines were developed to generate the finite element model and define the loads and constraints automatically. The model was meshed with a fixed static mesh. A finer mesh was used in the areas expecting higher stress. This provided accurate results at the cost of computation time. The contact

pressure distribution in the contact area was calculated from the nodal stresses of the nodes in the contact region. Damage accumulation caused due to wear was accounted for by using the Euler integration scheme,

$$h_{j,n} = h_{j-1,n} + \Delta h_{j,n} \qquad (14)$$

$\Delta h_{j,n}$ is the wear increment, n is the node number and j is the step number. To prevent the simulation results from becoming erratic, due to excessively large wear increments, a predetermined maximum wear increment limiter was defined, Δh_{lim}. A two dimensional half symmetry model was constructed. The model was verified by performing experiments involving a spherical steel pin sliding on a steel disc. Hegadekatte [2005] has created a finite element model which simulates wear between steel and brass contact system. Archard's wear law has been used for damage computation. Two dimensional and three dimensional models have been constructed to simulate wear. Wear is computed on both the interacting surfaces. In wear simulation the maximum amount of wear possible is limited by the surface element height. To overcome this limitation adaptive re-meshing has been used in this model. A wear simulation tool has been developed which solves the contact problem a number of times at different stages of the sliding process. Contact pressure is calculated at the surface nodes which are involved in wear. The contact pressure is calculated at the surface nodes from the normal vector and the stress tensor calculated at each surface node,

$$t_j = \sigma_{ij} * n_i \qquad (15)$$

$$P = t_j * n_j$$

t_j is the traction vector, σ_{ij} is the stress tensor, n_i is the inward surface normal at the corresponding surface node and P is the contact pressure. Archard's wear model is used to calculate wear at each of the surface nodes.

$$\frac{h}{s} = k_D * P \qquad (16)$$

h is the nodal wear, s is the sliding distance, k_D is the dimensional wear coefficient and P is the contact pressure at each surface node. This wear law is discretized with respect to the sliding distance as,

$$\frac{d}{ds} h = k_D * P \qquad (17)$$

An Euler integration scheme used explained in Equation 14 is used to integrate the wear law over the sliding process. The surface nodes in the contact region are shifted in the direction of the inward surface normal, depending on the amount of wear at that particular node. To allow this motion, the surface elements would have to be meshed such that they have enough height to accommodate this wear, resulting in a coarse mesh in the contact region. This problem was eliminated in this model by using Adaptive Remeshing. The element mesh in the contact region is re-meshed, which corrects the deformed mesh at the surface. The nodes are shifted towards the interior of the model, depending on the amount of wear. This refines the mesh and reduces the size of the elements. To apply the calculated wear, the model is fixed in space at its geometrical boundaries except at the surface nodes. At the surface nodes, the computed wear is applied as a displacement boundary condition, which moves the surface nodes inside the

material. These new nodal coordinates form the reference configuration for the next wear step. Dry sliding contact has been simulated in this model. Wear occurring due to the rotation of a hemispherical Brass ring on flat steel ring has been simulated. Load is applied on the top surface of the brass ring as it rotates on the steel ring, whose position is fixed. The contact is initially non-conformal contact which conforms with sliding due to wear. Hegadekatte's model doesn't take into consideration the changes in the model as wear progresses. The results obtained at individual nodes do not take into consideration, the history of the loading at those nodes. Thompson [2006] proposed a wear model which calculated wear in the solution process instead of calculating it in the post processor, to eliminate the drawbacks of Hegadekatte's model. A modified Archard's equation was used in this model,

$$W = K * S^{C2} * R^{C3} \qquad (18)$$

W is the change in volume, K, C2, C3 are constants which account for the materials in contact, S is the stress created by the contacting pairs and R is the number of repetitions of the load. A quantity known as wear strain was defined by dividing Equation 18 by the original volume,

$$e_{wr} = C1 * S^{C2} * R^{C3} \qquad (19)$$

e_{wr} is the wear strain, C1 is equal to K divided by the original volume

Unlike other strains, wear strain represents material that is removed from the system. Wear strain used in this model differs from wear, as proposed by Archard. In Archard's equation the applied loading is assumed to be distributed over the entire loading area, hence wear is expected to occur uniformly over the entire surface. The

Wear strain proposed in this model is a function of stress and load repetitions. Only those regions of the surface which are loaded, experience wear. Wear strain permits wear to be different at different locations of the surface, depending on the loading condition. This model uses a wear equation that is similar to creep equations. Creep is used to simulate wear. The strain hardening creep equation used is given by,

$$\frac{d}{dt}e_{cr} = C1 * stress^{C2} * e_{cr}^{C3} * \exp(-C4/T) \qquad (20)$$

C1, C2, C3, C4 are user defined constants. Incremental creep strain is calculated using Equation 20. The incremental creep strain is multiplied by the incremental time and added to the previous creep strain. The same procedure is used to calculate the wear strain. For each load step, the incremental wear strain is calculated, multiplied by the load step time and added to the previous wear strain.

CHAPTER 3

FINITE ELEMENT REPRESENTATION OF ELECTRICAL CONTACTS SUBJECTED TO VIBRATIONS

The wear simulation tool developed here can be used to simulate wear between electrical contacts subjected to vibrations. In today's electronic devices there exist thousands of electrical contacts. In this work, four different electrical contact systems have been studied, namely, Fuzz Buttons, SD Cards, Memory Cards and Zero Insertion Force (Z.I.F.) sockets. A finite element representation of each of these electrical contacts has been presented here.

3.1 Fuzz Buttons

Fuzz buttons are special interconnects used to connect an Integrated Circuit (I.C.) to a Printed Circuit Board (P.C.B.). Fuzz button interconnections have several advantages over traditional interconnections like soldering, socketing and plug in connectors due to their simple design, good performance and long life. Fuzz buttons provide a reliable and a cost effective interconnection for new chips which run at very high clock speeds and have very high package densities. Traditional interconnects like sockets require expensive plated through holes and fabrication. Plug connectors use metal fingers or prongs to make contacts which are prone to bending or breaking. The size of these connectors also limits

their density. Solder connections can be expensive and operations such as disassembling, replacing and repairing are cumbersome.

Fuzz button interconnects were invented by Tecknit Co. They were first used in static dissipation pads for computer chassis. Fuzz buttons were later used in radar and space applications. They were also used in ARM missiles as an interconnect between ring shaped PCB's. Fuzz buttons were able to cope with very severe vibrations without being damaged while maintaining a good connection which made them ideal for the above mentioned applications.

3.1.1 Construction of Fuzz Buttons

Fuzz buttons are constructed from a large quantity of gold plated Beryllium-Copper (BeCu) wire. This wire is compressed into a cylindrical shape by a purpose built machine. The wire used for manufacturing fuzz buttons is extremely thin. Standard fuzz buttons are manufactured from a single strand of 0.002 inch gold plated BeCu wire. Figure 5 shows a standard fuzz button.

Figure 5: Magnified view of a standard fuzz button [Courtesy of Tecknit Interconnection Products]

Fuzz buttons are available in diameters ranging from 0.010” to 0.125”. Their lengths may vary from 2X to 10X their diameter. Fuzz buttons are tiny. Figure 6 gives a general idea of the size of fuzz buttons.

Figure 6: Small size of fuzz buttons enabling high contact density [Courtesy of Tecknit Interconnection Products]

Fuzz buttons provide a low inductance value and a short signal path, resulting in a distortion free connection. Fuzz buttons are also currently used in test sockets, for various chip packages like Ball Grid Arrays, Pin Grid Arrays and Land Grid Arrays. Figure 7 shows the assembly of a fuzz button in a test socket.

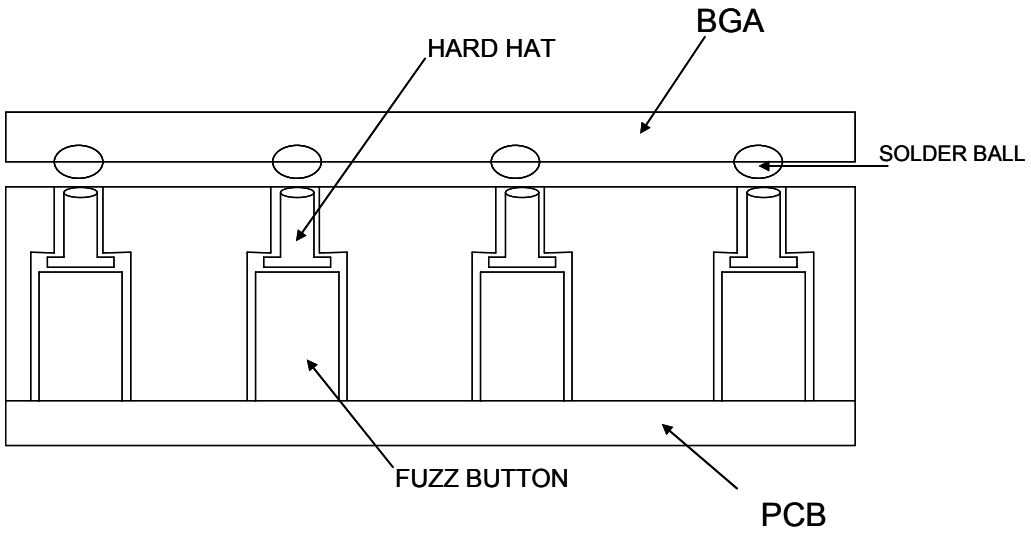

Figure 7: Fuzz button assembly

Spring characteristics of the fuzz button contacts are excellent as they are made from high tensile strength gold plated BeCu wire. This ensures long life of the contacts. Each fuzz button is designed to compress 15% with no compression set within the socket. When fuzz buttons are used in test sockets more than 500,000 insertions are possible on a single test socket, before the fuzz buttons have to be replaced. In test sockets, a single fuzz button can also be removed to isolate a connection to aid testing and fault finding on a particular chip package. The contact pressure required to use fuzz buttons is minimal, enabling them to be used with most delicate of packages. This reduction in pressure becomes important while testing Micro Electronic Packages. They have high test point density, result in high pressures per square inch.

Gold plated hard hats are used to connect Integrated circuits like BGA's, LGA's, PGA's and gull wing to Fuzz Buttons. These are miniature contact pins. These help minimize the damage to solder balls or pins of the IC. Typical hardhats are shown in Figure 8

Figure 8: Hard Hats [Courtesy of Tecknit Interconnection Products]

The skin effect is the tendency of an Alternating Electric Current (AC) to distribute itself within a conductor such that the current density near the surface of the conductor is greater than that at its core. The electric current tends to flow at the skin of the conductor. There is less surface area to pass the signal. The skin effect causes the effective resistance of the conductor to increase with the frequency of the current. Skin effect is due to eddy currents set up by the AC current. The random orientation of the wires within fuzz buttons negates the skin effect to a large extent. In case of fuzz buttons the small diameter of the wire also helps reduce skin effect.

3.1.2 Modeling a fuzz button contact

To represent the contact between a fuzz button and the PCB a two dimensional finite element model is constructed as shown in Figure 9

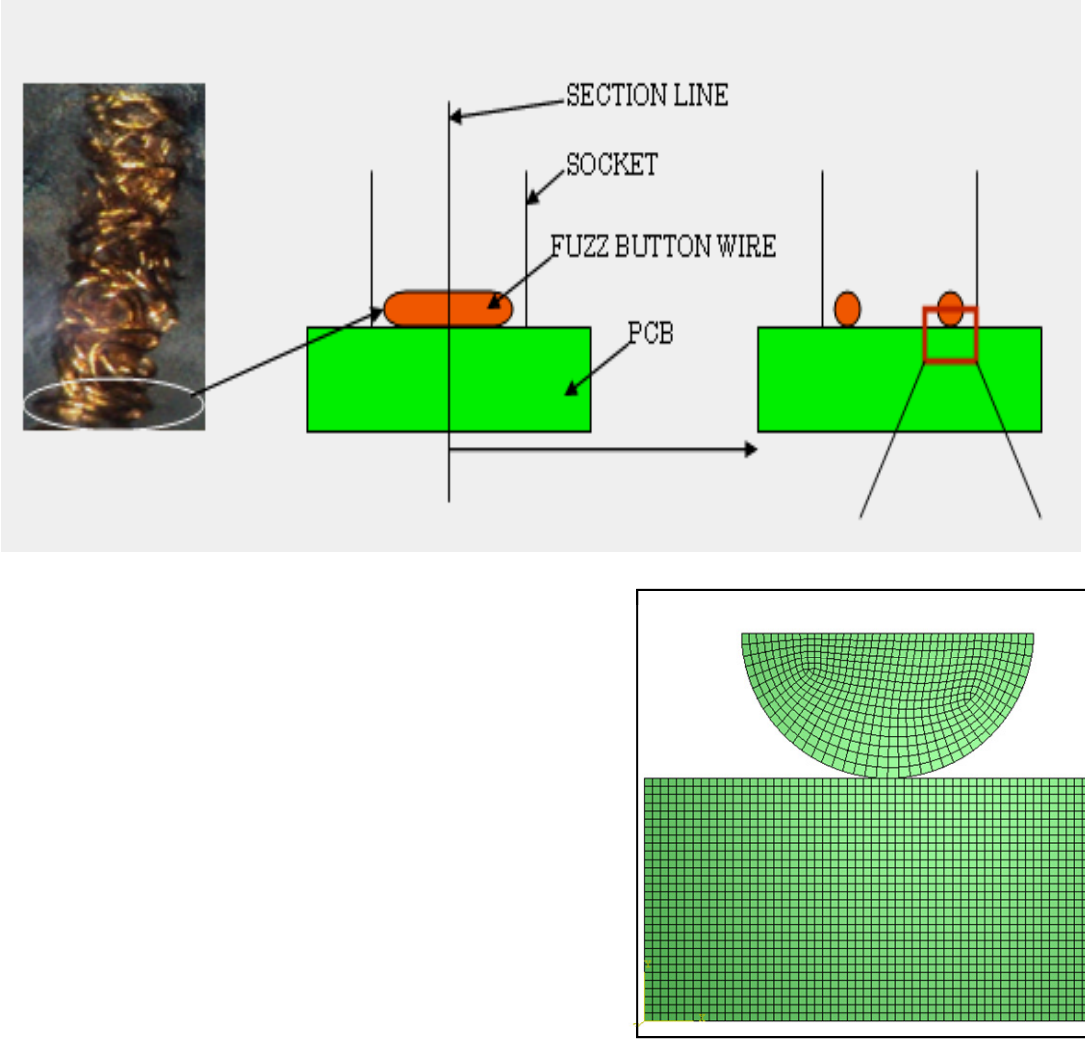

Figure 9: 2D modeling of a fuzz button and PCB contact

As shown in Figure 7 fuzz buttons are mounted in sockets. As mentioned earlier, fuzz buttons are used in applications involving severe vibrations. There exists a slight clearance between fuzz buttons and their respective sockets. The diameters of the sockets are slightly bigger than the diameters of fuzz buttons to facilitate easy removal of fuzz buttons during repair. When this assembly is subjected to external vibrations, the fuzz buttons oscillate at a high frequency inside sockets. After several oscillations, the surface

of the PCB wears off due to fretting wear. This might result in the loss of an electrical connection, leading to failure of component. When fuzz buttons are used in test sockets, they deform slightly when the test socket is loaded with a component. This might cause the fuzz button wire to slide against the PCB resulting in fretting wear. The contact between a fuzz button and PCB is simplified to enable modeling. The bottom of the fuzz button is assumed to be a complete circle of wire. A model is constructed which represents the cross-section of a circular wire on a flat PCB. Since the bottom of the wire is contacting the PCB, only the lower semicircular half of the wire is modeled. This semicircular slider oscillates on the rectangular receptacle, resulting in fretting wear. The wear model presented here will help predict the wear rate of the PCB, which will help to predict the life of the component.

3.2 Memory Cards

Memory Cards are used in several electronic devices like cell phones, cameras and gaming consoles. Amongst memory cards, SD card is a very popular configuration. Very often in these devices the memory card must be removed for data transfer and reinserted. Typically, an insertion force of 40N is required for these cards. After several insertions and removals the contacts of the sockets will wear off. These cards are used in several portable devices. During their usage these devices may be subjected to drops or shocks or vibrations generated due to neighboring components which might result in fretting wear.

3.2.1 Construction of Memory Cards (S.D. Cards)

A Secure Digital card is compact with dimensions, 24mm*32mm*2.1mm. It was jointly developed by Panasonic, SanDisk and Toshiba. The Secure Digital Card is a flash-based memory card that is specifically designed to meet the security, capacity, performance and environmental requirements, required in newly emerging audio and video consumer electronic devices. An SD card includes a copyright protection mechanism. It uses a nine pin interface for communication. These pins are subjected to fretting wear and eventually will get damaged resulting in card failure.

Figure 10 shows an SD card with nine contact pins.

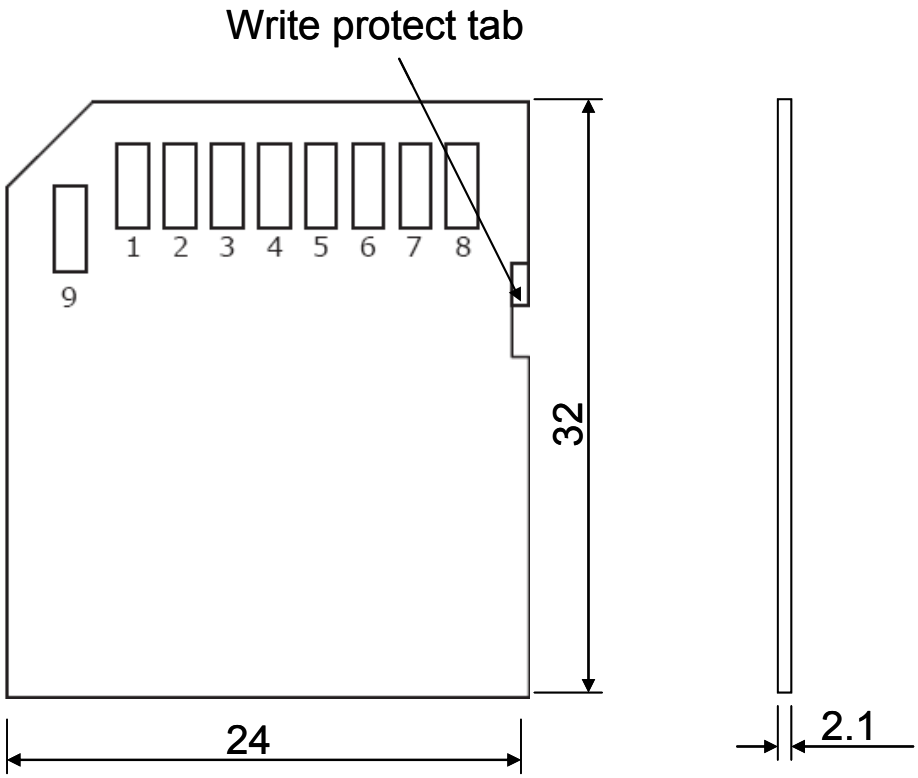

Figure 10: A typical SD Card construction

Each pin has a specific function. These pins perform the following functions, 1 pin for clock, 1 pin for command, 4 pins for data and 3 pins for power. Table 2 shows the pin numbers, names, their type and their specific functions.

PIN #	PIN NAME	PIN TYPE	FUNCTION
1	DAT3	Input/Output (I/O)	Card Detect/Data Line [Bit3]
2	CMD	I/O using push pull drivers	Command/Response
3	Vss1	Power Supply	Ground
4	VDD	Power Supply	Supply Voltage
5	CLK	Input	Clock
6	Vss2	Power Supply	Ground
7	DAT0	Input/Output (I/O)	Data Line[Bit0]
8	DAT1	Input/Output (I/O)	Data Line[Bit1]
9	DAT2	Input/Output (I/O)	Data Line[Bit2]

Table 2: SD Card pins and their functions

These SD cards are inserted into special SD card connectors. When fully inserted, the contact pins on the SD card, touch the connector. Figure 11 shows a typical SD card connector

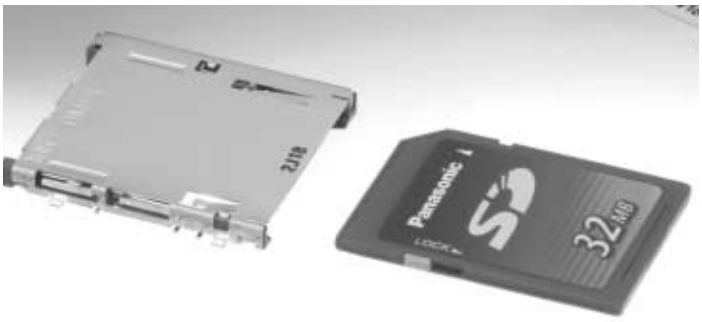

Figure 10: SD card connector with card [Courtesy of Panasonic]

3.2.2 Modeling a memory card contact

To represent the contact between an SD card and its respective connector, a two dimensional finite element model is constructed as shown in Figure 12

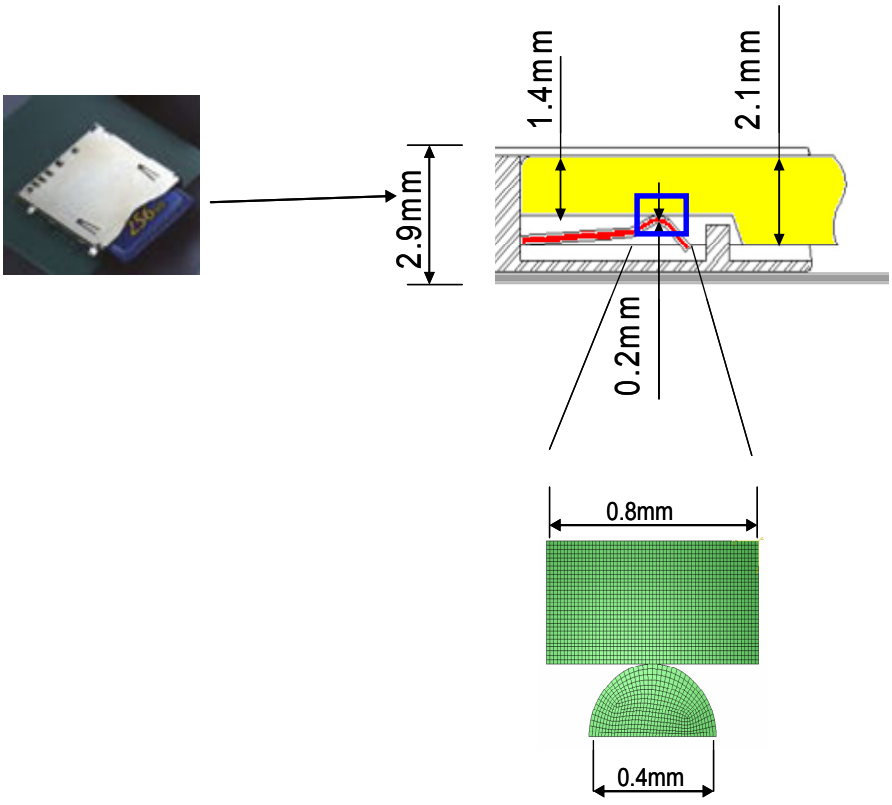

Figure 11: 2D Modeling of a Memory card and a memory card connector contact based on [SD Card Product Manual, Courtesy of Hirose Connectors]

When this assembly is subjected to vibrations, the card will vibrate in its socket. This will cause the pins of the card to oscillate rapidly with respect to the connector, which will result in fretting wear. This model can be used to predict the wear rate and hence, the life of the component.

3.3 Memory Modules

Memory modules are used in many electronic devices like servers, laptops and printers. They are mounted in special sockets which are mounted on the PCB. Portable devices like laptops may be subjected to external vibrations during usage. Devices like servers are run for extended periods of time. Vibrations generated by various components like cooling fans and hard-drives are transmitted throughout the system. When these vibrations reach memory module sockets, they might cause the memory modules to vibrate in their respective sockets, resulting in fretting wear. Figure 13 shows a typical dual in-line memory module (DIMM).

Figure 12: A Typical Dual In-line Memory Module [Courtesy of Kingston Technology]

Figure 14 shows a memory socket. As shown in Figure 14, the contact pins which enter the socket are at the bottom of the memory module. Fretting wear will degrade these contacts, causing the component to fail.

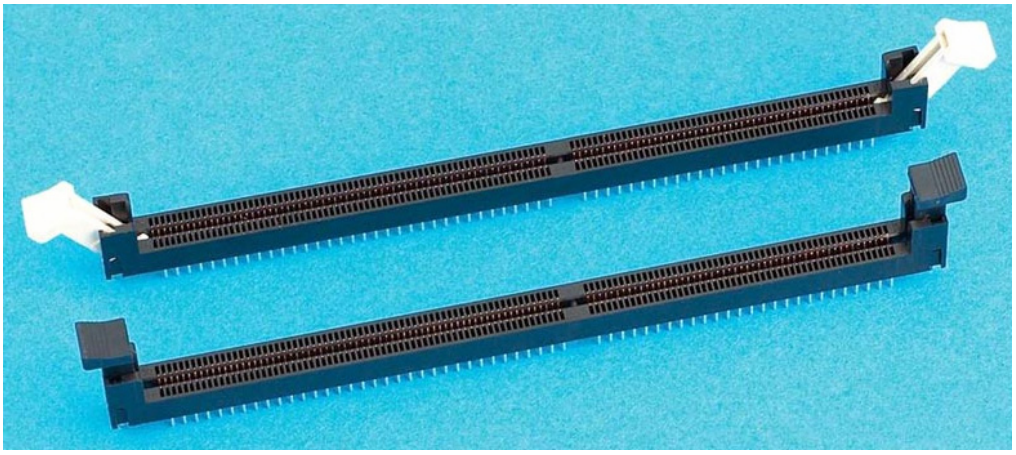

Figure 13: A Typical Memory Socket [Courtesy of Kingston Technology]

To represent the contact between a DIMM memory module and its socket, a two dimensional finite element model is constructed as shown in

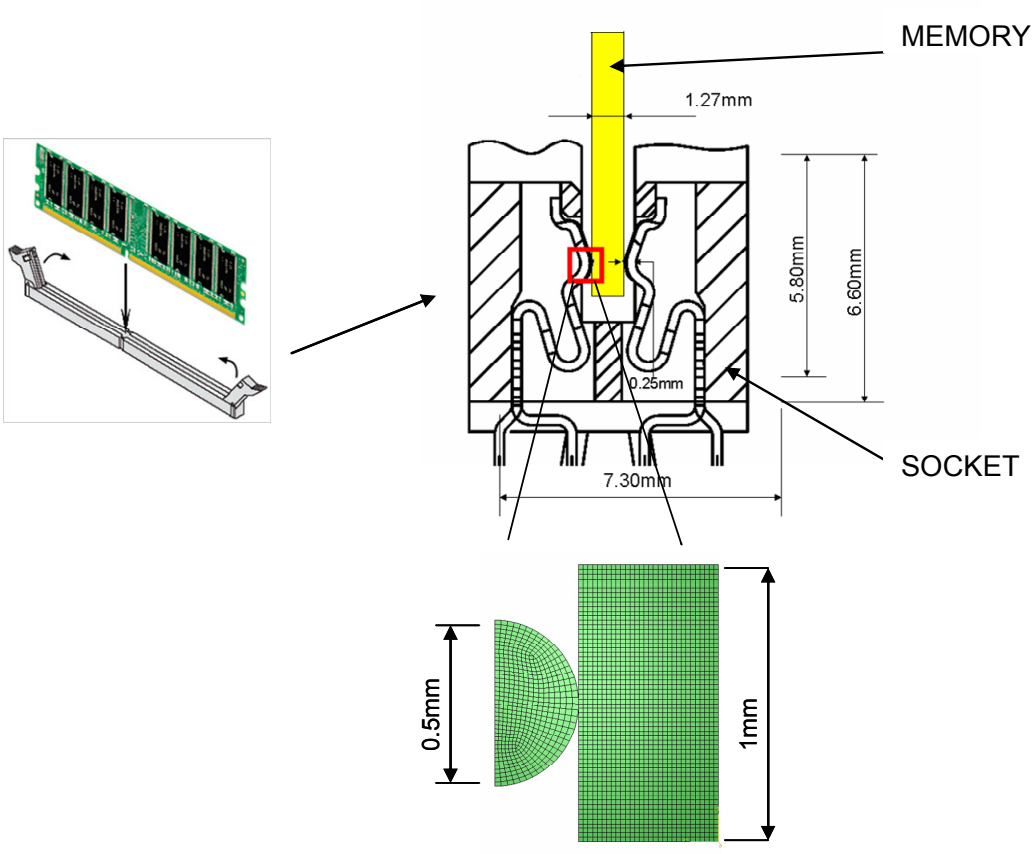

Figure 14: A 2D model representing a memory module and its corresponding socket based on DIMM Socket Manual [Courtesy of DDK Sockets]

An insertion force of 97N is required to insert these modules. The semicircular part represents the connector in the socket. The rectangular part represents a contact pin of the memory module.

3.4 Zero Insertion Force Sockets

Zero Insertion force (Z.I.F.) sockets are Integrated Circuit (I.C.) sockets invented to avoid problems caused by applying force during insertion and extraction of microprocessors. A normal IC socket requires the IC to be pushed into sprung contacts which then grip by friction. In the case of microprocessors, the IC has hundreds of pins, therefore the total insertion force will be very large, which might damage the IC or the PCB. In case of a ZIF socket, before the IC is inserted, a lever or slider on the side of the socket is moved, pushing all the sprung contacts apart, so that the IC can be inserted with very little force. The weight of the IC is sufficient and no external downward force is required. The lever is then moved back, allowing the contacts to close and grip the pins of the IC. Large ZIF sockets are mounted on PC motherboards.

This assembly of ZIF socket and IC is subjected to vibrations. Vibrations may arise from neighboring components like CD drives, hard drives or cooling fans which are mounted above the IC to extract heat. These vibrations may cause relative motion between the sprung contacts and the IC pins. After several cycles, the sprung contacts wear out due to fretting wear. This will result in failure of the electric contact and the component. Figure 16 shows a 2D model representation of ZIF socket and pin contact.

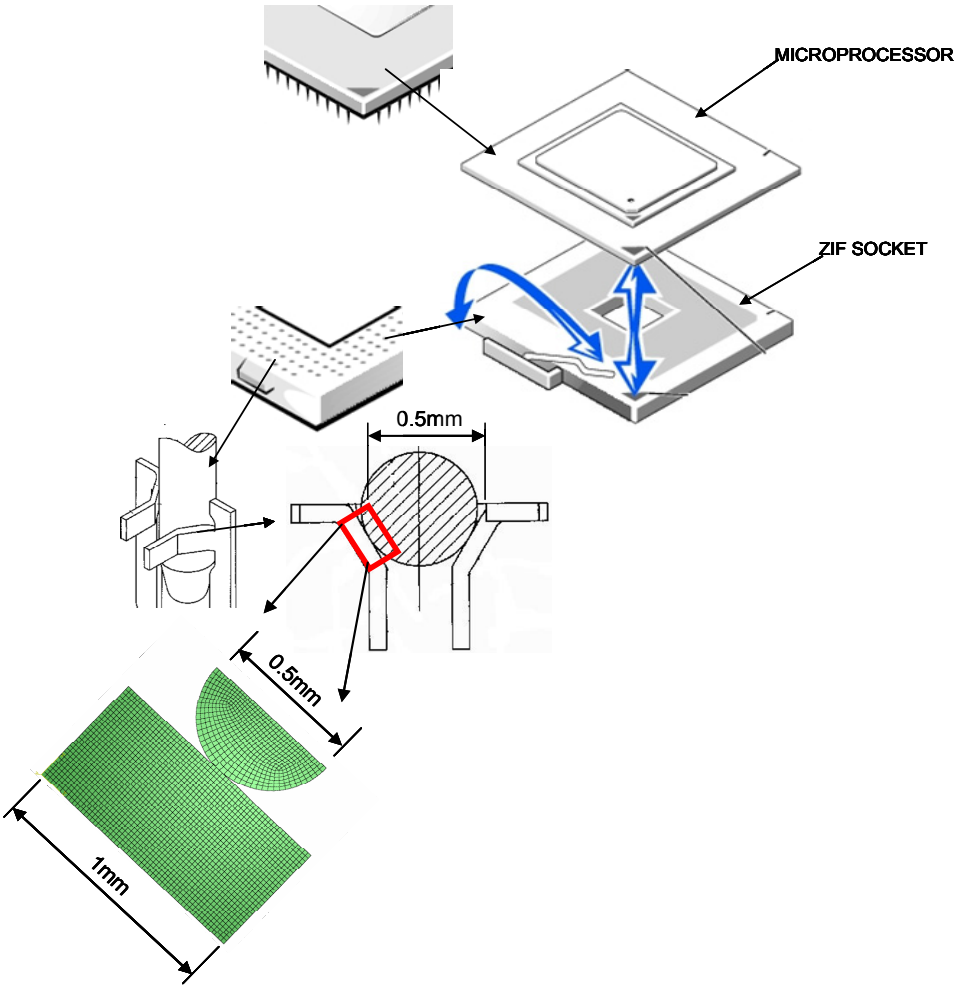

Figure 15: 2D model representing a ZIF socket and IC pin contact based on Lin [2003]

All these applications prove that the model developed in this study can be used to predict the wear rate of various electrical contacts. For each case considered, the material properties of the contacting surfaces are inputted, the dimensions are changed and load is applied depending upon the contact force in the system considered. The model helps predict the wear rate, which in turn can predict the rate of degradation of the contacting surface. Once the surface of the electrical contact wears off, it ceases to function resulting

in failure of the component. This model can therefore be used for life prediction of components.

CHAPTER 4

MODELING OF ELECTRICAL CONTACTS

As shown in Figure 12, Figure 15 and Figure 16, electrical contact between various electrical systems can be modeled using a two dimensional model of a slider which slides on a receptacle. Two dimensional and three dimensional models have been constructed to model electrical contacts. The slider represents the part which undergoes repetitive motion when subjected to vibrations. This sliding portion of the electrical contact, contacts the fixed portion, which is represented by the rectangular receptacle.

4.1 Two Dimensional Model (First Model with Coarse Mesh)

A two dimensional model is constructed to represent the contact between a fuzz button and PCB. To simplify the model, a single wire from the fuzz button which contacts the PCB has been modeled. Instead of modeling the entire wire, a circular cross-section of the wire has been modeled. During contact, only the bottom half of the wire will contact the PCB. To simplify the model further, only the bottom half of the wire is modeled i.e. a semicircular cross-section, representing the bottom half of the wire has been constructed which slides on the PCB.

Since the amplitude of oscillation of the wire on the PCB is very small, instead of modeling the entire PCB, only a small rectangular section of the PCB has been modeled. The semicircular slider, representing the wire oscillates on the rectangular receptacle, representing the PCB. After several oscillations, the surface of the PCB wears off due to fretting wear. Figure 17 shows the two dimensional model representing the contact system.

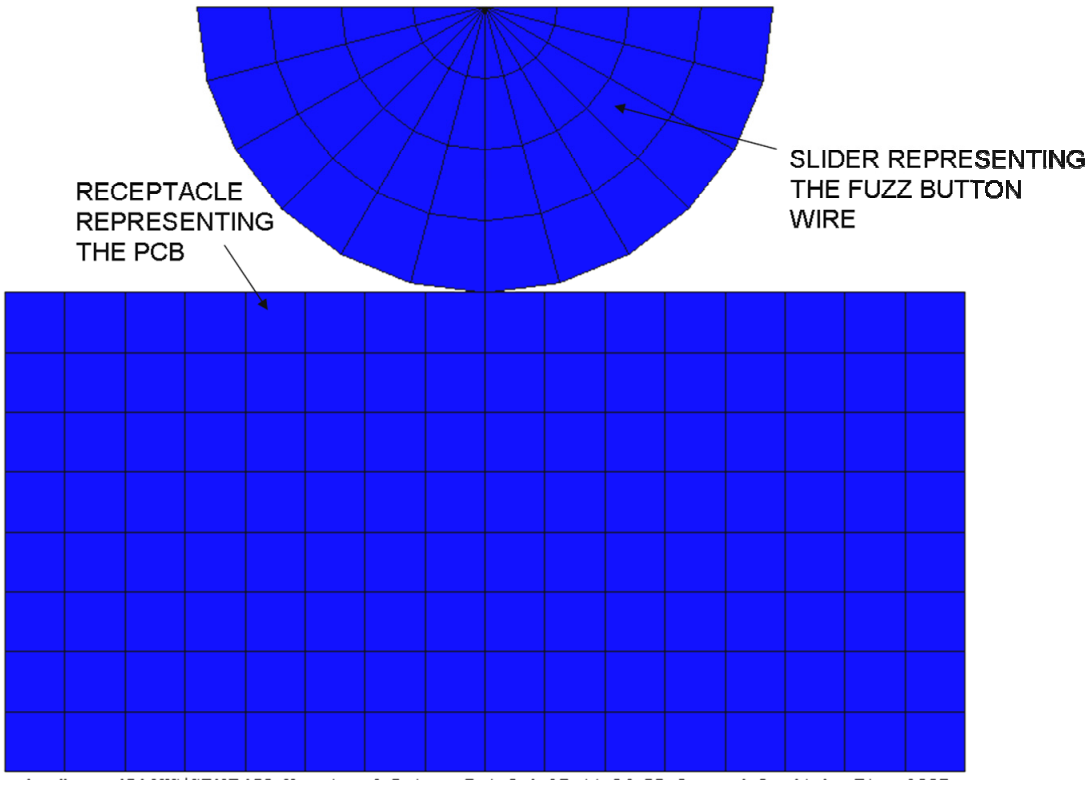

Figure 16: 2D Model Representation of Fuzz Button contacting the PCB

This two dimensional model is constructed in HYPERMESH. Material properties are assigned to the model. The fuzz button is made of Beryllium Copper wires. The slider, which represents the fuzz button, is assigned the properties of BeCu, namely the density, modulus of elasticity and poisson's ratio. The top surface of the PCB is made of copper.

The receptacle, which represents the PCB, is assigned the material properties of copper. The entire model is made of plain strain elements. The semicircular slider is modeled using CPE4, which is a Q4 quad element and some CPE3, linear constant strain triangular (CST) elements. Q4 is a solid 4-node bilinear plane strain element. CST is a 3-node linear plane strain element. The rectangular PCB is modeled using Q4 elements. Figure 18 shows a CST element.

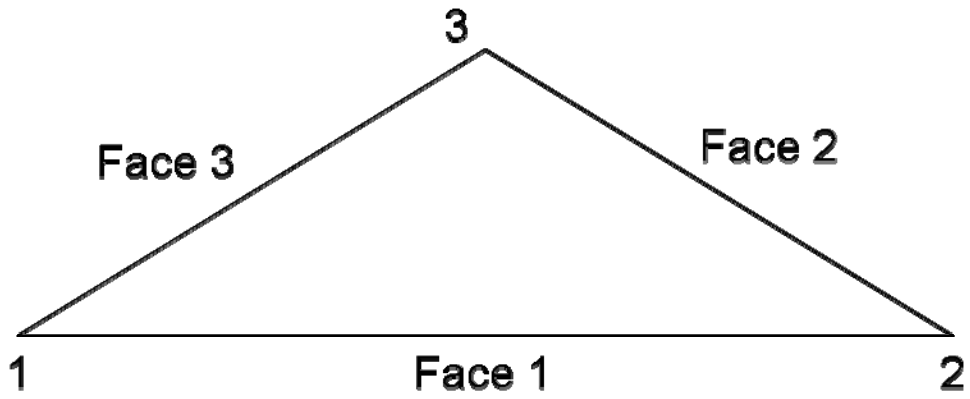

Figure 17: A standard Constant Strain Triangle 3 noded linear plane strain element

Figure 19 shows a standard Q4 element. The face numbers of these elements are important while applying load on the top face of the fuzz button wire. The top face of the fuzz button is made of Q4 elements. It is important to apply pressure on that face of the element which is pointing upwards to ensure correct load application

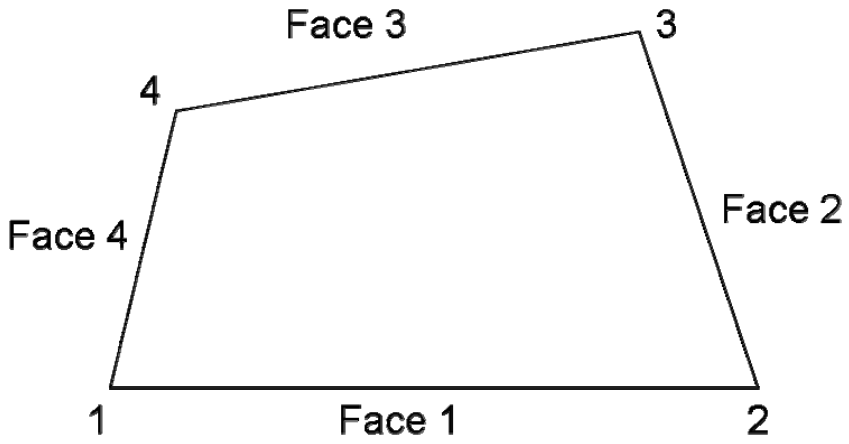

Figure 18: A standard Q4 4 noded bilinear plane strain element

These elements support adaptive meshing; hence they are used in this model. Load is applied on the top surface of the semicircular slider as it oscillates on the receptacle.

A coarse mesh was used in this model. A coarse mesh was initially selected to reduce the simulation running time at the cost of accuracy of results. Once it was established, that the analysis was running successfully, a new 2D model was constructed with a finer mesh. This resulted in the increase of computation time but at the same time better results would be obtained

4.2 Two Dimensional Model (Second Model with a Finer Mesh)

A new 2D model was constructed in HYPERMESH using a finer mesh. Material properties were assigned to the model. The slider, which represents the fuzz button, was assigned the properties of BeCu, namely the density, modulus of elasticity and poisson's ratio. The top surface of the PCB, where the fuzz button contacts is made of copper. The receptacle, which represents the PCB, was assigned the material properties of copper. The semicircular slider was modeled using Q4 quad elements and some CST triangular

elements. Q4 is a solid 4-node bilinear plane strain element. CST is a 3-node linear plane strain element. The rectangular PCB was modeled using Q4 quad elements. Figure 20 shows the fine mesh model.

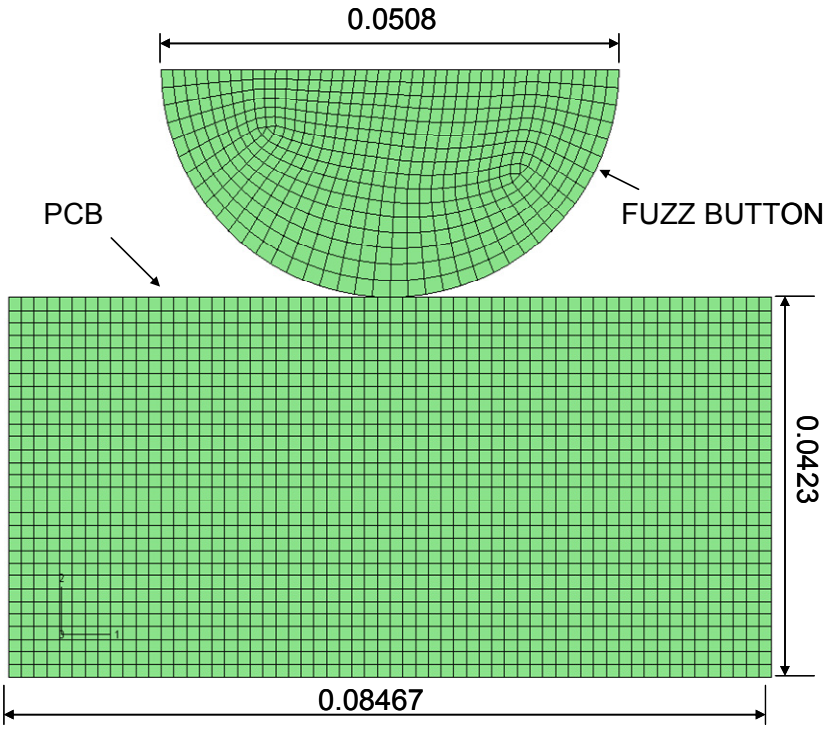

Figure 19: 2D Model with a finer mesh representing the fuzz button and PCB

The dimensions of the model are selected to represent the actual size of the electrical contact. As shown in Figure 20, the fuzz button wire has a diameter of 0.0508mm. This wire is subjected to vibrations. The fuzz buttons are mounted inside sockets. These sockets are slightly larger than the diameter of the fuzz button. The amplitude of vibration of the fuzz button depends on the size of these sockets. The PCB is 0.08467mm long and its length is selected by taking into consideration the amplitude of oscillation during vibrations. As shown in Figure 7, a hard hat presses down on a fuzz button. The IC rests on the hard hat. The contact force required to ensure proper contact

of fuzz buttons with the PCB, is specified by fuzz button manufacturers. For the size of the fuzz button used in this model, a contact force of 0.834N is used. The magnitude of force required is given by the manufacturer, Tecknit Co. This force is applied on an annular area whose width is equal to the diameter of the wire.

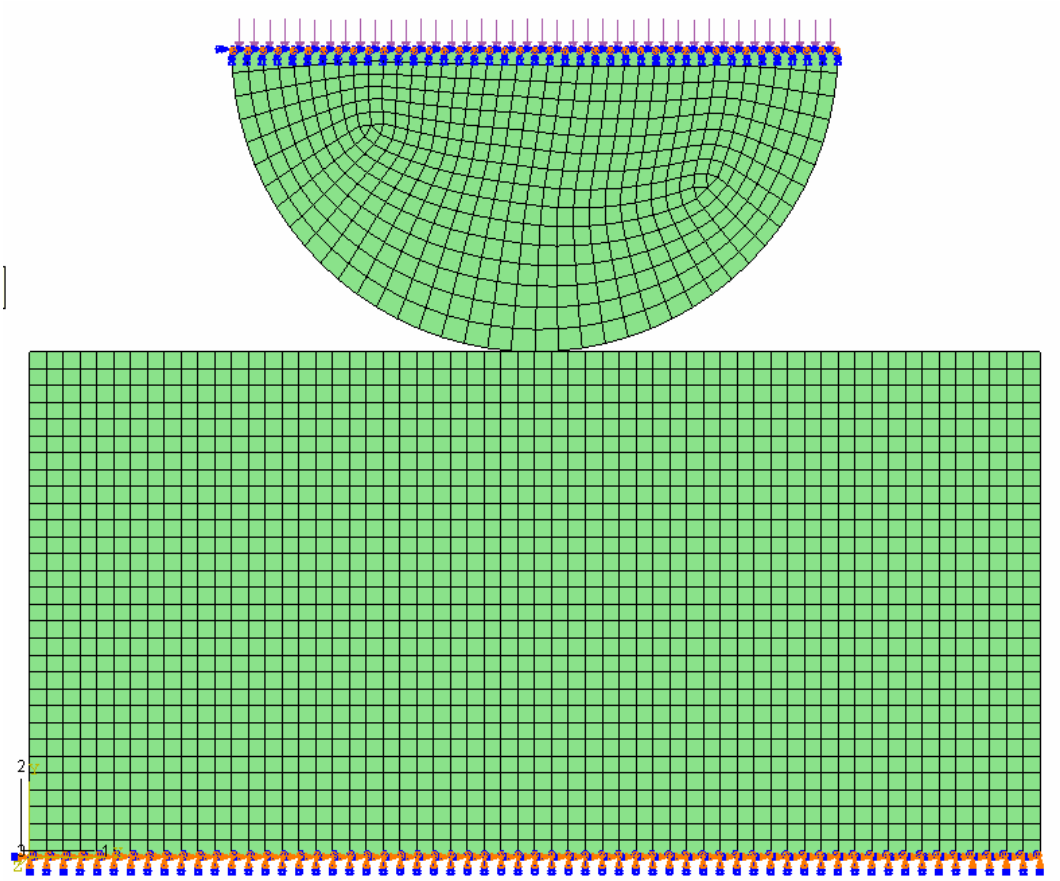

Figure 20: Loading applied on the top face of the slider

The contact pressure was found by dividing the contact force by the contact area. It was found to be 51.71 MPa. Since the hard hat transmits the contact pressure to the fuzz button, this pressure is applied on the top face of the slider. This is shown in Figure 21. As the slider slides over the PCB, the pressure is continuously applied on the slider.

The slider slides over the PCB for a large number of cycles. At the start of the cycle, the slider is positioned at the centre of the PCB as shown in Figure 22

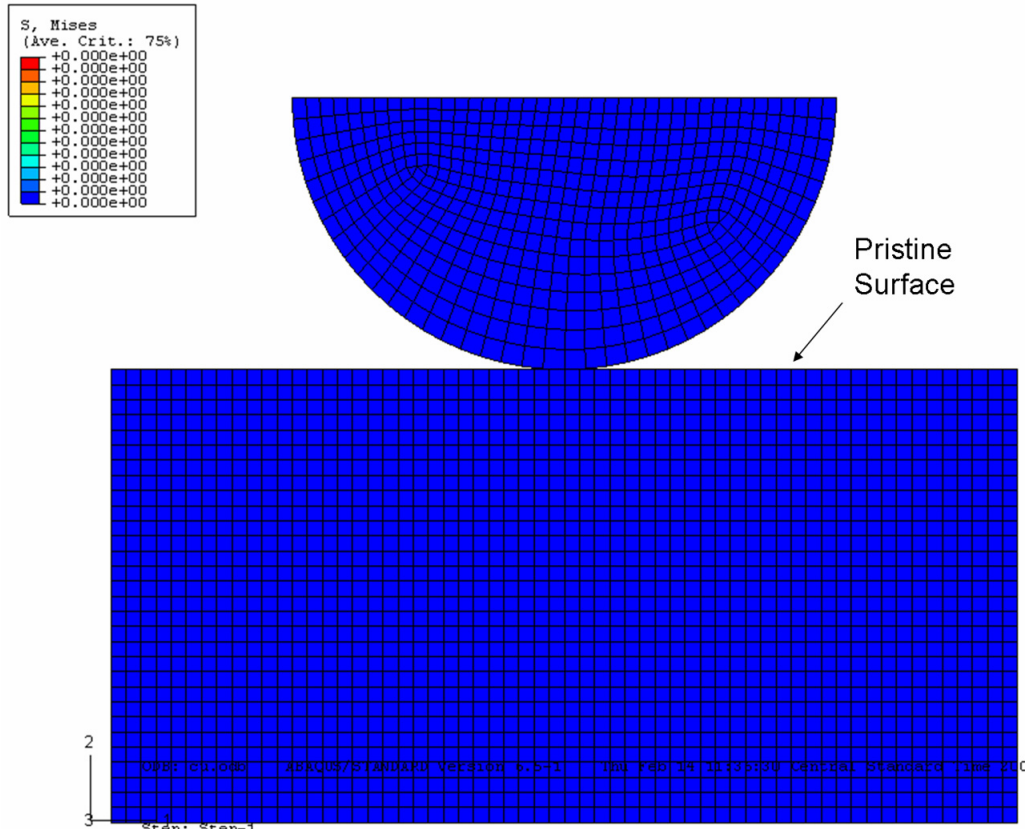

Figure 21: Von Mises stress plot with the position of the slider at the start of a cycle

After this, the slider moves to the right extreme of the PCB. The magnitude of this movement is decided by the size of the PCB. The dimensions of the PCB depend on the amplitude of vibration. Figure 23 shows the slider in the rightmost position. During this motion pressure is continuously applied on the top face of the slider. At this position one quarter of the cycle is complete.

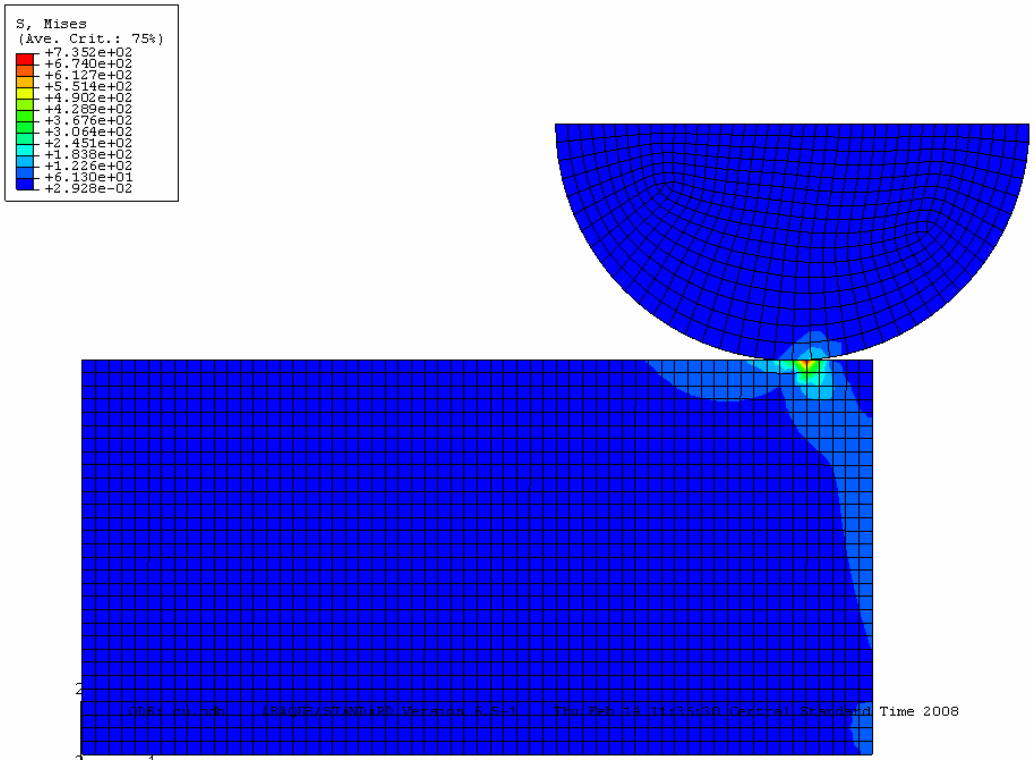

Figure 22: Von Mises stress at the rightmost position of slider after completion of one quarter of a cycle

At the position shown in Figure 23 the slider reverses direction and heads back towards the central position. Once it reaches the centre, one half of the cycle gets completed. The slider continues to move leftward till it reaches the position shown in Figure 24. This position marks the completion of 3/4th of the cycle.

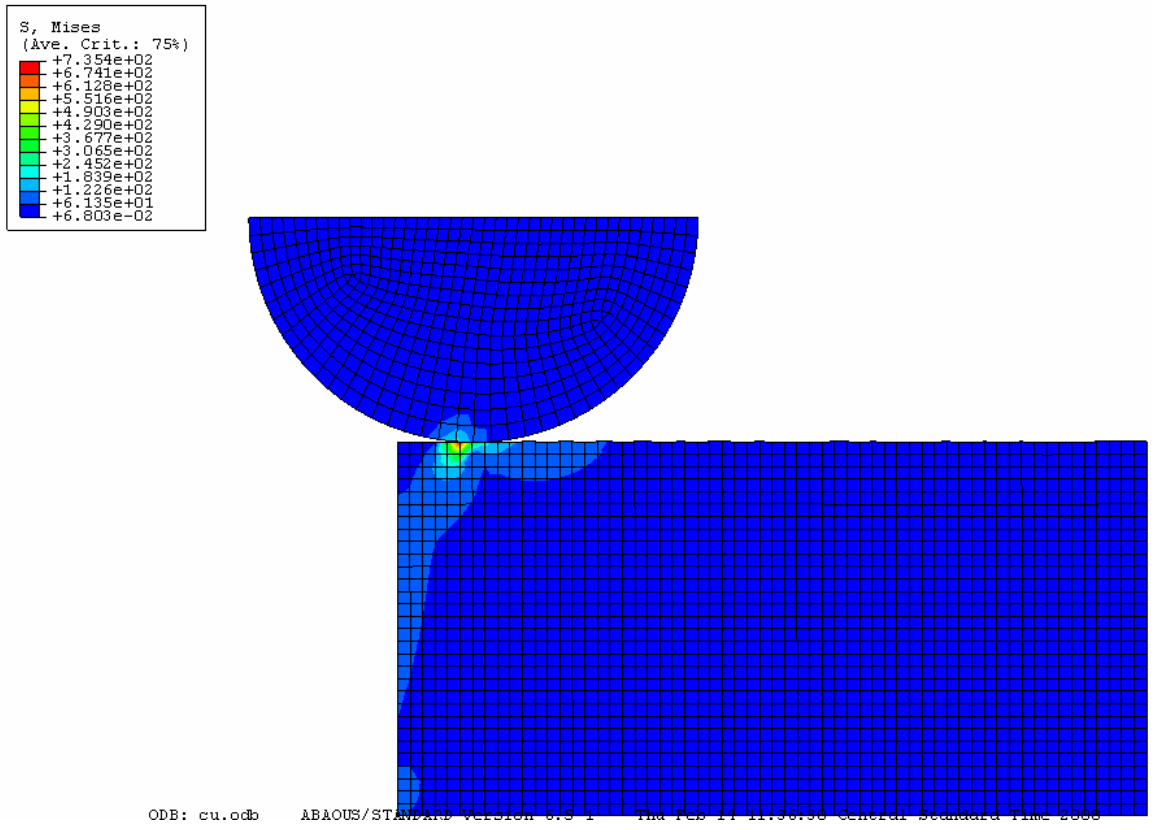

Figure 23: Von Mises stress at the leftmost position of the slider after completion of 3/4th of the cycle

During this entire motion pressure is applied on the top face of the slider. As the slider moves from the rightmost position, shown in Figure 23 to the leftmost position, shown in Figure 24, the PCB surface gets damaged. These are the first signs of wear on the PCB surface. At this position, the slider reverses direction and heads back to the central position. This marks the completion of one cycle. The slider is allowed to slide over the PCB for several number of cycles. The PCB surface gets worn out which causes a change in the electrical resistance. This is shown in Figure 25. When the PCB surface gets worn, the surface elements get severely distorted. A method had to be devised to

remesh these elements in order for the simulation to continue running for a large number of cycles. Adaptive meshing has been used to remesh the elements of the PCB, so they would be able to show severe damage accumulation.

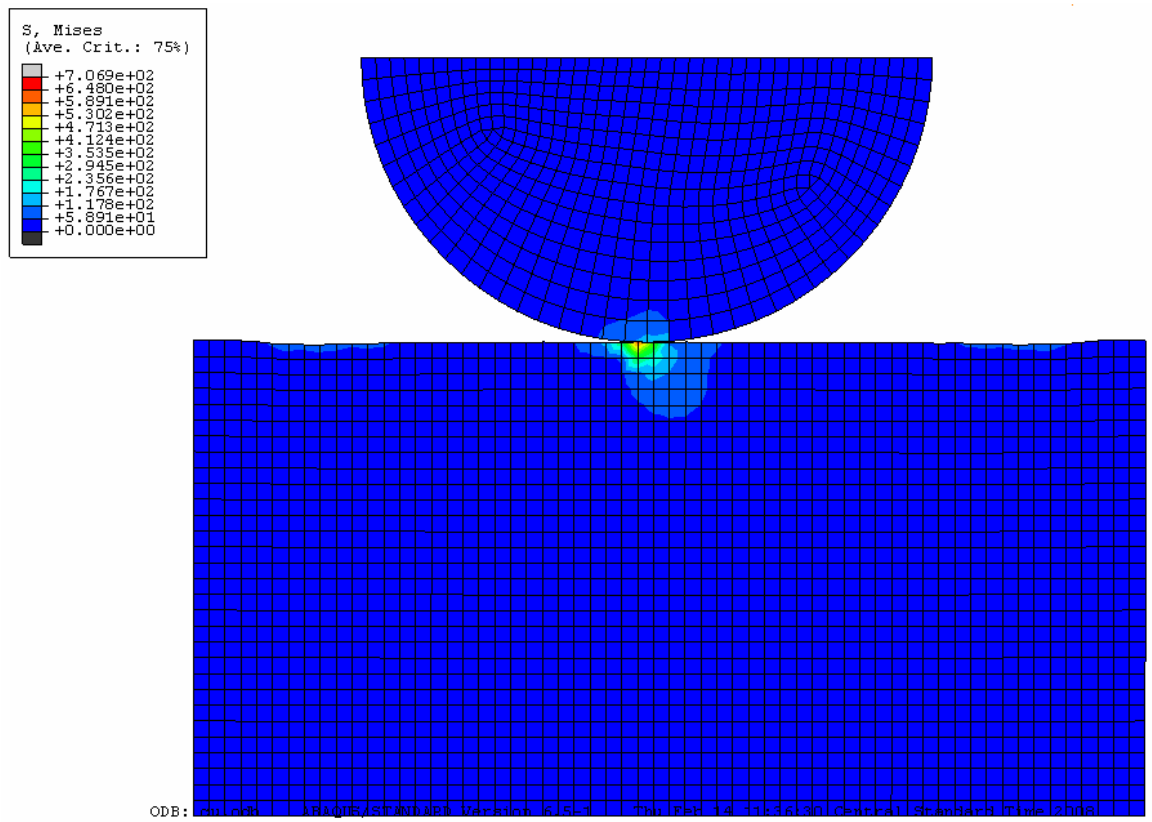

Figure 24: Von Mises stress on a worn out PCB surface after several cycles

4.3 Three Dimensional Model

Once the 2D model ran successfully a 3D model was constructed to simulate wear. Initially two different 3D models were constructed. In the first model the fuzz button wire, which represents the slider was modeled as a cylinder. The PCB, which represents the receptacle was modeled as a rectangular block. Since the bottom half of the

fuzz button wire contacts the PCB, the wire is modeled as a half cylinder. To simulate wear this entire half cylinder slides on the rectangular block.

Figure 25 shows the three dimensional model.

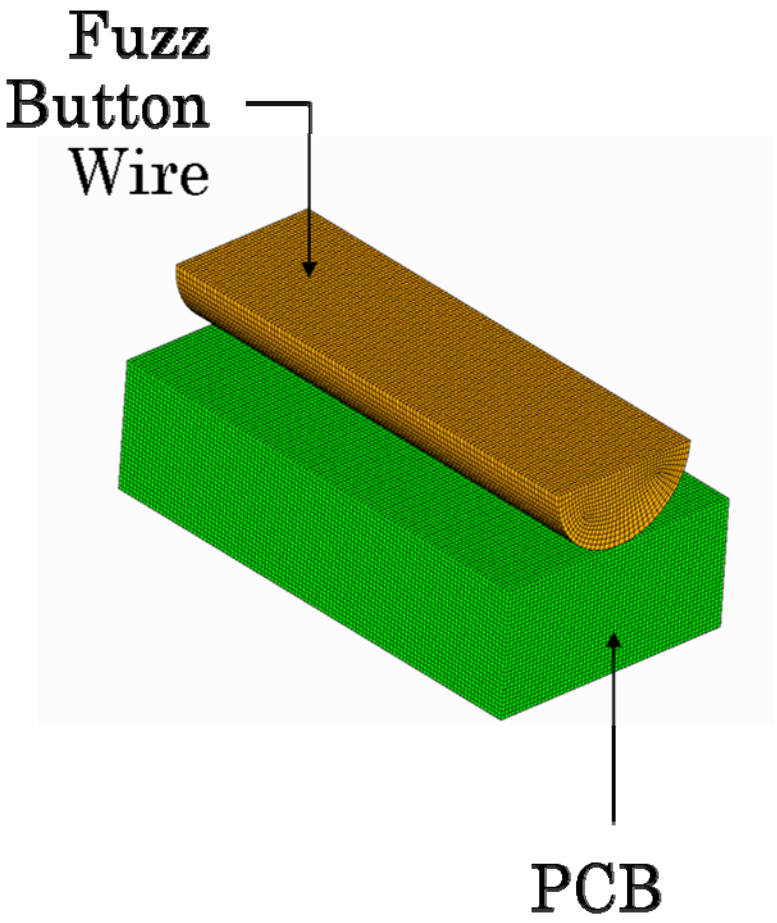

Figure 25: 3D model representing a fuzz button contact on a PCB

Initially the fuzz button was modeled as a half cylinder having length equal to the outer circumference of a fuzz button. This length was equal to 3.192mm. The PCB was modeled as a rectangular block whose length was equal to the length of the fuzz button. The cylinder oscillated over the rectangular block causing wear on the PCB surface. Due to the length of this model, it proved computationally expensive to simulate wear using this model. To reduce the running time of the simulation, the model was constructed with

a reduced length. The slider was modeled having a length equal to the width of two elements. This length was equal to 0.01058mm. The PCB was modeled with a length equal to the length of the slider. This model is shown in Figure 27

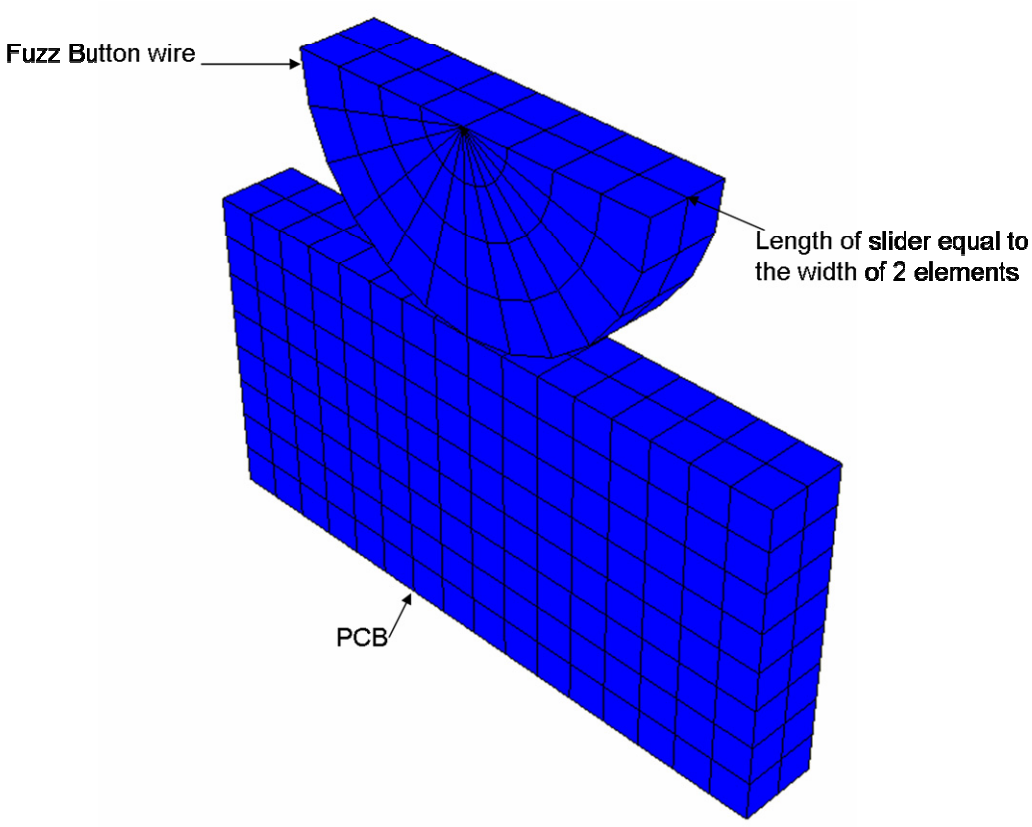

Figure 25: Modified 3D Model with model length equal to the width of two elements

The fuzz button is made of brick and pie elements, namely brick elements C3D8 and pie element C3D6. The pie element is a solid continuum element. It is a 6-node linear triangular prism. Figure 28 shows a pie element. The brick element is a solid continuum element. It is an 8 noded linear brick element. This element supports adaptive meshing. The PCB is entirely made up of brick elements. The 3D model aims to replicate the contact conditions in the actual contact.

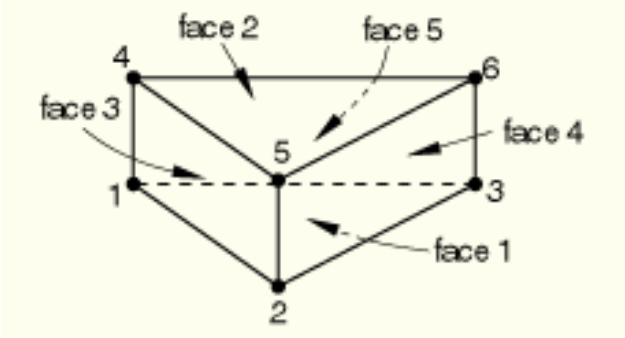

Figure 26: A standard 6 noded linear pie element

Load is applied on the top face of the fuzz button. The face numbers of brick are important while applying load on the top face of the fuzz button wire. The top face of the fuzz button is made of brick and pie elements. It is important to apply pressure on that face of the element which is pointing upwards to ensure correct load application

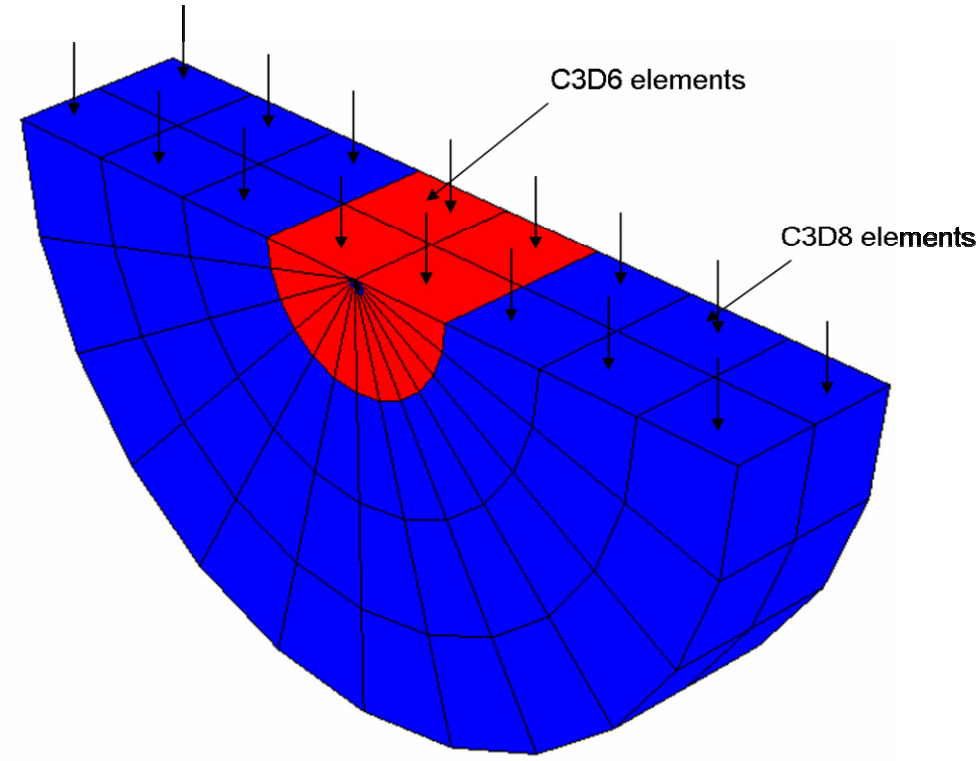

Figure 27: Top face of the slider consisting of two different elements on which load is applied

In the 3D model the slider oscillates over the receptacle and causes fretting wear. Figure 30 shows the neutral position of the slider with load applied.

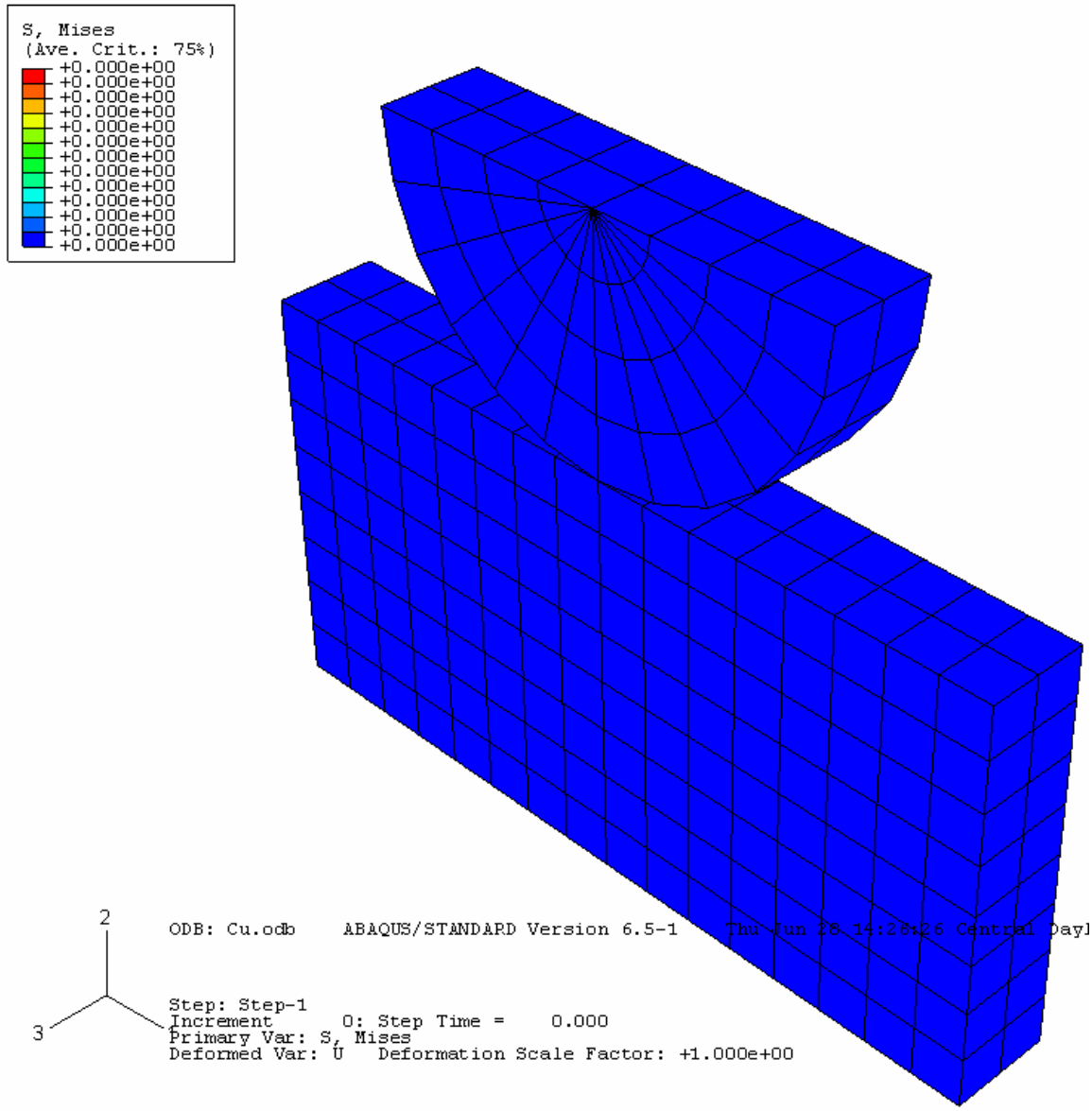

Figure 28: Von Mises stress shown at the neutral position of the slider at the start of a cycle

This happens at the beginning of each cycle. The slider first moves to the right extreme of the PCB with load applied on the top face of the slider. This position is shown in Figure 31

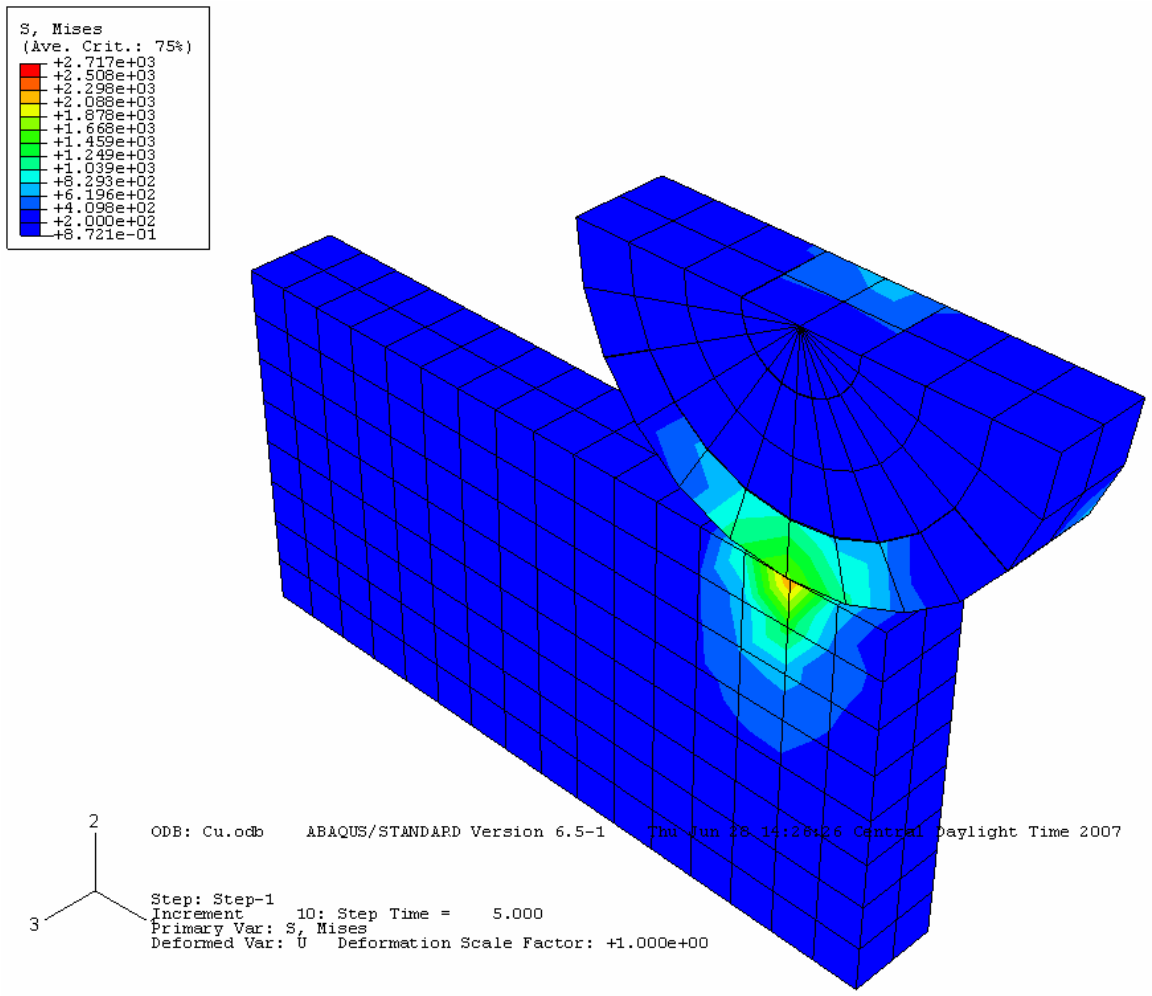

Figure 29: Von Mises stress plot with slider at the right extreme of the receptacle

After this, the slider reverses direction and travels to the left extreme of the PCB. This is shown in Figure 32. The slider again reverses direction and heads back to the neutral position. This marks the completion of one cycle.

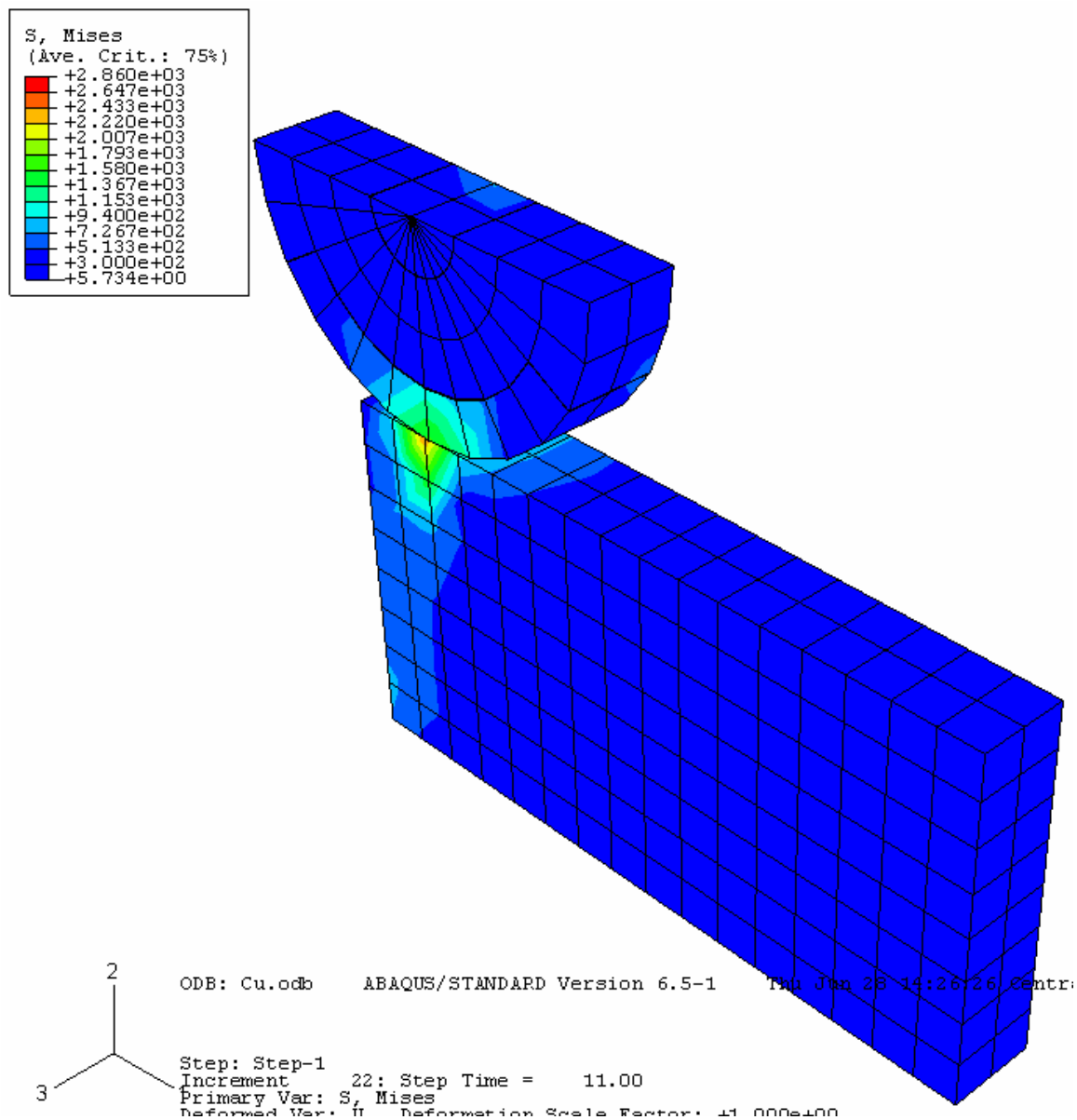

Figure 30: Von Mises stress plot with slider at the left extreme of the receptacle

After several such cycles the PCB surface gets worn out as shown in Figure 33. It is easy to understand the effects of fretting wear in electrical contacts by looking at the results of the 3D model. The worn out PCB surface may cause failure of the electrical contact resulting in failure of the component.

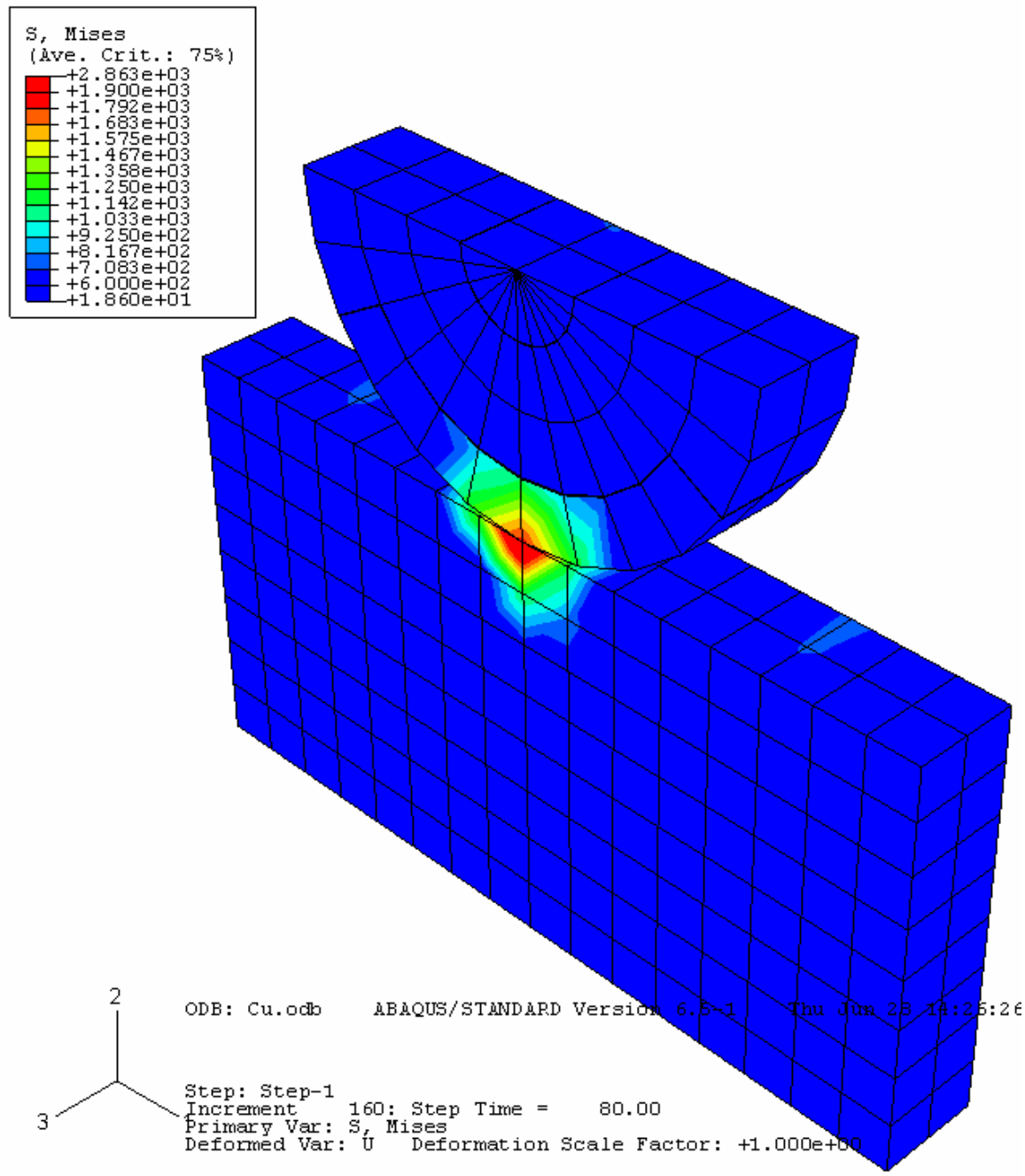

Figure 31: Von Mises stress plot of a worn out PCB after several wear cycles

A second three dimensional model was constructed. In this model the PCB was modeled as a circular ring with a rectangular cross-section. The fuzz button was modeled as a circular ring having a semi circular cross-section. The fuzz button was allowed to

oscillate on the PCB which resulted in ring on ring contact. This model is shown in Figure 34

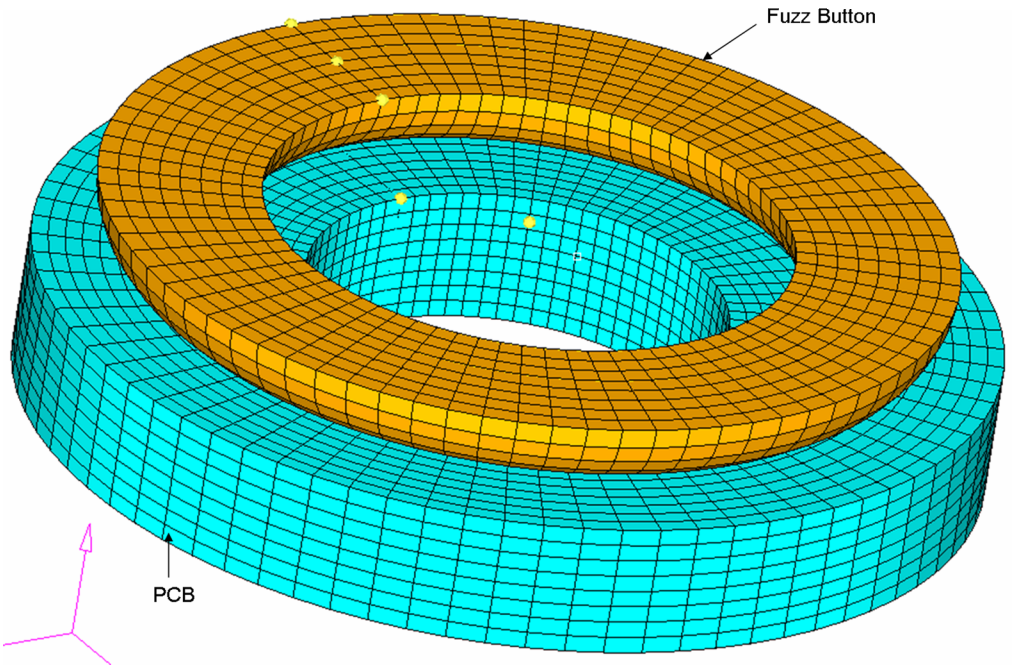

Figure 32: A circular model representing a fuzz button contacting a PCB

The bottom face of the PCB ring was fixed. It was found that modeling wear in this model was computationally expensive. To run the wear simulation using this model for a large number of cycles was computationally expensive and the running time was 7 days. As a result, this model was abandoned and the 3D model shown in Figure 33 was used.

4.4 Boundary Conditions

Boundary conditions were enforced both in the 2D model and 3D model to constrain the motion of the fuzz button wire. In the 2D model, the slider, which represents the fuzz button was constrained to move only in the X and Y direction. Only the displacement dof was active. Rotation of the slider about the X and Y axis was not permitted. It was not allowed to move in the Z direction or rotate about the Z direction. This was enforced using the command *BOUNDARY in the input file. The command used was,

***BOUNDARY**

slidertopsurfnodes, 3, 6

A nodeset 'slidertopsurfnodes' is defined which contains all the nodes on the top surface of the slider. In Abaqus each number corresponds to a specific dof. This is shown in Table 3. The number 3 defines the first dof constrained. The number 6 defines the last dof constrained. This meant that dof 3,4,5 and 6 are constrained.

No.	Degrees of freedom corresponding to that number
1	X Displacement
2	Y Displacement
3	Z Displacement
4	Rotation about the x-axis, in radians
5	Rotation about the y-axis, in radians
6	Rotation about the z-axis, in radians

Table 3: Numbers corresponding to dof used in Abaqus

Once the motion of the slider was constrained it was necessary to fix the position of the PCB, which acts as the receptacle. This was achieved by using the command *BOUNDARY in the inp file. The command used was,

***BOUNDARY**

PCBbotnodes, ENCASTRE

A nodeset PCBbotnodes was defined which contained all the nodes on the bottom face of the PCB. The ENCASTRE command makes dof 1 to 6 zero i.e. all dof are zero. The PCB is not allowed to displace or rotate in any direction. All the Boundary Conditions applied to the slider and the receptacle are shown in Figure 35

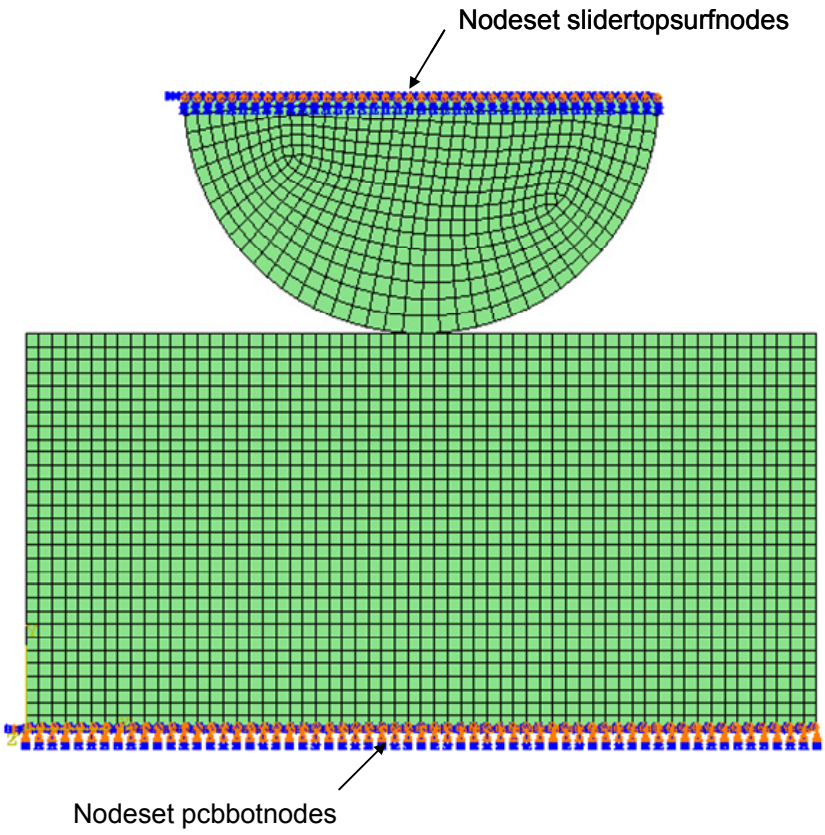

Figure 33: 2D contact model with applied constraints

In case of the 3D model similar boundary conditions are enforced. The slider is constrained to displace only in the X and Y directions. All rotational degrees of freedom are constrained. This was enforced by using the command *BOUNDARY. The command used was,

***BOUNDARY**

topnodes,3,6

A nodeset topnodes is defined which contains all the nodes on the top surface of the slider. The numbers 3, 6 indicate that dof from 3 to 6 are constrained. In ABAQUS each number stands for a specific dof. This list is given in Table 3. The receptacle, which represents the PCB needs to be fixed i.e. all dof's must be constrained. This is achieved by using the command ENCASTRE. ENCASTRE makes dof 1 through 6 zero. As a result of this all displacement dof and all rotational dof are zero. The command used was,

***BOUNDARY**

_PickedSet16,ENCASTRE

_PickedSet16 is a nodeset which contains all the node on the bottom surface of the PCB. The fixed receptacle is shown in Figure 36

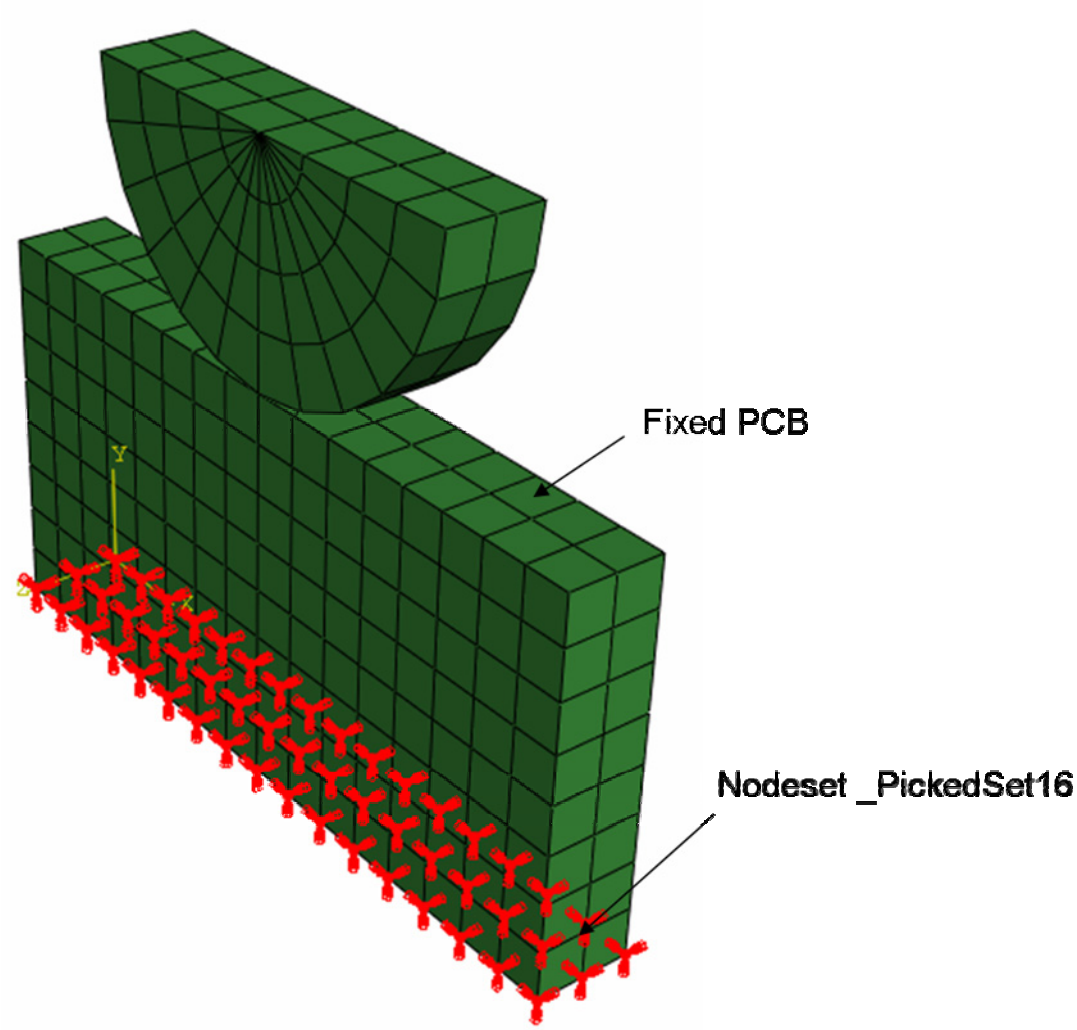

Figure 34: 3D model with a fully constrained receptacle

The receptacle is fully constrained using the command ENCASTRE. The PCB is fixed as the fuzz button oscillates on the PCB. The slider is allowed to slide in the X and Y directions. Displacement degree of freedom in the z direction and all rotational degrees of freedoms are constrained. This is shown in Figure 37

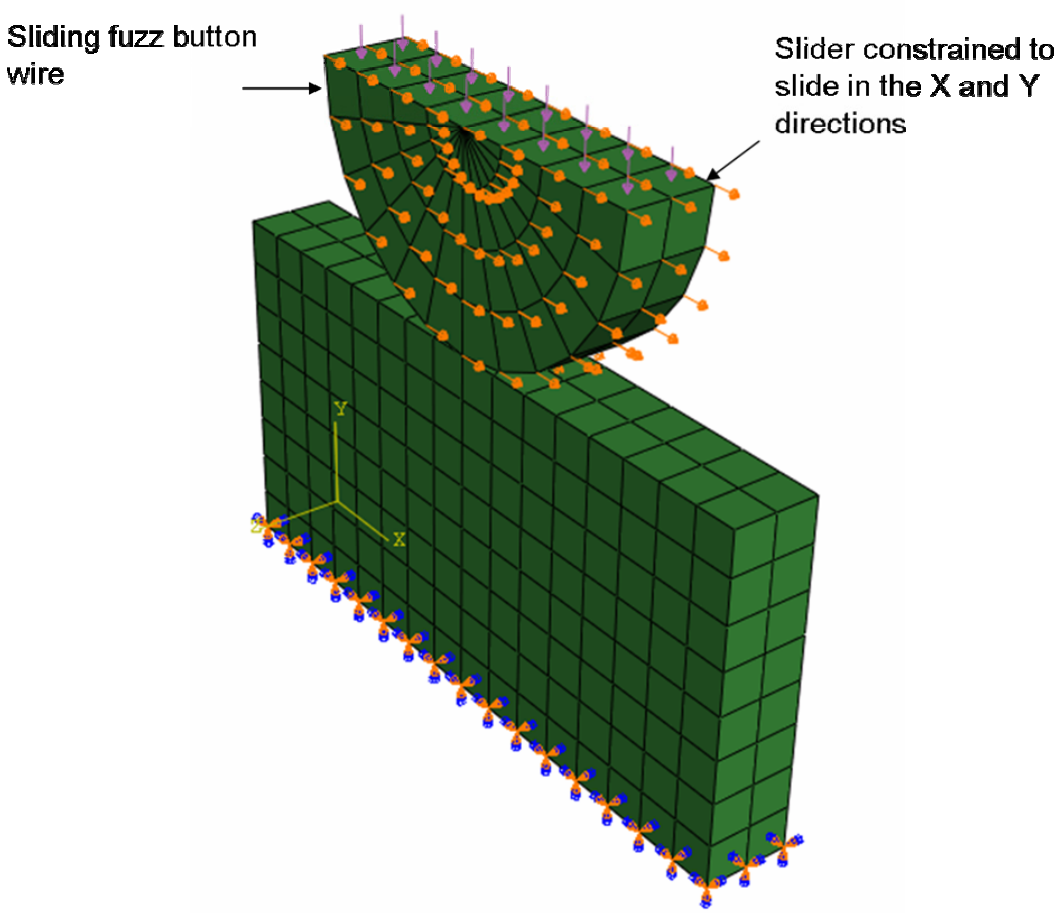

Figure 35: 3D Model with a partially constrained slider

As the slider slides on the receptacle, load is applied on the top face of the slider. The loaded slider is shown in Figure 38. The top face of the slider consists of brick and pie elements. While applying load it is important to ensure that load is applied on the correct element face. This element face number may vary depending on the orientation of the element. This is done by picking the faces of the elements manually in ABAQUS. Figure 38 shows the slider with the load applied.

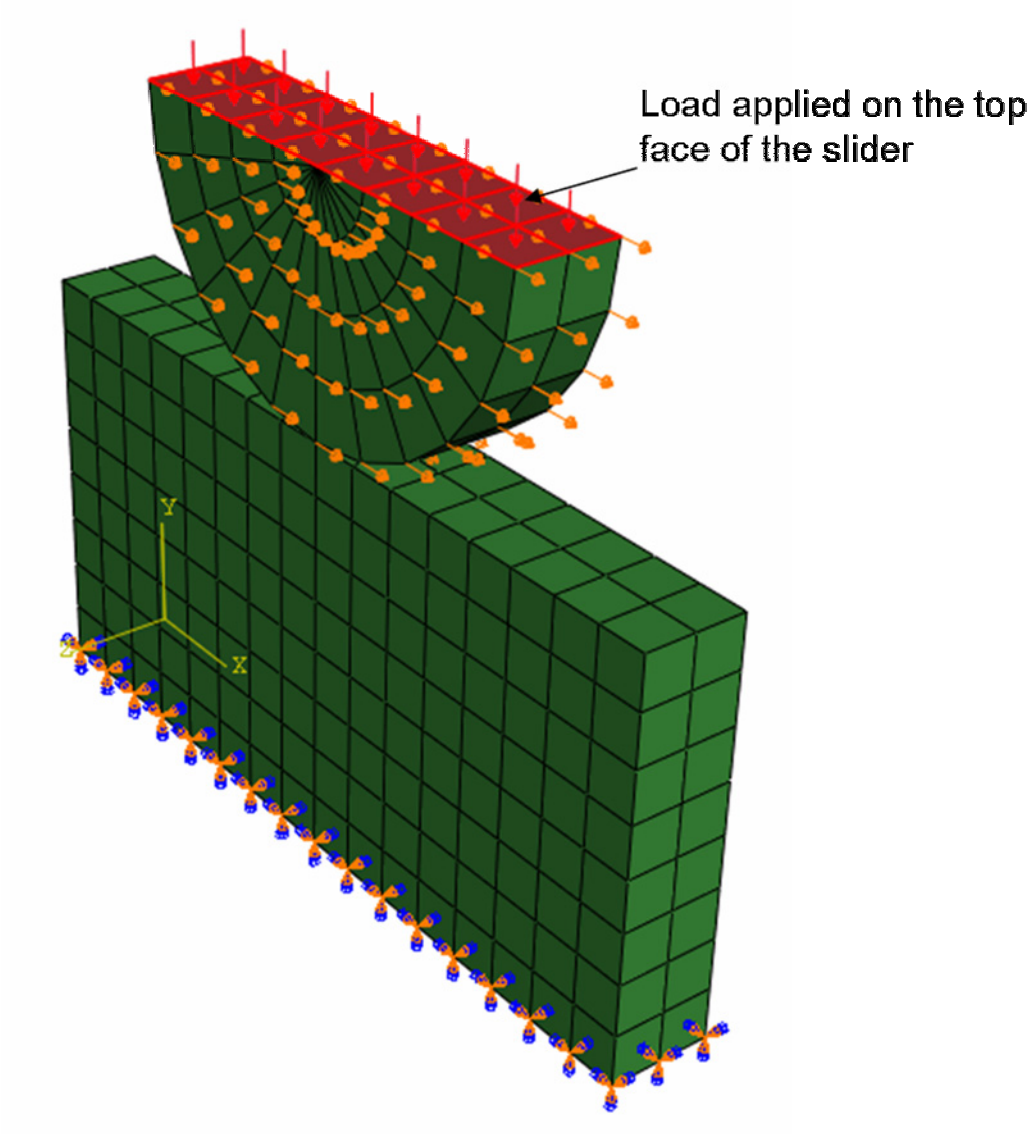

Figure 36: 3D Model with pressure load applied on the top face of the slider

CHAPTER 5

IMPLEMENTATION OF THE WEAR LAW IN THE FINITE ELEMENT MODEL

Archard's model predicts wear with a sufficient degree of accuracy while predicting mild wear in metal contacts. Archard's model has been used by Molinari [2000], Podra [1999], Cantizano [2002], Agelet [1999], Hegadekatte [2005] to predict wear. Archard's wear law has been used in the model to predict wear. Archard's wear model is given by,

$$\frac{V}{A*s} = \frac{k}{H} * \frac{F}{A}$$

This law can also be expressed in terms of wear depth as,

$$h = \frac{k}{H} * s * P \qquad (21)$$

h is the wear depth

k is Archard's wear coefficient

H is the hardness of the softer material

s is the sliding distance

P is the contact pressure.

Archard's wear coefficient has been interpreted in various ways. It is the fraction of asperities yielding wear particles, ratio of volume worn to volume deformed, a factor inversely proportional to critical number of load cycles, number of repeated asperity

encounters for producing ruptures, as a factor reflecting the inefficiencies associated with the various processes involved in generating wear particles. [Rigney 1994]

This wear law is integrated in the model in the form of wear rate. Both sides of Equation 21 are divided by time.

$$\frac{h}{t} = \frac{k}{H} * \frac{s}{t} * P \qquad (22)$$

The left hand side of the equation is the wear-rate h/t. s/t is the sliding velocity. This equation has been used in this model.

5.1 User subroutine UMESHMOTION

User subroutine UMESHMOTION is used in ABAQUS. The wear model is integrated in this user subroutine. UMESHMOTION is used to define the motion of nodes in an adaptive mesh domain. The magnitude of movement of these nodes is controlled by the wear law. UMESHMOTION is a fortran subroutine. The subroutine used in this work is presented here. Different parts of the code have been explained.

```
SUBROUTINE UMESHMOTION (UREF,ULOCAL,NODE,NNDOF,
    $  LNODETYPE,ALOCAL,NDIM,TIME,DTIME,PNEWDT,
    $  KSTEP,KINC,KMESHSWEEP,JMATYP,JGVBLOCK)
```

All the words present inside the brackets are variables. They can be classified into three types depending on their function, variables which have to be defined, variables that can be updated and variables that are passed in for information.

UREF

This is the value of the user specified velocity provided as part of the adaptive mesh constraint definition. This value is updated based on any amplitude definitions used with the adaptive mesh constraint.

ULOCAL

ULOCAL contains components of the mesh displacement or velocity of the adaptive mesh constraint node, described in the coordinate system ALOCAL. ULOCAL will be passed into the routine as values determined by the mesh smoothing algorithm. In this model ULOCAL contains components of the nodal velocity. This value of nodal velocity is controlled by the wear-rate.

NODE

NODE contains the node numbers which are passed in UMESHMOTION from ABAQUS

NNDOF

NNDOF determines the number of degrees of freedom at each node

LNODETYPE

LNODETYPE defines the node type flag. Nodes are classified depending on their position, constraints and their grouping into master or slave nodes. Table 4 shows all node types with their explanation.

Node type	Function
LNODETYPE=1	This indicates that the node is on the interior of the adaptive mesh region.
LNODETYPE=2	This indicates that the node is involved in a tied constraint
LNODETYPE=3	This indicates that the node is at the

	corner of the boundary of an adaptive mesh region
LNODETYPE=4	This indicates that the node lies on the edge of a boundary of an adaptive mesh region
LNODETYPE=5	This indicates that the node lies on a flat surface on a boundary of the adaptive mesh region.
LNODETYPE=6	This indicates that the node participates in a constraint as a master node.
LNODETYPE=7	This indicates that the node participates in a constraint as a slave node.

Table 4: Classification of nodes in UMESHMOTION

The different nodetypes present in this model are shown in Figure 39

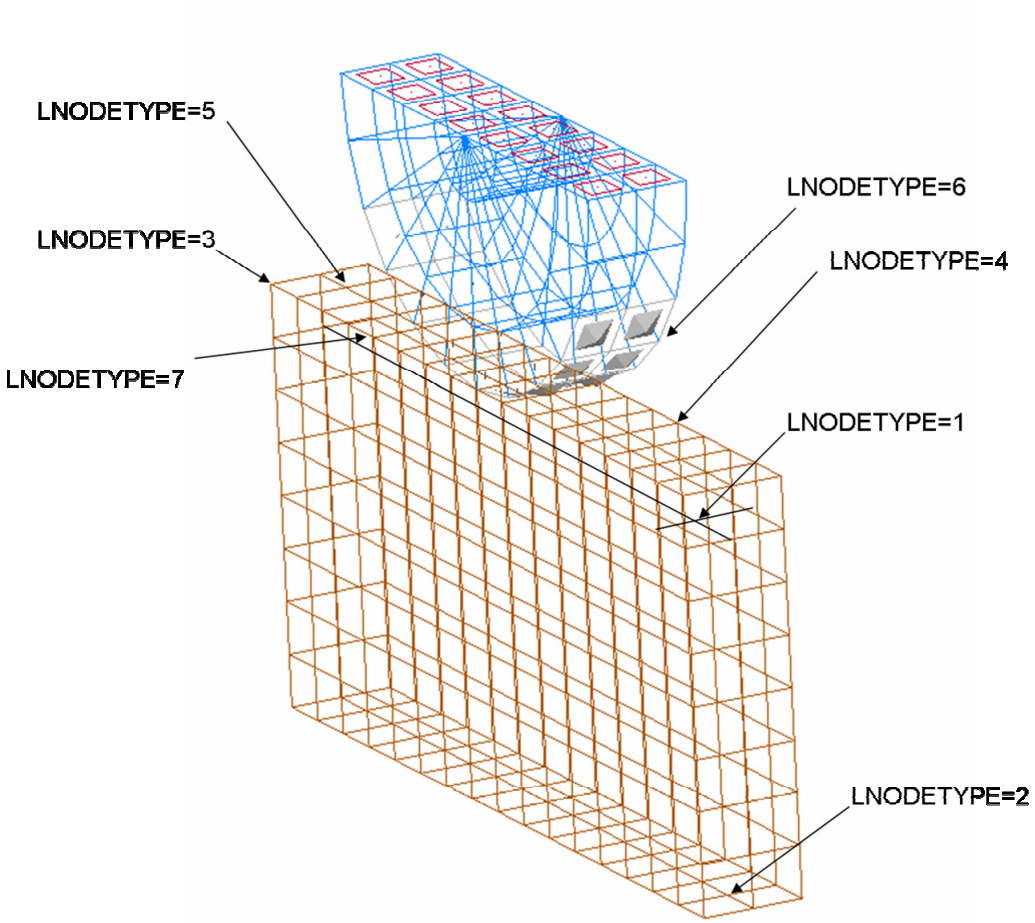

Figure 37: Node types used in the model

NDIM

NDIM is equal to the number of coordinate dimensions

ALOCAL

ALOCAL is defined as the local coordinate system aligned with the tangent to the adaptive mesh domain at the node. If the node is on the interior of the adaptive mesh domain, ALOCAL is set to the identity matrix. In case of the 2D model, NDIM=2, the 2-direction is normal to the surface. Wear occurs along this direction. Figure 40 shows the wear direction in the 2D model and 3D model. The nodes are moved in the direction shown in Figure 40 to simulate wear. The magnitude of motion is determined from

ULOCAL. In case of the 3D model, NDIM=3, the 2-direction also lies in the plane of a flat surface or is arbitrary if the node is on an edge. When NDIM=3 the 3-direction is normal to the surface. Wear occurs along this direction.

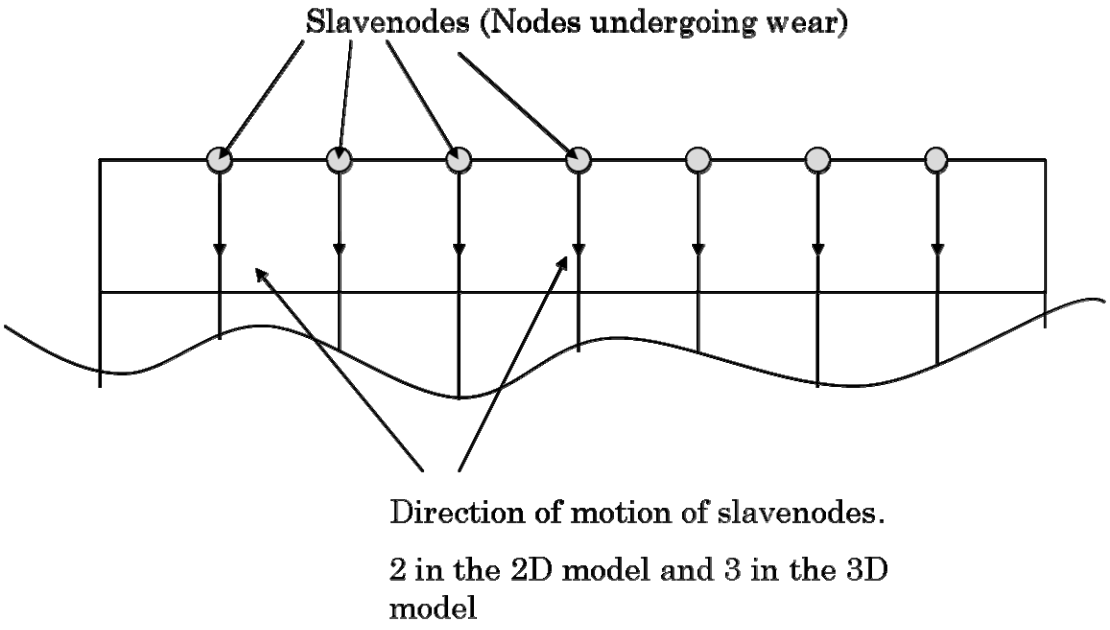

Figure 38: Direction of motion of nodes which undergo wear

TIME

TIME indicates the current value of the timestep

DTIME

DTIME indicates the time increment used in the code. This is defined in *STATIC in the input file

KSTEP

Each simulation is divided into steps. KSTEP defines which Step number is progressing in the simulation.

KINC

KINC indicates the Increment number.

KMESHSWEEP

KMESHSWEEP indicates the mesh sweep number

JMATYP

JMATYP is the variable that must be passed into the GETVRMAVGATNODE utility routine to access local results at the node

JGVBLOCK

JGVBLOCK is the variable that must be passed into the GETVRN, GETNODETOELEMCONN, and GETVRMAVGATNODE utility routines to access local results at the node.

PNEWDT

PNEWDT is the ratio of suggested new time increment to the time increment currently being used

5.2 Defining model properties and slider sliding frequency

All material properties are defined in the input file. Steel on steel contact is modeled in both 2D and 3D model. Material properties for steel are entered in the input file using '*MATERIAL'. This option is used to indicate the start of a material definition. The slider is made of steel. The code used in the input file is defined here,

**MATERIAL, NAME=fuzzbutton,*

**DENSITY*

7.85E-09

**ELASTIC, TYPE = ISOTROPIC*

200000.0 ,0.29

The first line defines the name under which the material properties defined will be stored. NAME is a required parameter and its set equal to a label, in this case, fuzzbutton, that will be used to refer to the material in element property options. The slider is made of steel. *DENSITY assigns the density to the material. The slider is assigned a density of 7.85E-09 tonnes/mm^3. The material is assumed to be isotropic. This is defined in *ELASTIC. *ELASTIC is used to define linear elastic modules. The modulus of elasticity of steel is defined as 200000 MPa. The Poisson's ratio is defined as 0.29. Using *MATERIAL the material properties of the receptacle which represents the PCB are also defined. The slider needs to contact the receptacle. A surface to surface contact is defined in the model. Initially a surface is defined on the slider using the *SURFACE command. *SURFACE is used to define surfaces for contact simulations. The command is defined as,

**SURFACE, NAME = SURFACE2, TYPE = ELEMENT*

slidersurface

The NAME parameter is set equal to a label that will be used to refer to that surface, in this case, SURFACE2. Set TYPE=ELEMENT defines a free surface automatically for the elements specified. It can also be used to define a surface on the elements by using element face identifiers. An element number or element set name is specified as the first entry of each data line. In this model an element set slidersurface is defined which contains all the elements which make up the slider surface. A second surface is defined which represents the top face of the PCB.

**SURFACE, NAME = SURFACE1, TYPE = NODE*

PCB, 1

TYPE=NODE defines a surface by specifying a list of nodes or node set labels. In this model a node set PCB is defined at the top face of the receptacle. The surface formed from the node set PCB is called SURFACE1. The contacting surfaces SURFACE1 and SURFACE2 are shown in Figure 41

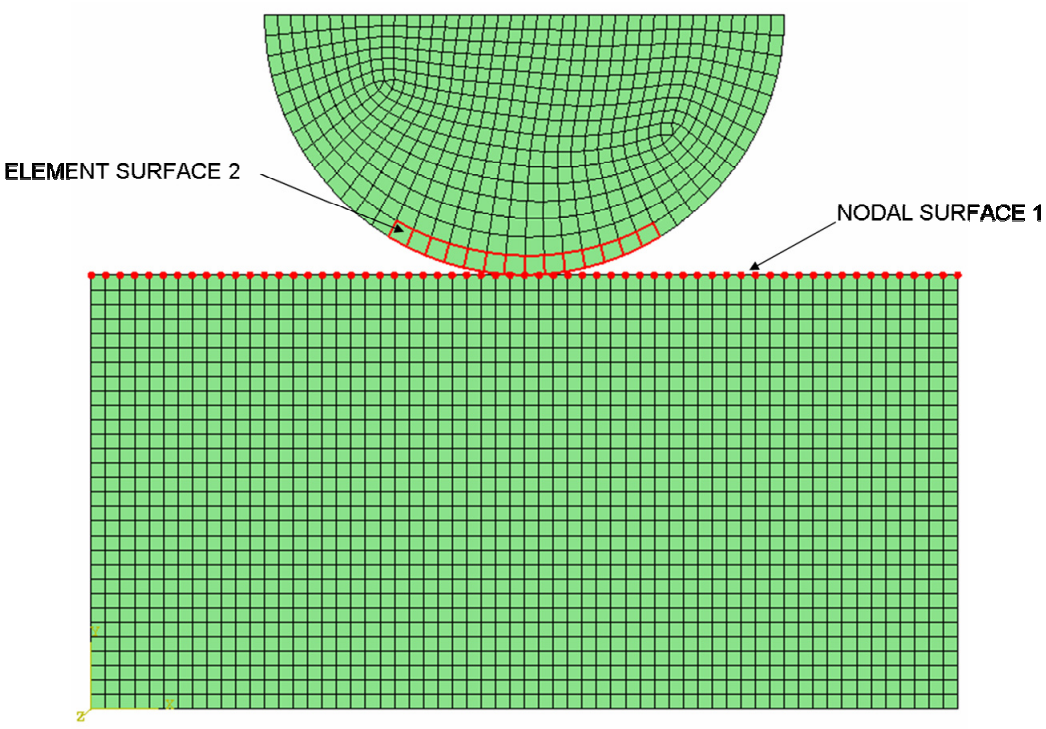

Figure 39: Contacting surfaces used in the 2D contact model

A third surface called slidertopsurface is defined.

**SURFACE, NAME = SLIDERTOPSURFACE, TYPE = ELEMENT*

slidertopsurfelem_s2,S2

slidertopsurfelem_s3,S3

This surface consists of two element sets. The first element set slidertopsurfelem_s2 consists of elements with their face 2 pointing upwards. The second element set slidertopsurfelem_s3 consists of elements with their face 3 pointing upwards. When slidertopsurface is defined, all the top element faces are selected. S2 represents face 2 of all elements in element set slidertopsurfelem_s2. S3 represents face 3 of all elements in the element set slidertopsurfelem_s3. Both these element sets are shown in Figure 42

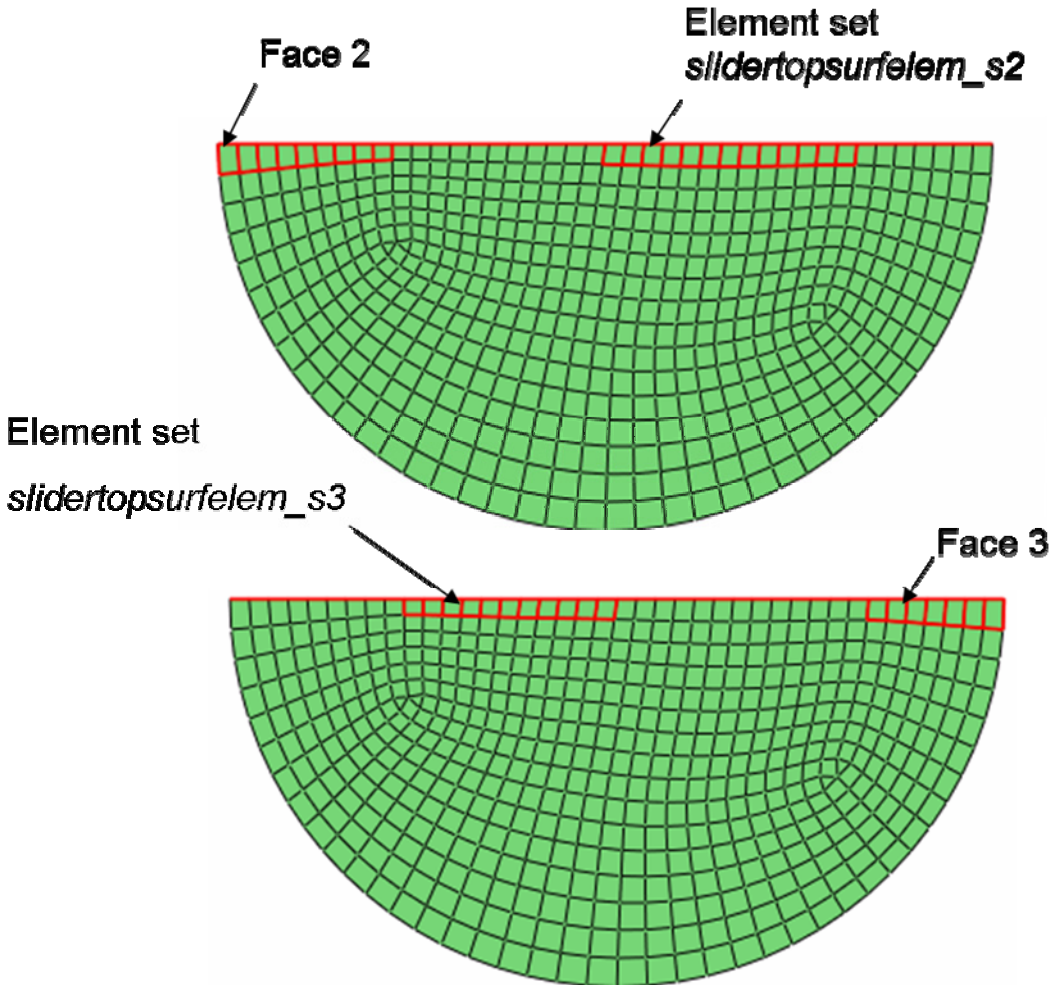

Figure 40: Elements with different orientations make up the loading surface

.

After defining the surfaces, a contact is defined between the two contacting surfaces. This is done using the command *CONTACT PAIR. This option is used to define pairs of surfaces or pairs of node sets and surfaces that may contact or interact with each other during the analysis. The code used is,

**CONTACT PAIR, INTERACTION=fricbhv*

SURFACE1, SURFACE2

Contact is defined using the node to surface discretization. With node-to-surface discretization the contact conditions are established such that each slave node on one side of a contact interface effectively interacts with a point of projection on the master surface on the opposite side of the contact interface. Thus, each contact condition involves a single slave node and a group of nearby master nodes from which values are interpolated to the projection point. This is shown in Figure 43

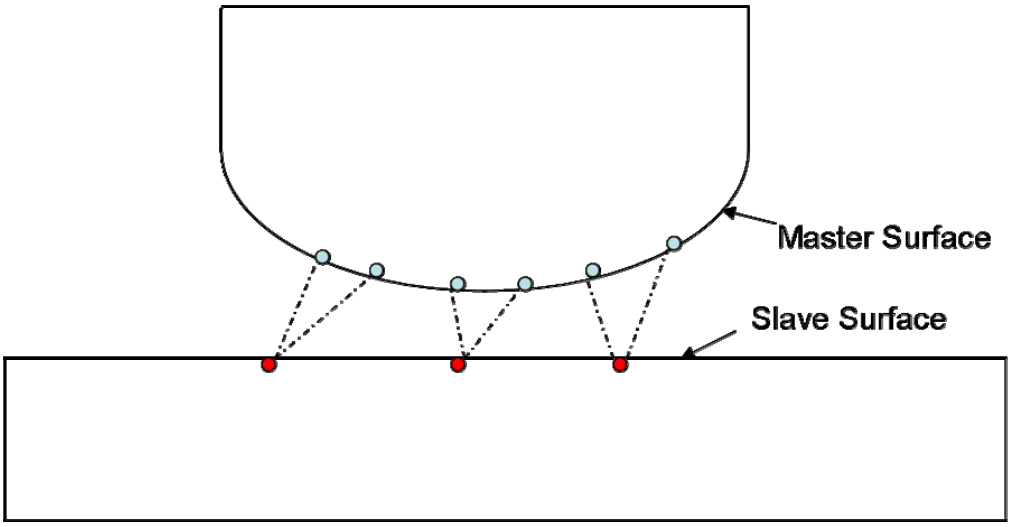

Figure 41: Node to Surface contact discretization

In node-to-surface discretization, the slave nodes are constrained not to penetrate into the master surface. The contact discretization is based on the normal of the master surface.

Abaqus enforces the following rules related to the assignment of master and slave surfaces. A rigid element based surface must always be a master surface. A node based surface can act only as a slave surface. Slave surfaces must be attached to deformable bodies.

The INTERACTION parameter is set equal to the name of the *SURFACE INTERACTION property definition associated with the contact pair being defined. The first surface in the data line, *SURFACE1* is the slave surface. The second surface in the data line, *SURFACE2* is the master surface The master surface is an elemental surface and the slave surface is a nodal surface. Since the PCB is supposed to wear off, it is assigned to be the slave surface. *SURFACE INTERACTION is an option used to create a surface interaction property definition. The surface interaction properties will govern any contact interactions that reference this surface interaction. The command used is,

**SURFACE INTERACTION, NAME = fricbhv*

The parameter NAME is set equal to a label that will be used to refer to this surface interaction property. This label is used in the INTERACTION parameter of the *CONTACT PAIR option. The *FRICTION option is used to introduce friction properties into a mechanical surface interaction model governing the interaction of contact surfaces. The command used is,

**FRICTION*

0.78

A friction coefficient value of 0.78 is used for steel on steel contact. [Dieter 1986]. *FRICTION must be used in conjunction with *SURFACE INTERACTION.

*CONTACT DAMPING is used to define viscous damping between two interacting surfaces. It must be used in conjunction with *SURFACE INTERACTION. The command used is,

**CONTACT DAMPING, DEFINITION = DAMPING COEFFICIENT*

1.0 ,0.02

In the data line, 1 refers to the damping coefficient and 0.02 is the clearance at which the damping coefficient is zero. In Abaqus this option is primarily used to damp relative motions of the surfaces during approach or separation. *STEP option is used to begin each step definition. It must be followed by a procedure definition option. The command used is,

**STEP,nlgeom=yes ,inc=1000000*

NLGEOM=YES is used to indicate that geometric nonlinearity should be accounted for during the stress analysis. Once the NLGEOM option has been switched on, it will be active during all subsequent steps in the analysis. INC is set equal to the maximum number of increments in a step. This value is only an upper bound. In this analysis the maximum number of increments is set at 1000000. *STATIC is used to indicate that the step should be analyzed as a static load step. The command used is,

**STATIC*

0.5 ,3 ,0.000000005 ,0.5

In the data line the first number, 0.5 indicates the initial time increment. This value will be modified as required if the automatic time stepping scheme is used. In this model automatic time stepping scheme is used. The second number, 3 indicates the time period of the step. If this entry is zero or is not specified, a default value of 1 is assumed. The

third number, 0.00000005 is the minimum time increment allowed in the automatic time increment. .

If ABAQUS finds it needs a smaller time increment than this value, the analysis is terminated. A small value is selected for the minimum time increment to prevent the analysis from getting terminated.

If this entry is zero, a default value of the smaller of the suggested initial time increment or 10^{-5} times the total time period is assumed. The last number, 0.5 is the maximum time increment allowed. A very high value of increment may cause the simulation to fail.

*CONTACT CONTROLS is used to provide additional optional solution controls for models involving contact between bodies. The command used is,

**CONTACT CONTROLS, FRICTION ONSET = IMMEDIATE*

FRICTION ONSET=IMMEDIATE instructs the model to include friction in the increment when contact occurs. *DSLOAD is used to prescribe distributed surface loading. A surface slidertopsurface is defined at the top face of the slider. This surface is shown in Figure 44. *DSLOAD is used to apply pressure on this surface

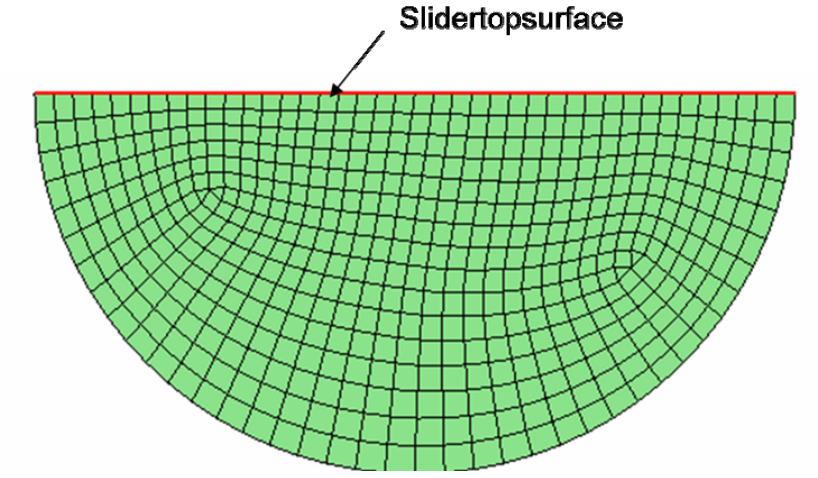

Figure 42: Loading surface Slidertopsurface

**Dsload*

SLIDERTOPSURFACE,P ,10

The first word in the data line represents the surface on which load is applied, in this case it is slidertopsurface. P stands for the distributed load type label, in this case pressure. The number 10 stands for the actual magnitude of the pressure applied.

*AMPLITUDE allows arbitrary time or frequency variations of load, displacement, and other prescribed variable magnitudes to be given throughout a step. The command used is,

**AMPLITUDE, NAME =ampl, TIME=STEP TIME, DEFINITION = PERIODIC,*

VALUE=ABSOLUTE

1,0.3927,0,0

0,0.033868,

The parameter NAME is set equal to a label that will be used to refer to the amplitude curve. For *AMPLITUDE an amplitude curve must be defined. In this model an amplitude curve is defined which allows arbitrary time variations of displacement to be given throughout a step. The amplitude curve is defined as a mathematical function as a sinusoidal variation. TIME=STEP TIME indicates that the amplitude is defined as a function of step time. VALUE=ABSOLUTE indicates that absolute magnitudes are specified for the amplitude curve. DEFINITION=PERIODIC defines the amplitude as a fourier series,

$$a = A_0 + \sum_{n=1}^{N}\left[A_n \cos n\omega(t - t_0) + B_n \sin n\omega(t - t_0)\right] \qquad (23)$$

In this model, only the first term of the fourier series is used, i.e. till n=1. The amplitude equation becomes,

$$a = A_0 + A_1 \cos\omega(t - t_0) + B_1 \sin\omega(t - t_0)$$

In the first data line, the first number corresponds to the number of terms in the fourier series, in this case it's one. The second term is the circular frequency in radians per time. In this model a time period of 16 has been used. The circular frequency is equal to $2\pi/16$. The third number corresponds to the starting time, t_0. In this case, t_0=0. The fourth number corresponds to the constant term in the Fourier series, A_0. In this case A_0=0. In the second data line, the first number, A_1 corresponds to the first coefficient of the cosine terms. In this model, a sinusoidal motion is required; therefore the cosine term is eliminated by making A_1 equal to zero. B_1 corresponds to the first coefficient of the sine terms. In this model it is equal to the max amplitude of oscillation from the central position. The max amplitude of oscillation from the central position is equal to 0.033868.

The *BOUNDARY option is used to prescribe boundary conditions at nodes. In this model *BOUNDARY controls the movement of the entire slider. The AMPLITUDE parameter is set equal to the name of the amplitude curve defining the magnitude of the prescribed boundary conditions. The amplitude curve is defined in *AMPLITUDE. The TYPE parameter is used in a stress or displacement analysis to specify whether the magnitude is in the form of a displacement history, a velocity history, or an acceleration history. In this case the magnitude is specified in the form of a displacement history. The command used is,

**BOUNDARY, AMPLITUDE = ampl, TYPE=DISPLACEMENT*
slider,1,1,0.033868

The first entry in the data line indicates the node number or node set label. Here slider refers to the nodeset which contains all the nodes which make up the slider. This is shown in Figure 45

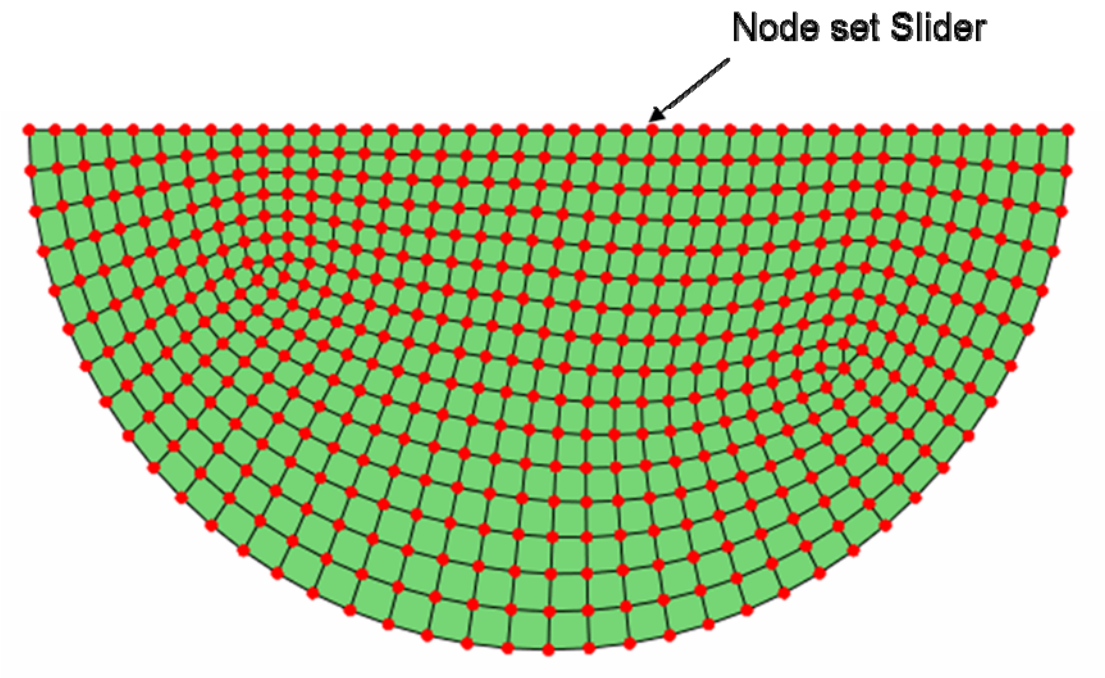

Figure 43: The node set Slider used in *BOUNDARY to define slider displacement

The second entry in the data line refers to the first degree of freedom constrained. The number 1 indicates that the slider is constrained to move in the x direction according to the boundary conditions specified. The third entry refers to the last degree of freedom constrained. In this model the last degree of constrained is still 1. The third entry refers to the actual magnitude of the displacement. In this case it is 0.033868mm which is equal to the max amplitude of oscillation from the central position.

The *ADAPTIVE MESH option is used to define an adaptive mesh domain and to specify the frequency and intensity of adaptive meshing for that domain. The parameter

ELSET is set equal to the name of the element set that contains all the solid elements in the adaptive mesh domain. In this model the element set PCBcontact contains all the elements of the receptacle. The command used is,

**ADAPTIVE MESH, ELSET=PCBcontact, FREQ=1,MESH=5*

The FREQ parameter is set equal to the frequency in increments at which adaptive meshing is to be performed. In this model the frequency is set to 1. This ensures that adaptive meshing is performed frequently and the model geometry is updated as the simulation progresses. The MESH parameter is set equal to the number of mesh sweeps to be performed in each adaptive mesh increment. This number cannot be set to a very high number as this would increase computation time. Only those elements which are specified in the adaptive mesh domain will be allowed to undergo wear. Figure 46 shows the adaptive mesh domain used in this model defined by element set PCB contact

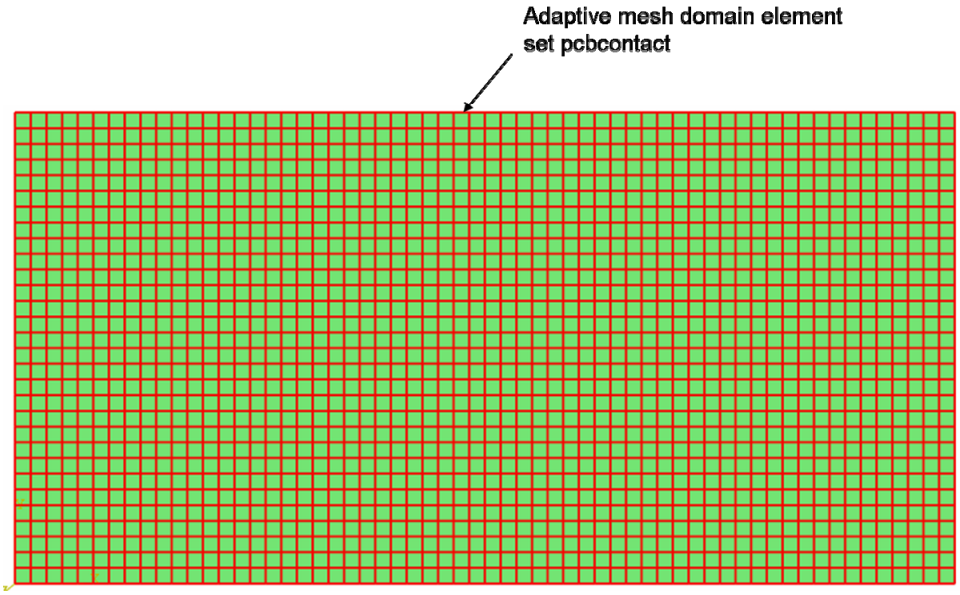

Figure 44: Adaptive mesh domain defined using element set PCBcontact

Arbitrary lagrangian-eulerian (ALE) formulation with adaptive meshing has been used to simulate wear in this model. ALE has been used to combine the advantages of the

Lagrangian and Eulerian descriptions. In the Lagrangian representation of the model, each individual node of the computational mesh follows the associated material particle during motion. This is shown in Figure 47. The material points represented by triangles overlap the nodes. The particle motion solid lines overlap the mesh dashed lines.

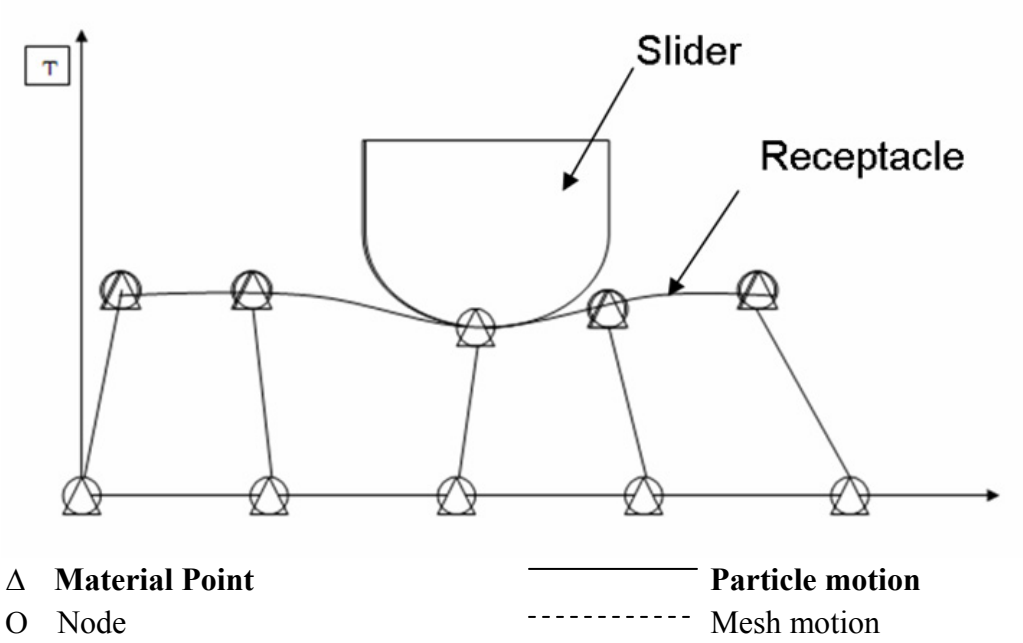

Figure 45: Lagrangian description of sliding contact

Lagrangian description allows an easy tracking of free surfaces and interfaces between different materials. It also facilitates the treatment of materials with history dependent constitutive relations. The main disadvantage of the Lagrangian representation of the model is its inability to follow large distortions of the computational domain without frequent re-meshing.

In the Eulerian description the computational mesh is fixed and the continuum moves with respect to the grid. As a result of this the interface definition and resolution of details are sacrificed. Figure 48 shows the Eulerian description of the sliding contact.

The mesh is shown in Figure 48 using the dotted lines and nodes. Although the material deforms the mesh remains fixed.

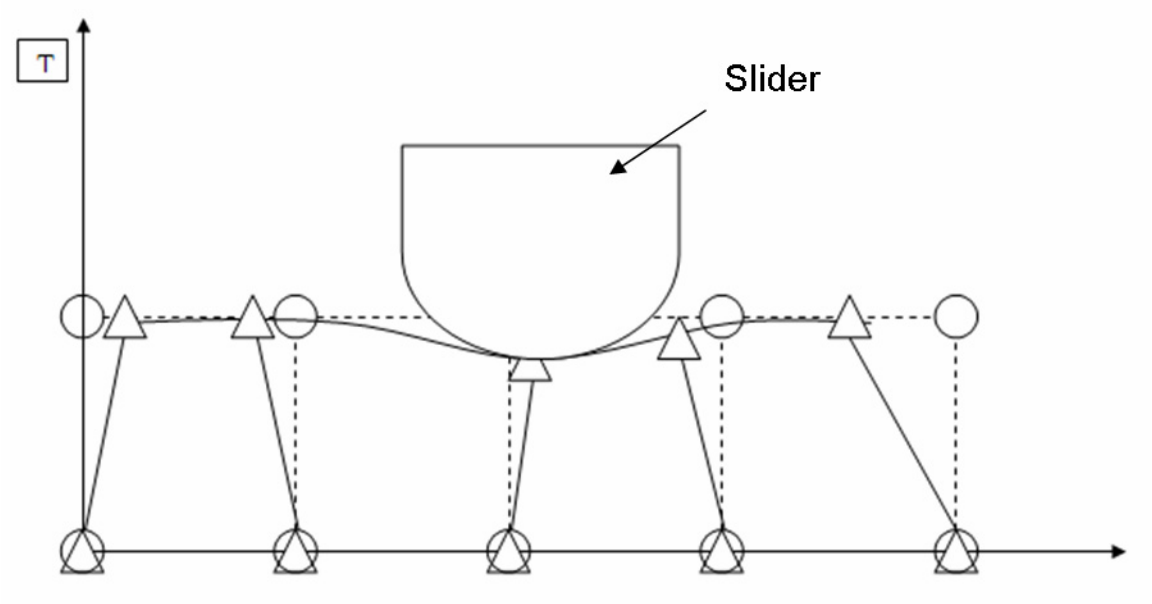

Δ **Material Point** ——— **Particle motion**
O Node - - - - - - - - - - Mesh motion

Figure 46: Eulerian Description of the sliding contact

ALE to a certain extent succeeds in combining the best features of both the Lagrangian and Eulerian approaches. In the ALE description, the nodes of the computational mesh may be moved with the continuum in normal Lagrangian fashion, or be held fixed in Eulerian manner, or, as shown in be moved in some arbitrarily specified way. Because of this freedom in moving the computational mesh offered by the ALE description, greater distortions of the continuum can be handled than would be allowed by a purely Lagrangian method, with more resolution than that afforded by a purely Eulerian approach.

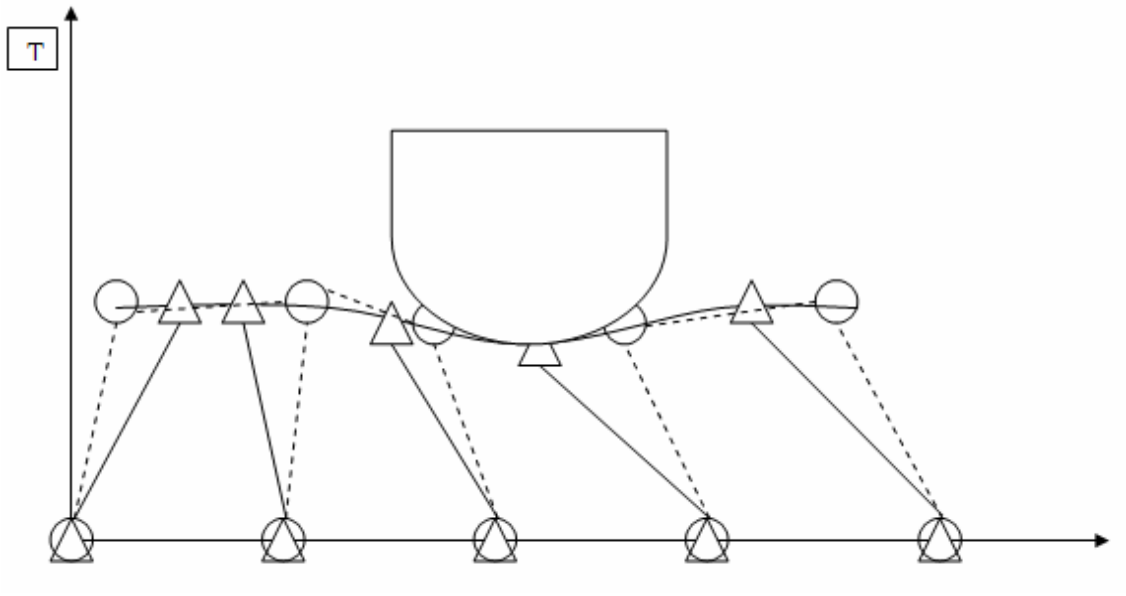

Figure 47: Arbitrary Lagrangian-Eulerian description of the model

The use of ALE in the sliding contact wear problem, allows a topologically similar mesh throughout the analysis, without creating or destroying elements, allowing the mesh to move independently of the material. ALE adaptive meshing enables the maintenance of a high quality mesh throughout an analysis, even when the contact surface gets worn out, by allowing the contact surface mesh to move independently of the material. The topology and connectivity of the elements is not altered. Abaqus applies the user-specified spatial mesh constraint without regard to the current material displacement at the node. This behavior allows a mesh displacement that differs from the current material displacement at the free surface of the adaptive mesh domain, effectively eroding material at the boundary. The analysis is performed in two steps, a Lagrangian step followed by an Eulerian step. In the Lagrangian step, material displacements are

obtained by solving the governing equations. In the Eulerian step, a new mesh is generated for the deformed domain. All kinematic and static variables are then transferred from the distorted mesh to the new mesh. The mapping is performed using a first order expansion of Taylor's series, which is also known as the convection equation in the ALE literature.

The *ADAPTIVE MESH CONSTRAINT option is used to prescribe independent mesh motion for nodes in an adaptive mesh domain or to define nodes that must follow the material. It can be used only in conjunction with the *ADAPTIVE MESH option. The command used is,

**ADAPTIVE MESH CONSTRAINT, CONSTRAINT TYPE=SPATIAL,*

TYPE=VELOCITY,USER

PCB,1,1,0.0004657

The parameter CONSTRAINT TYPE=SPATIAL is used to prescribe mesh motions that are independent of the underlying material. The parameter TYPE=VELOCITY is used to prescribe mesh velocity to the nodes in an adaptive mesh domain. The USER parameter is used if the mesh motion is to be defined in user subroutine UMESHMOTION. This parameter cannot be used when CONSTRAINT TYPE=LAGRANGIAN.

The first entry in the data line indicates the node number or node set label, in this case it is the node set PCB. The second entry indicates the first degree of freedom constrained. The third entry indicates the last degree of freedom constrained. The last entry indicates the actual magnitude of mesh motion. This command allows transfer of control from the input file to the fortran code written as a part of user subroutine UMESHMOTION.

5.3 Calculation of wear in user subroutine UMESHMOTION

In the fortran code, the first step is to define all the arrays which are going to be used in the code. This is done using the dimension statement. A DIMENSION statement is used to specify the symbolic names and dimension specifications of arrays. The form of a DIMENSION statement is:

DIMENSION a(d), b(e)

where each a(d) and b(e) are array declarators. Each symbolic name 'a' appearing in a DIMENSION statement declares 'a' to be an array in that program unit. 'd' and 'e' are dimension declarators. The code used is,

DIMENSION ULOCAL(NDIM),JELEMLIST(50)

DIMENSION ALOCAL(NDIM,),TIME(2)*

DIMENSION JMATYP(*),JGVBLOCK(*)

In this code, the line DIMENSION ULOCAL(NDIM) declares an array ULOCAL of length NDIM. In the 2D model, NDIM=2 and in case of the 3D model NDIM=3.

The CHARACTER type specification statement explicitly assigns the CHARACTER data type to symbolic names. The command used here is,

*CHARACTER*80 PARTNAME*

The name 'PARTNAME' is defined as a type character and as 80 characters long.

The arrays ARRAY and VEL are defined using the commands,

DIMENSION ARRAY(3)

DIMENSION VEL(6)

The array ‘ARRAY’ is used to store the nodal stress acting on the surface nodes of the receptacle. The array ‘VEL’ is used to store the sliding velocity of node 21, which is the bottom node of the slider. The position of this node is shown in

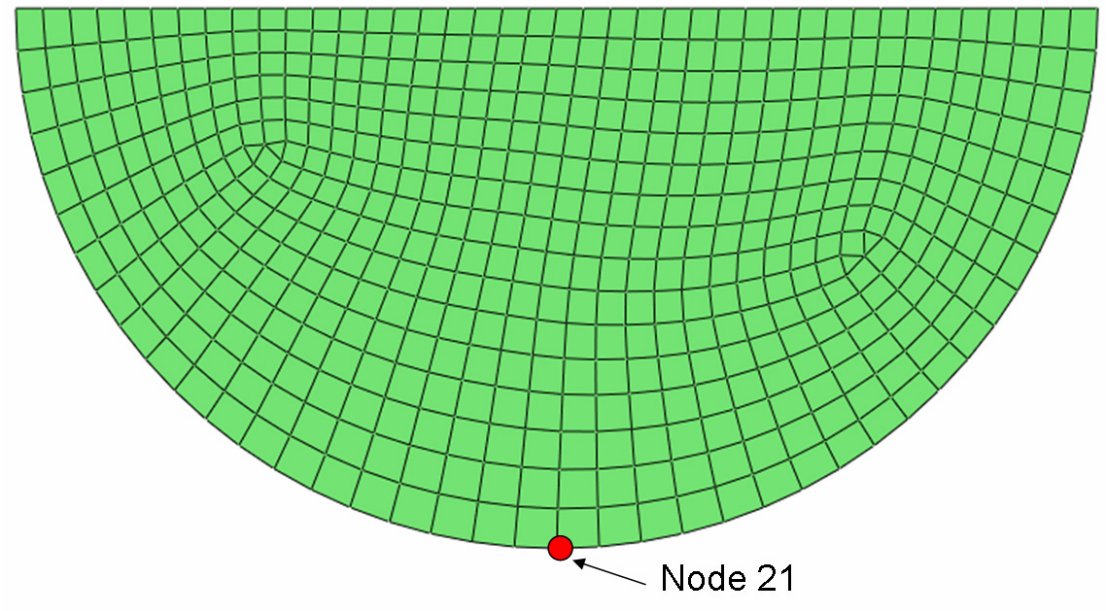

Figure 48: Nodal sliding velocity of Node 21 used to calculate wear

These values of pressures and velocities are used to calculate wear on the surface nodes. The PARAMETER statement is used to define constants which appear many times in a program. It is then often desirable to define them only once, in the beginning of the program. This is done using the PARAMETER statement. The command used is,

PARAMETER

CPRESS=0.0D0

VELOCITY=0.0D0

CPRESS is the pressure component of the array ‘ARRAY’. VELOCITY is the sliding velocity component of the array ‘VEL’. They are initially set to zero at the start of the program.

A nodeset ‘NODE’ is passed into the subroutine. This nodeset contains node 21 and all the surface nodes of the PCB which undergo wear. The IF-ELSE statement helps to differentiate node 21 from the other nodes. Nodal velocity of node 21 is required to calculate wear at the surface nodes shown in Figure 40. It is essential that velocity is extracted just at node 21. This is ensured using the if-then statement. The command used is,

IF (NODE==21) THEN

ULOCAL(NDIM)=0

When the node number is 21, there is no need to find out the mesh velocity in ULOCAL, since its not a part of the PCB and will not undergo wear. Therefore for node 21, ULOCAL(NDIM) is set to zero. The sliding velocity at node 21 is extracted using GETVRN. Utility routine GETVRN is called from user subroutine UMESHMOTION to access node point information. The command used is,

CALL GETVRN(NODE,'V',VEL,JRCD,JGVBLOCK,LTRN)

Node refers to the node number from which the node point information is extracted. ‘V’ is the output variable key selected from the table in Abaqus/Standard output variable identifiers of the Abaqus analysis user’s manual. The variable V includes all velocity components, including rotational velocities at nodes with rotational degrees of freedom. There are a total of 6 components, 3 translational and 3 rotational. Out of the 3 translational components only the first component which represents sliding along the X direction is required. VEL is a real array containing individual components of the output variable. JRCD is a return code which is returned as 0 when no error is present or 1 when there exists an output request error or all components of the output request are zero.

JGVBLOCK is a variable that must be passed into the GETVRN utility routine. LTRN is a variable indicating the coordinate system the nodal quantity is to be returned in. A value of zero specifies that the results are to be returned in the global coordinate system, regardless of any transformation applied at the node. A value of one specifies that the results are to be returned in the local transformed system. In this model all results are returned in the global coordinate system. Once the sliding velocity is obtained at node 21, the next step is to find the pressures at the surface nodes of the PCB. Pressure is not calculated at node 21 and this is ensured using the ELSE statement. The command used is,

ELSE

CALL GETPARTINFO(NODE,0,PARTNAME,LOCNUM,JRCD)

Getpartinfo is used to obtain part instance information from the global node number. NODE is the internal node number to be looked up. The second entry is JTYP, which is an integer flag indicating whether NODE is a node or element number. JTYP is set equal to 0 to look up a node number or 1 to look up an element number. PARTNAME is the name of the part instance that contains NODE. LOCNUM is the part-local node number corresponding to NODE. JRCD returns a code zero if there is an error and one if there's no error. Utility routine GETNODETOELEMCONN is called from user subroutine UMESHMOTION to retrieve a list of elements connected to a specified node. The code used is,

CALL GETNODETOELEMCONN(NODE,NELEMS,JELEMLIST,JELEMTYPE,

$ JRCD,JGVBLOCK)

NODE corresponds to the user node number, in this case, PCB. NELEMS is the maximum allowable length of JELEMLIST. JELEMLIST returns an array of element numbers for elements connected to NODE. The list will contain elements only in adaptive mesh domains active in the step as well as any contact elements associated with the domain. JELEMTYPE contains an array describing the element types for each element entry in JELEMLIST. The number 1 in the array indicates a solid element. The number 2 in the array indicates a contact element. . JRCD is a return code which is returned as 0 when no error is present or 1 when there exists an output request error or all components of the output request are zero. JGVBLOCK is a variable that must be passed into the GETNODETOELEMCONN utility routine. Contact pressure at each node is calculated using GETVRMAVGATNODE. Utility routine GETVRMAVGATNODE is called from user subroutine UMESHMOTION to access material integration point information averaged at a node. The results variables available from GETVRMAVGATNODE are nearly the same as those available from GETVRM. Since it will average results, GETVRMAVGATNODE will operate only on real valued results. The command used is,

CALL GETVRMAVGATNODE(NODE,'CSTRESS',ARRAY,JRCD,JELEMLIST,NELEMS,

$ JMATYP,JGVBLOCK)

NODE refers to the node number, in this case nodeset PCB, which contains all the nodes on the top face of the receptacle. Pressure is extracted from these nodes. The second input in the data line corresponds to the output variable key. This key is selected from the Abaqus/Standard output variable identifiers table. This key is listed in the output table as

being available for results file output at the element integration points. The key used in this model is 'CSTRESS'. This output variable CSTRESS contains three components, CPRESS which indicates the contact pressure, CSHEAR1 which indicates contact traction in the local 1 direction and CSHEAR2 which indicates contact traction in the local 2 direction. The third component is returned only in the 3D model. ARRAY is a real valued array containing individual components of the output variable. ARRAY contains 3 components, CPRESS, CSHEAR1 and CSHEAR2. JRCD is a return code which is returned as 0 when no error is present or 1 when there exists an output request error or all components of the output request are zero. JELEMLIST is an array of element numbers for elements connected to NODE for which you want material point quantities considered in the average result. Results from each element in the list that contain the node will be extrapolated to that node and averaged. JELEMLIST can be obtained from utility routine GETNODETOELEMCONN. NELEMS is the maximum allowable length of JELEMLIST. JMATYP and JGVBLOCK are variables that must be passed into the GETVRMAVGATNODE utility routine. An array CPRESS is defined. The first variable from ARRAY is stored in CPRESS. The command used is,

CPRESS = ARRAY(1)

The contact pressure on the nodes which are located on the top face of the PCB is stored in CPRESS. The sliding velocity of node 21 in the X1 direction, which is located on the slider, is used to calculate wear. Six components of velocity are stored in the array VEL. Out of these; just the 1st component is required. The command used is,

VELOCITY = VEL(1)

The sliding velocity of node 21 is stored in VELOCITY.

Once the sliding velocity and contact pressure are obtained, the wear rate is calculated using formula,

$$\frac{h}{t} = \frac{k}{H} * \frac{s}{t} * P \qquad (24)$$

s/t is the sliding velocity, P is the contact pressure, k is the Archard's coefficient, H is the hardness of the softer material and h/t is the wear rate. In this model the formula used varies with the contact system used. If a steel-on-steel contact system is used,

Archard's coefficient for steel is 0.0150 [Rabinowicz 1995]. Archard's coefficients for some common contact systems are given in Table 5

Contact System	Archard's coefficient
Cadmium on cadmium	0.0057
Zinc on zinc	0.0530
Silver on silver	0.0040
Copper on copper	0.0110
Platinum on platinum	0.0130
Mild steel on mild steel	0.0150
Stainless steel on stainless steel	0.0070
Cadmium on mild steel	0.00003
Copper on mild steel	0.0005
Mild steel on copper	0.00017

Table 5: Archard's Wear Coefficients Table [Rabinowicz 1995]

The value of Hardness used for steel is 424MPa. The formula used is,

*WEARRATE=0.000035377*VELOCITY*CPRESS*

If a copper-on-copper contact system is used, Archard's coefficient for copper is 0.0110. The hardness value used for copper is 427MPa. The formula used is,

*WEARRATE=0.000025761*VELOCITY*CPRESS*

Once the wear rate is calculated, the wear occurring at the nodes is calculated using the formula,

ULOCAL(NDIM)=ULOCAL(NDIM)-WEARRATE

ULOCAL contains components of the mesh velocity of the adaptive mesh constraint node. Wear rate is subtracted from ULOCAL to simulate ablation. The nodes undergoing wear move in a direction normal to the surface with a velocity equal to ULOCAL.

CHAPTER 6

MODEL PREDICTIONS AND MODEL VALIDATION

6.1 Model Predictions

The simulation was allowed to run for 2000 fretting cycles. Wear accrues on the contact surface of the connector with increase in fretting cycles. As the simulation progresses the nodes at the surface of the receptacle move in a direction shown in Figure 40. The velocity at which these nodes move is governed by the formula,

*WEARRATE=0.000025761*VELOCITY*CPRESS*

The wear rate is in turn governed by the VELOCITY and CPRESS. VELOCITY indicates the velocity of node 21. Node 21 is located on the bottom of the slider. Therefore VELOCITY indicates the velocity of the slider. The velocity of the slider is continuously varying. It's maximum at the central position and zero at the extremes, this is shown in Figure 51. As the surface of the PCB degrades, the contact pressure keeps varying. The contact pressure is continuously updated using CPRESS to maintain the accuracy of the results. All these factors result in an uneven wear rate

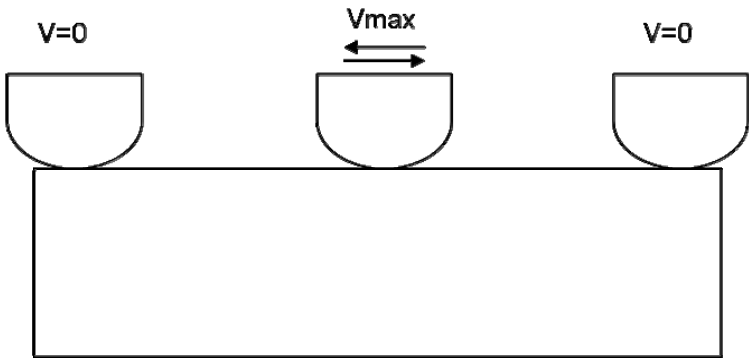

Figure 49: Velocity variation of the slider affecting wear rate

The accrued wear has been plotted versus fretting cycles as shown in Figure 52. 'S' is defined as the distance of nodes from the neutral position. Starting from the neutral position left side is negative and the right side is assigned positive values. Several such plots have been prepared to include nodes spanning across the top face of the receptacle. This plot is prepared by plotting the nodal displacement of a node, located on the top face of the PCB. As the number of fretting cycles increase, the node moves

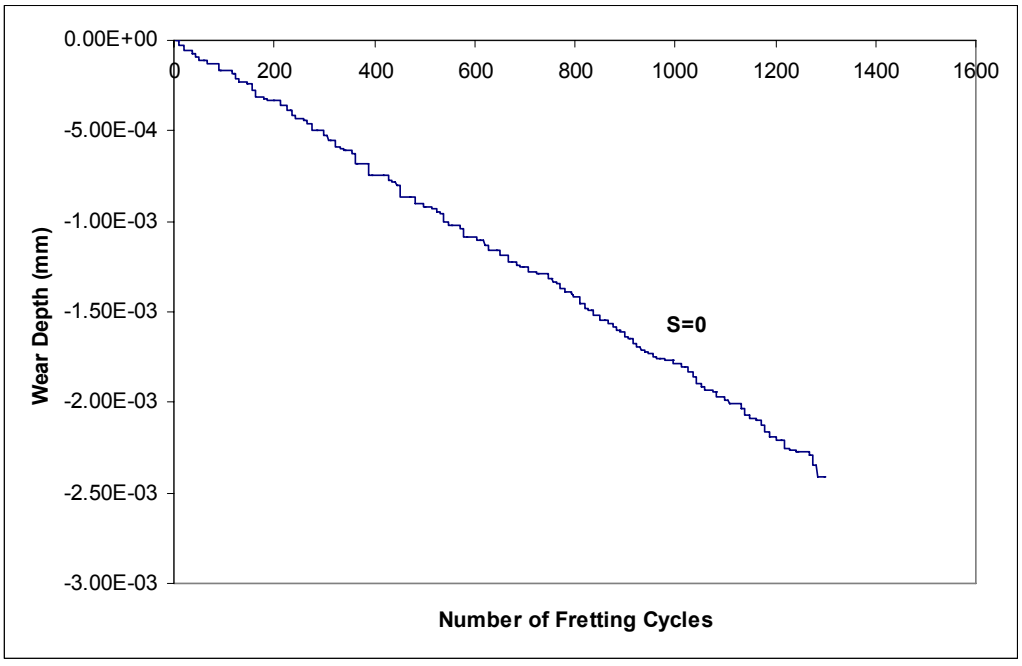

Figure 50: Simulated Wear Depth versus Number of Fretting Cycles at S=0

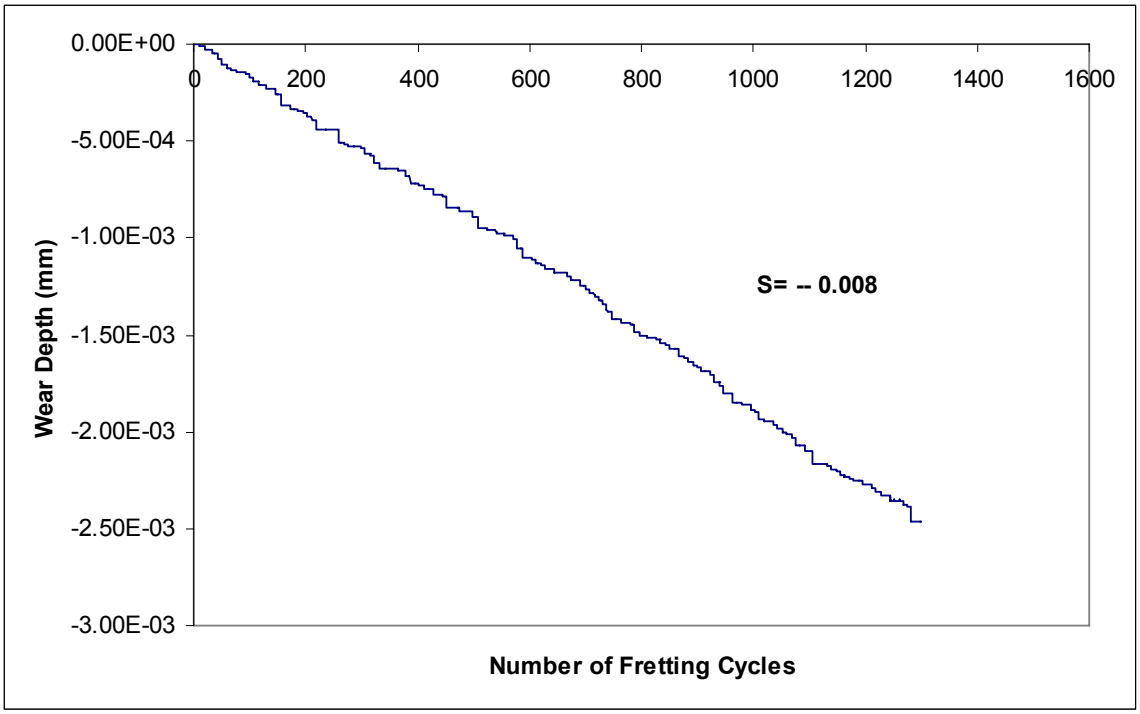

Figure 51: Simulated Wear Depth versus Number of Fretting Cycles at S=-0.008mm

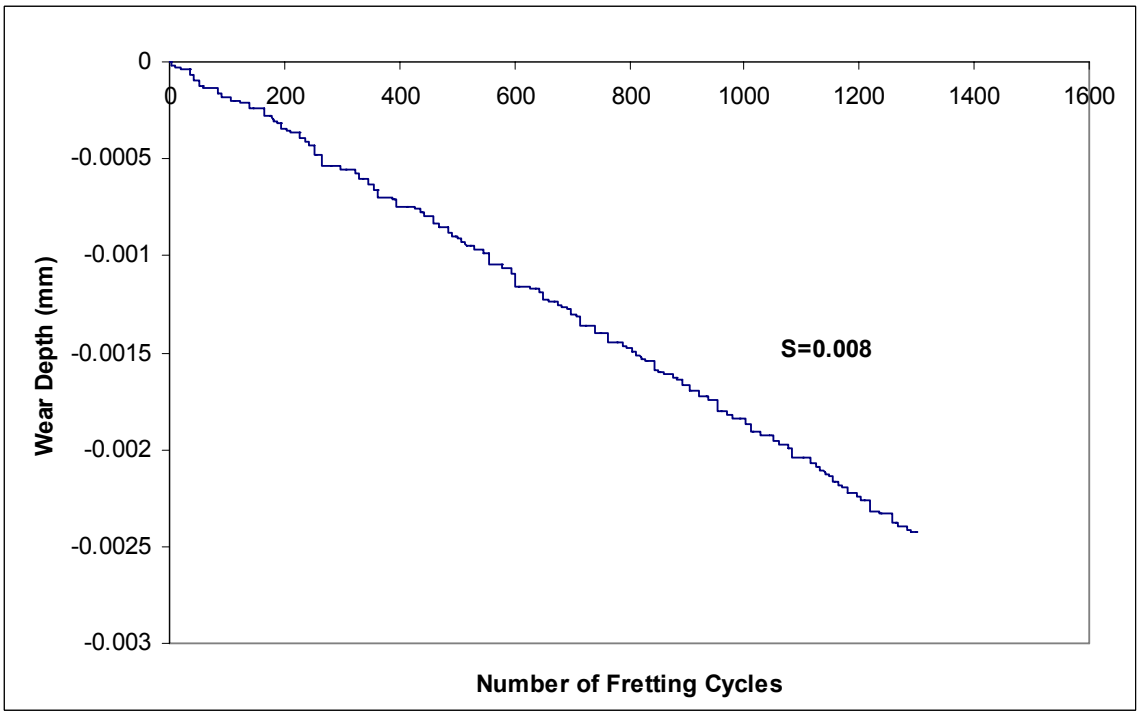

Figure 52: Simulated Wear Depth versus Number of Fretting Cycles at S=0.008mm

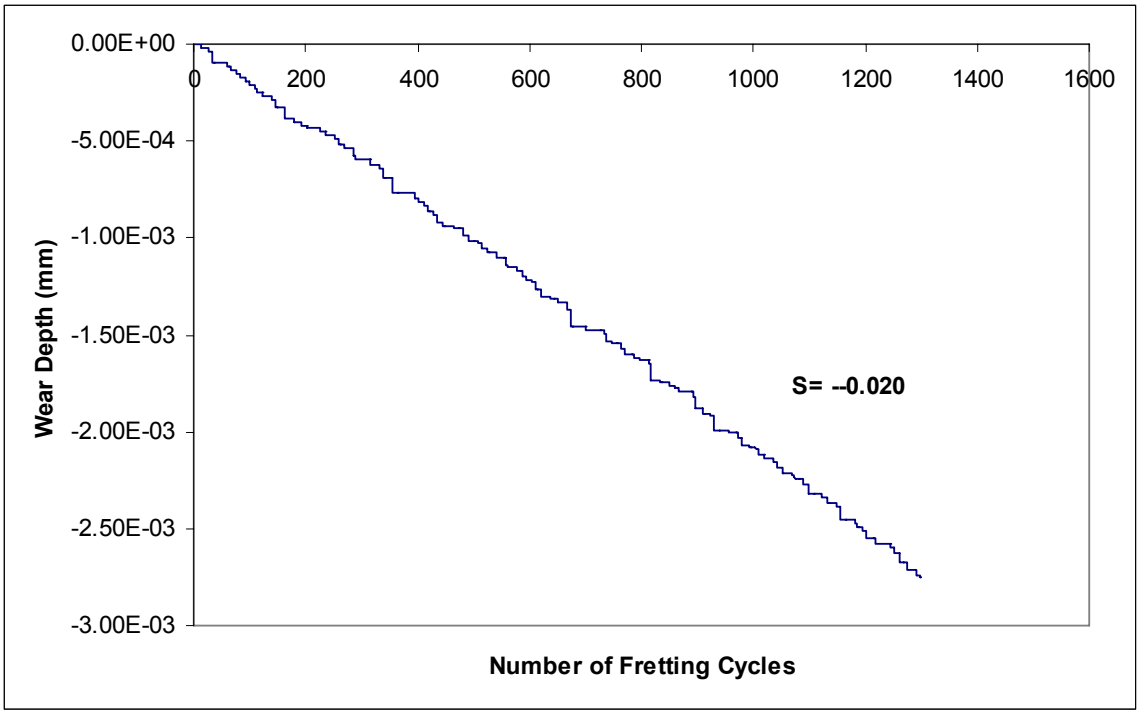

Figure 53: Simulated Wear Depth versus Number of Fretting Cycles at S=-0.020mm

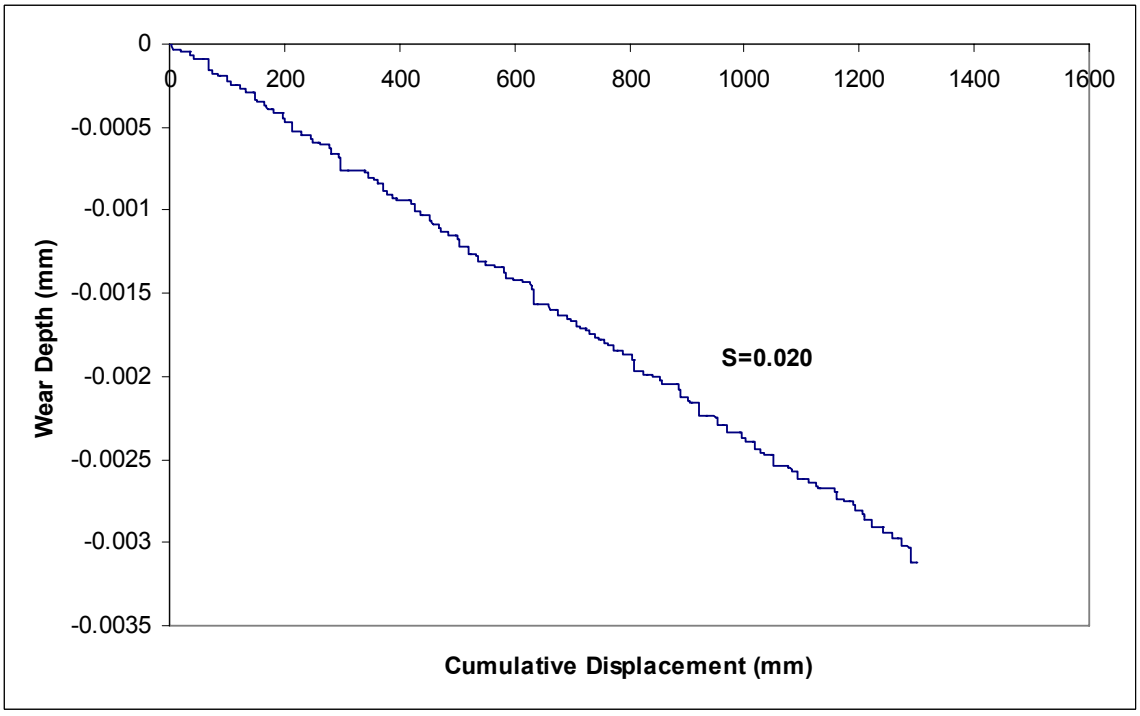

Figure 54: Simulated Wear Depth versus Number of Fretting Cycles at S=0.020mm

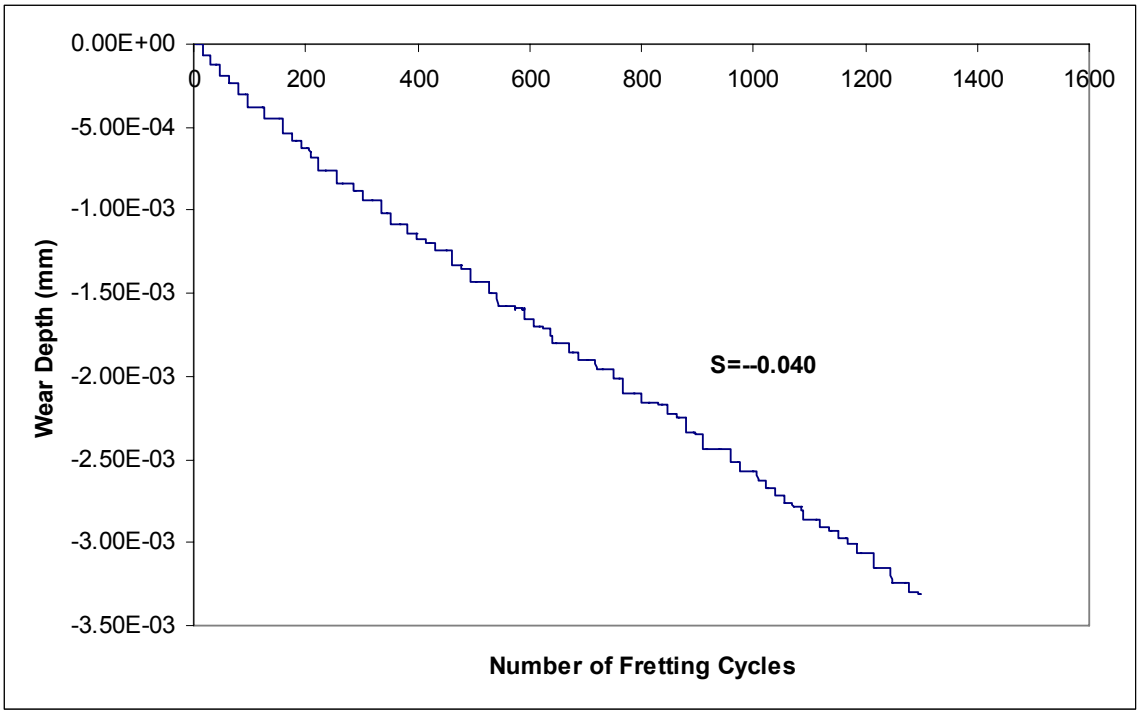

Figure 55: Simulated Wear Depth versus Number of Fretting Cycles at S=-0.040mm

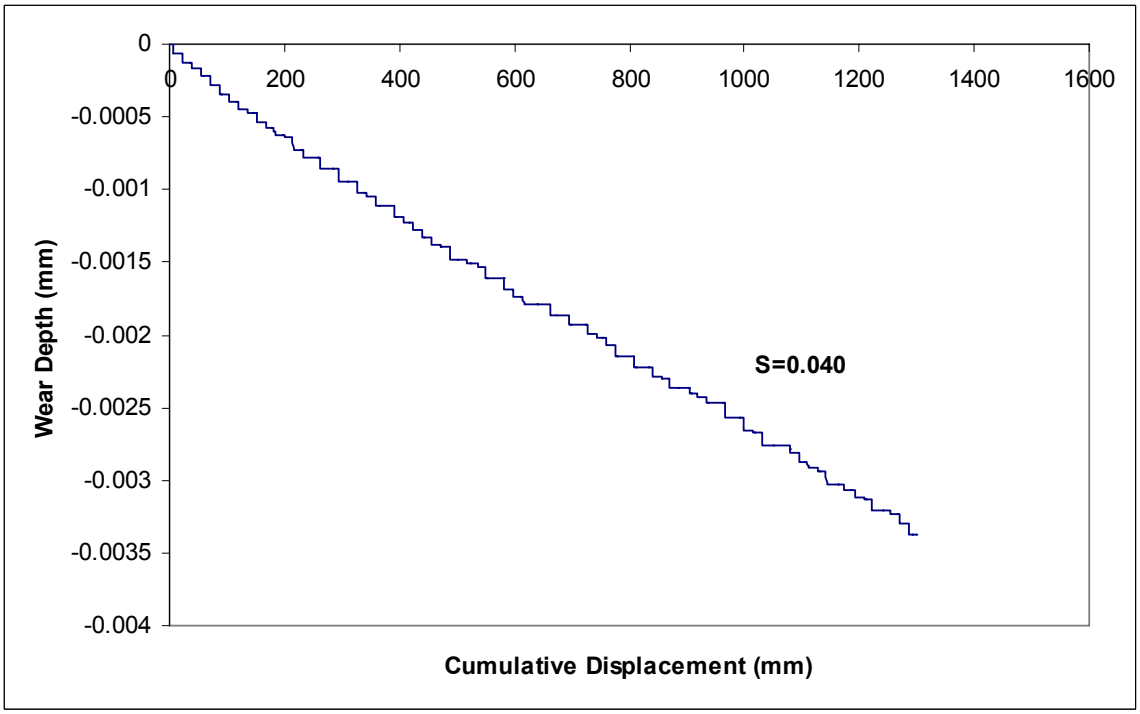

Figure 56: Simulated Wear Depth versus Number of Fretting Cycles at S=0.040mm

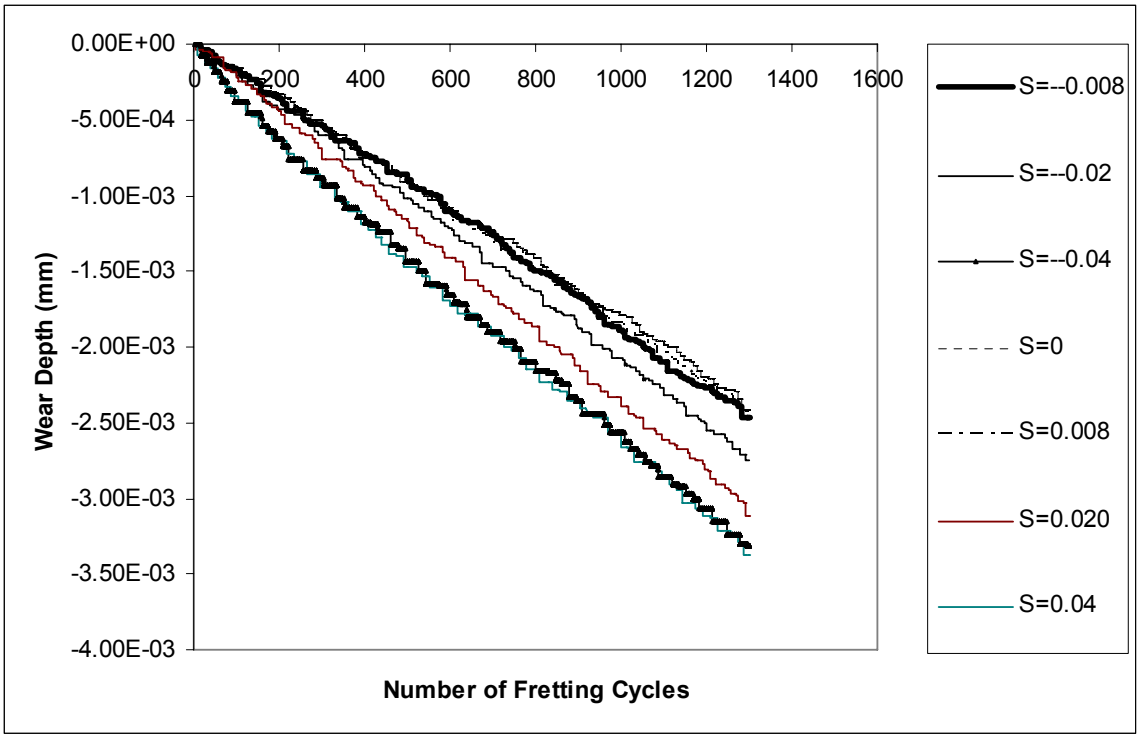

Figure 57: Simulated wear depth versus Number of fretting cycles for 7 nodes spanning across the receptacle surface from S=-0.040 to 0.040mm

inside the material due to wear occurring at the surface. As seen from Figure 52 the plot is not smooth. The uneven wear rates are because of the changes in the surface profile, contact pressure and instantaneous relative velocity with the evolution of the wear process. It can be concluded from Figure 59 that the maximum wear rate was present at the right and left extremes of the receptacle.

Through show the displacement of nodes in the receptacle as wear progresses. The legend in these figures indicates the magnitude of displacement. Blue color indicates minimal nodal displacement and red color indicates maximum nodal displacement. Figure 60 shows the displacement on nodes at the start of the simulation. The uniform blue color indicates zero displacement of the nodes at the start of the simulation

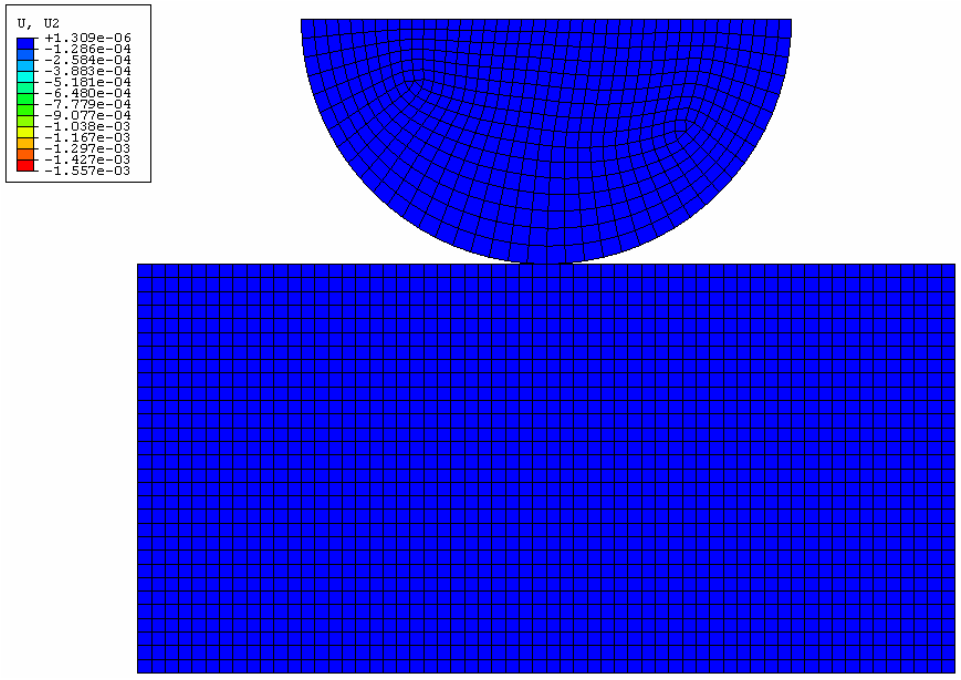

Figure 58: Displacement plot showing Zero Displacement on the receptacle at the start of the simulation

As the simulation progresses, the nodes at the receptacle surface move downwards, inside the material to simulate wear. This can be seen in Figure 61 where the light blue band just below the receptacle surface represents nodal displacement. Figure 62 shows the nodes have displaced further indicating that the wear depth increases with an increase in the number of fretting cycles. Figure 63 shows the nodes keep displacing inwards as the simulation progresses. Since the entire receptacle has been defined as an adaptive mesh domain, the nodes deep inside the receptacle also undergo downward movement. This can be seen by the light blue band in Figure 63

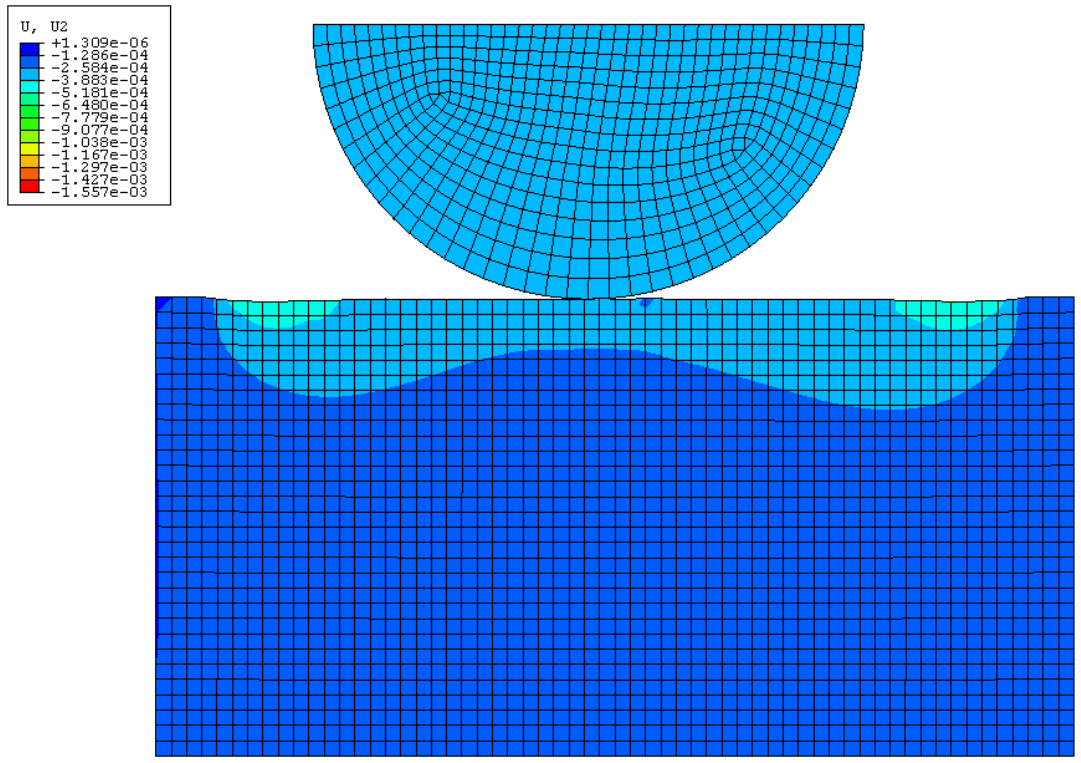

Figure 59: Nodal Displacement plot in the receptacle at 150 fretting cycles

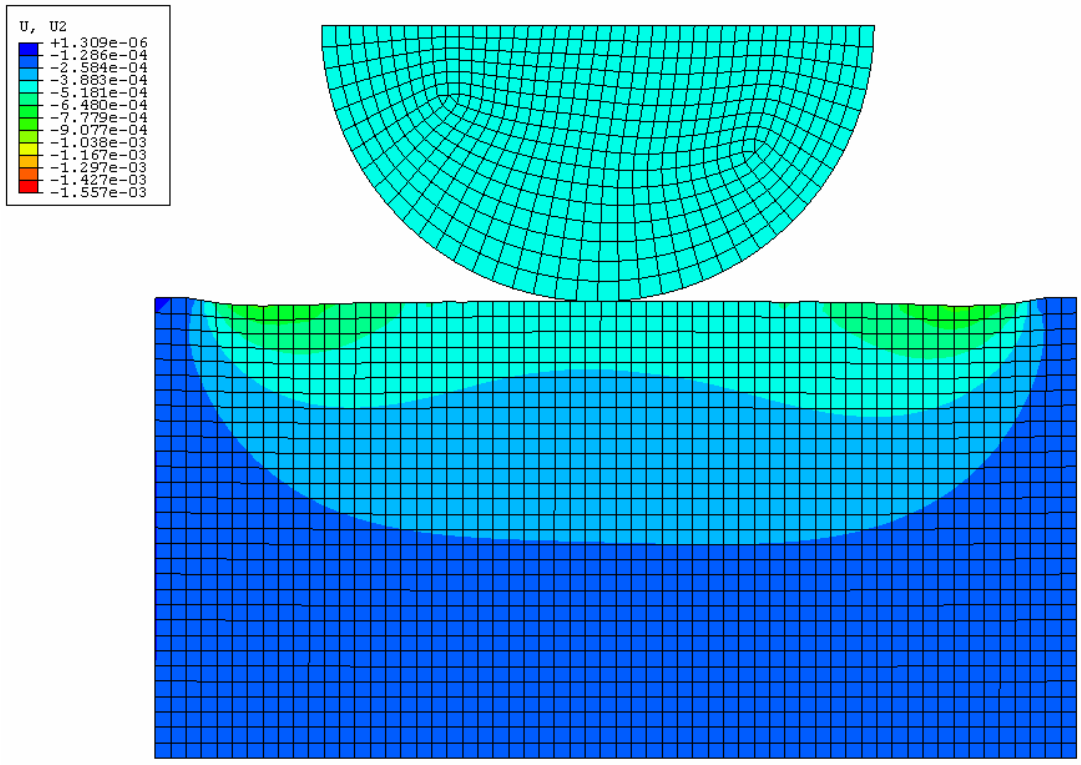

Figure 60: Nodal Displacement plot in the receptacle at 240 fretting cycles

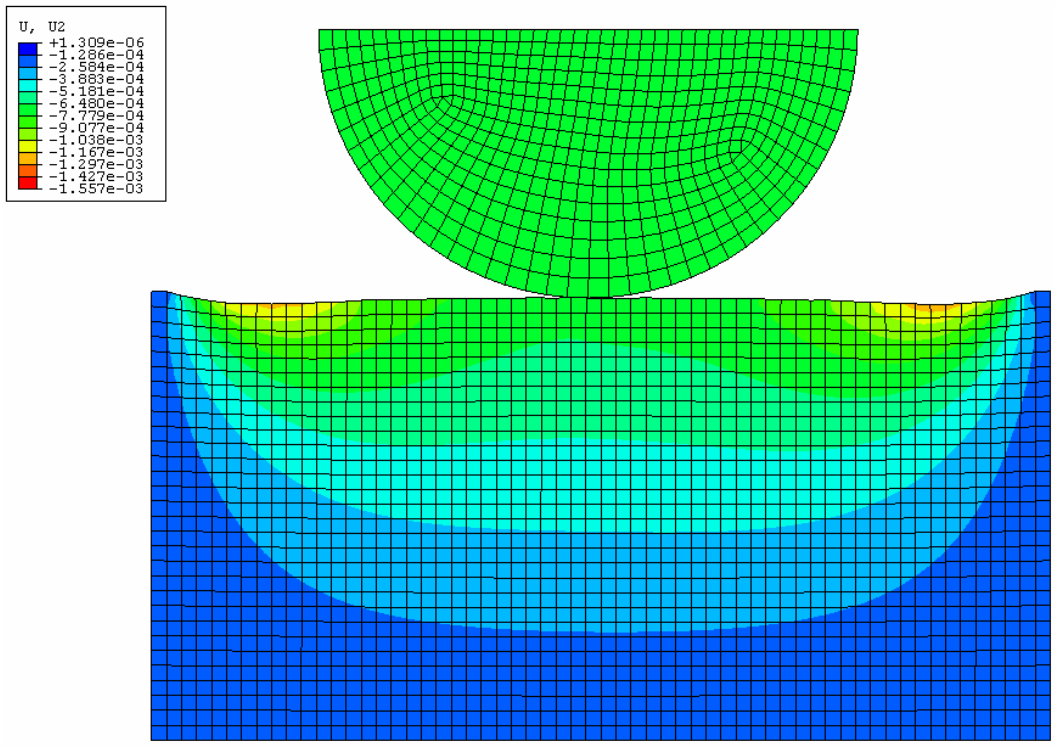

Figure 61: Nodal Displacement plot in the receptacle at 360 fretting cycles

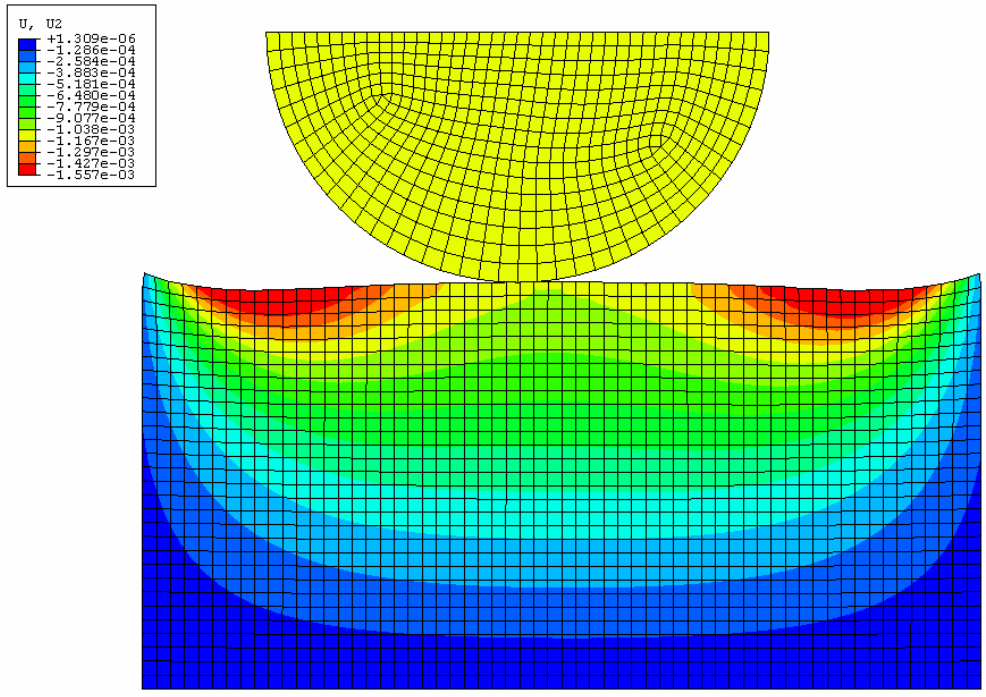

Figure 62: Nodal Displacement plot in the receptacle at 480 fretting cycles

The yellow band in Figure 64 indicates wear is continuously occurring as the simulation progresses

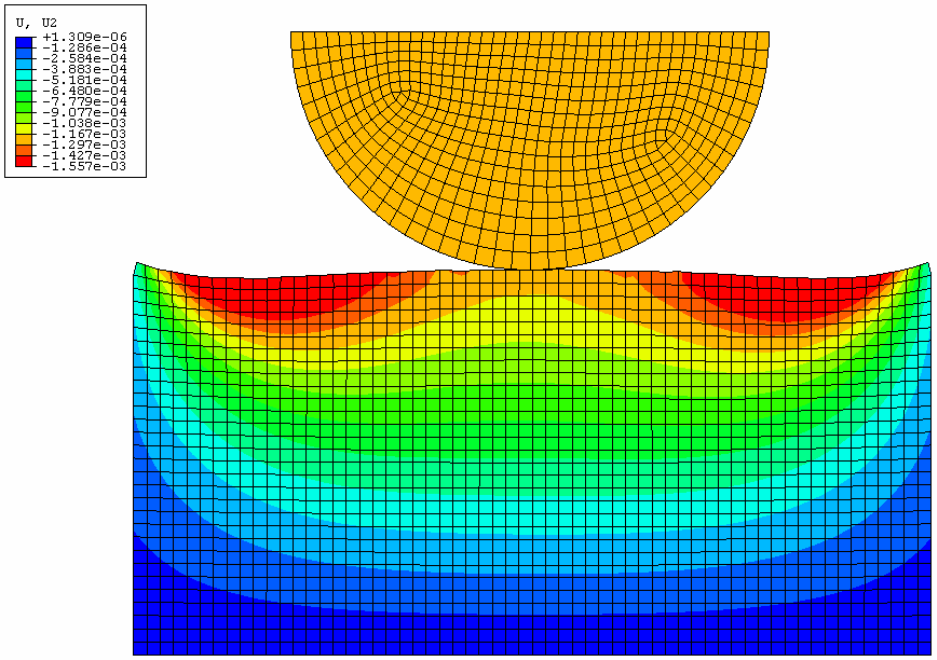

Figure 63: Nodal Displacement plot in the receptacle at 585 fretting cycles

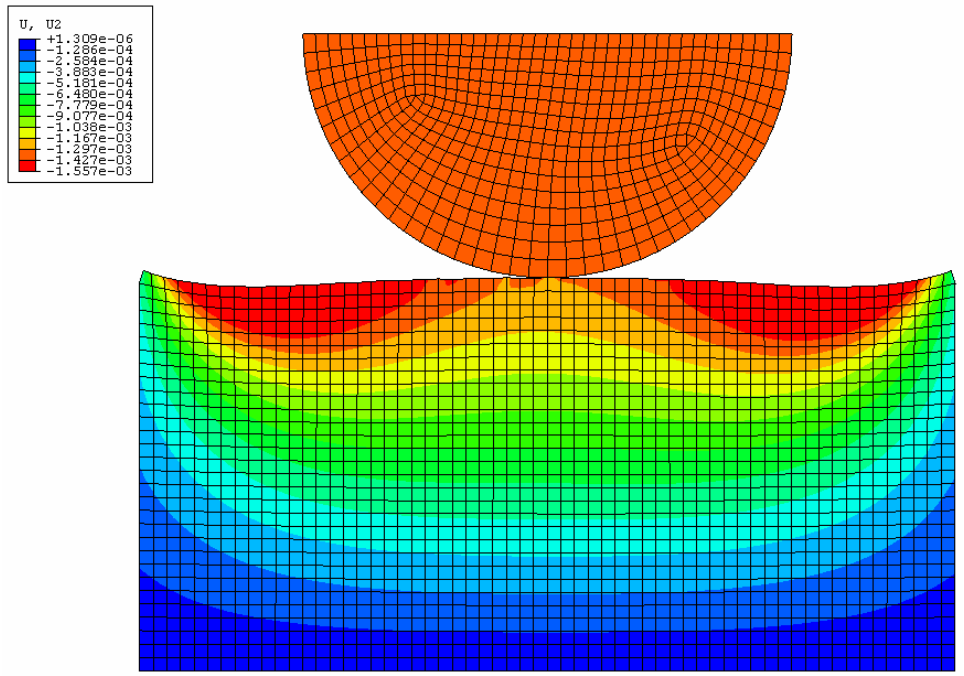

Figure 64: Nodal Displacement plot in the receptacle at 800 cycles

The red regions in Figure 66 indicate the areas of maximum wear

Once the new model was constructed, the simulation was allowed to run for 1600 cycles. Figure 67 shows the change in the surface profile and stress distribution in the pristine contact and the contact system after 1600 cycles in the new 2D model

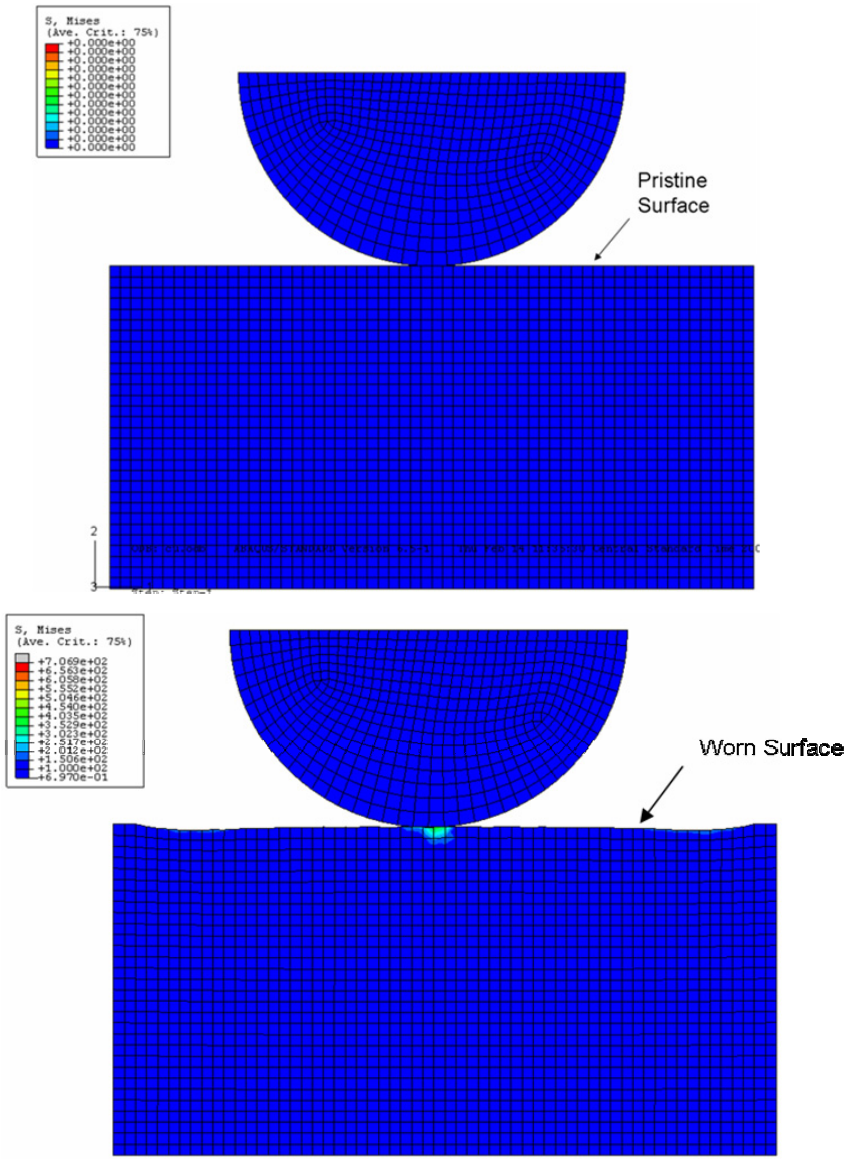

Figure 65: Von Mises stress plot showing wear on the contact surface due to fretting as seen in the 2D model

The 3D model was allowed to run for 1600 cycles. shows the change in the surface profile and stress distribution in the pristine contact and the contact system after 1600 cycles in the 3D model

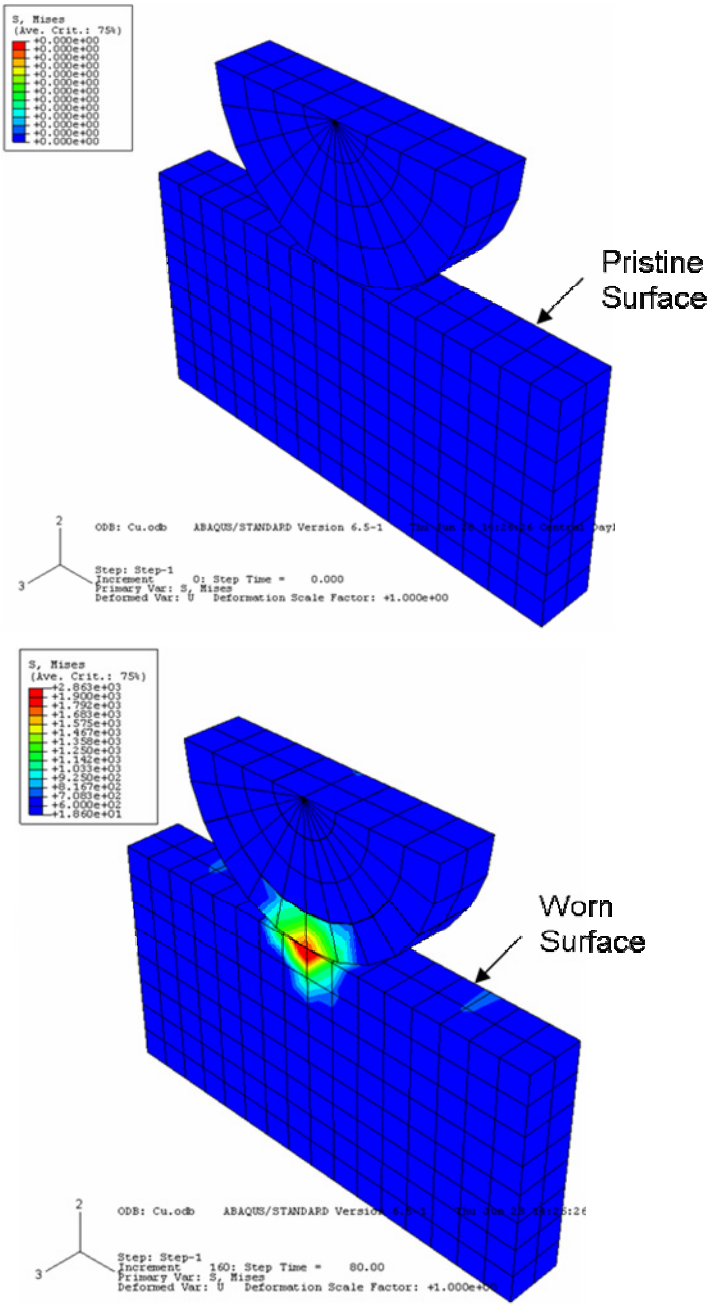

Figure 66: Von Mises stress plot of wear on the contact surface due to fretting as seen in the 3D model

As wear progresses the contact pressure at the nodes varies because of changing surface profile. Thus the wear rate fluctuates continuously as wear progresses. This is shown in Figure 69

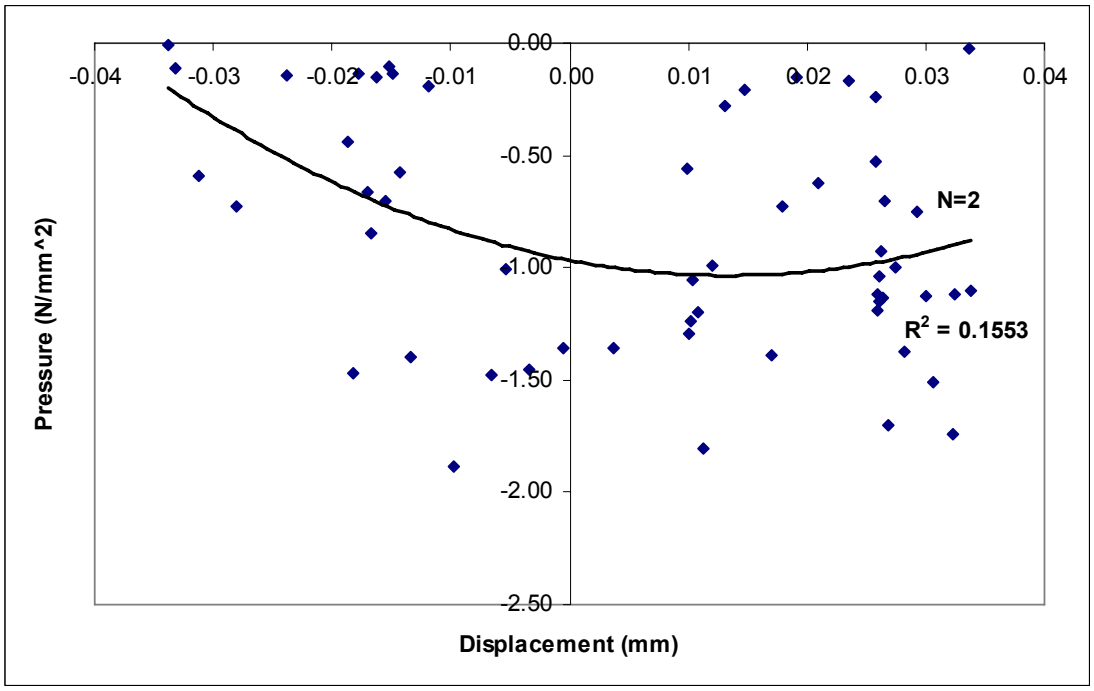

Figure 67: Contact Pressure Variation across Vibration Amplitude with Wear Evolution due to Fretting Cycles

In Figure 69 the pressure variation is almost flat as the surface is not degraded and the contact pressure at all nodes on the receptacle is almost the same. As the number of fretting cycles increase, the surface gets degraded and the contact pressure exerted at various nodes changes. This variation is clearly shown in the pressure versus displacement plots. The X axis represents the vibration amplitude with the origin representing the neutral position. The Y axis represents the pressure variation as the slider slides over the receptacle. The Y axis has negative values since the pressure is compressive. Several pressure plots have been plotted to show the change in pressure

values as the simulation progresses. N, represents the cycle number for which the pressure plot has been plotted.

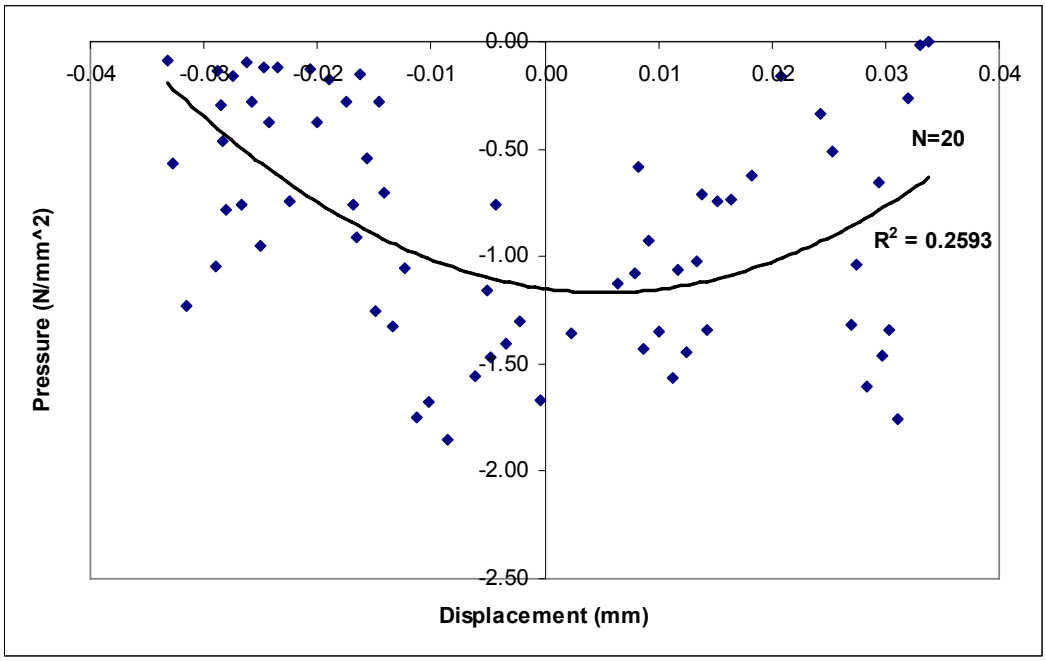

Figure 68: Contact Pressure Variation across Vibration Amplitude with Wear Evolution due to Fretting Cycles

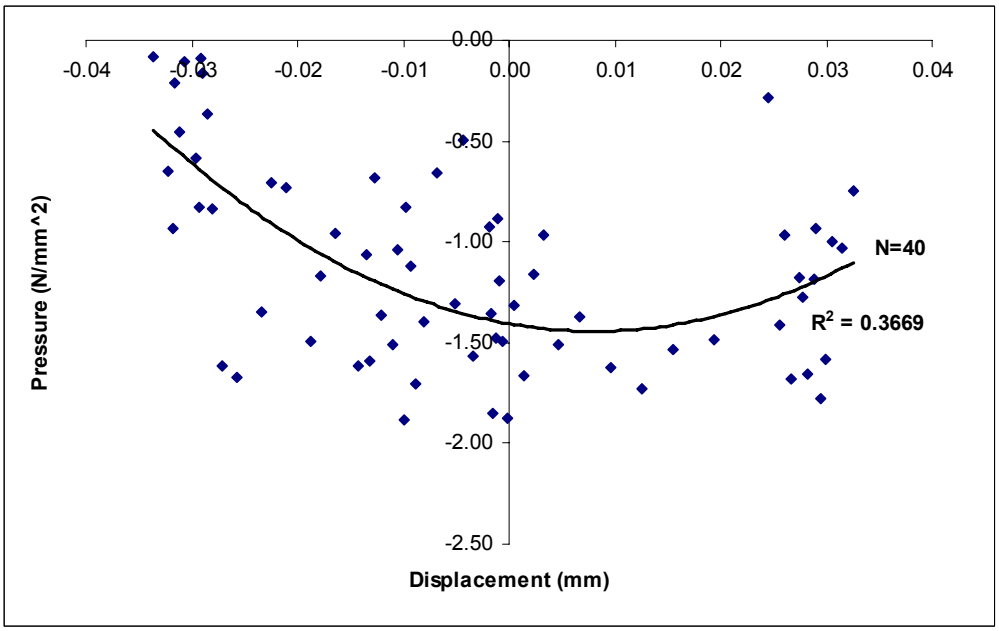

Figure 69: Contact Pressure Variation across Vibration Amplitude with Wear Evolution due to Fretting Cycles

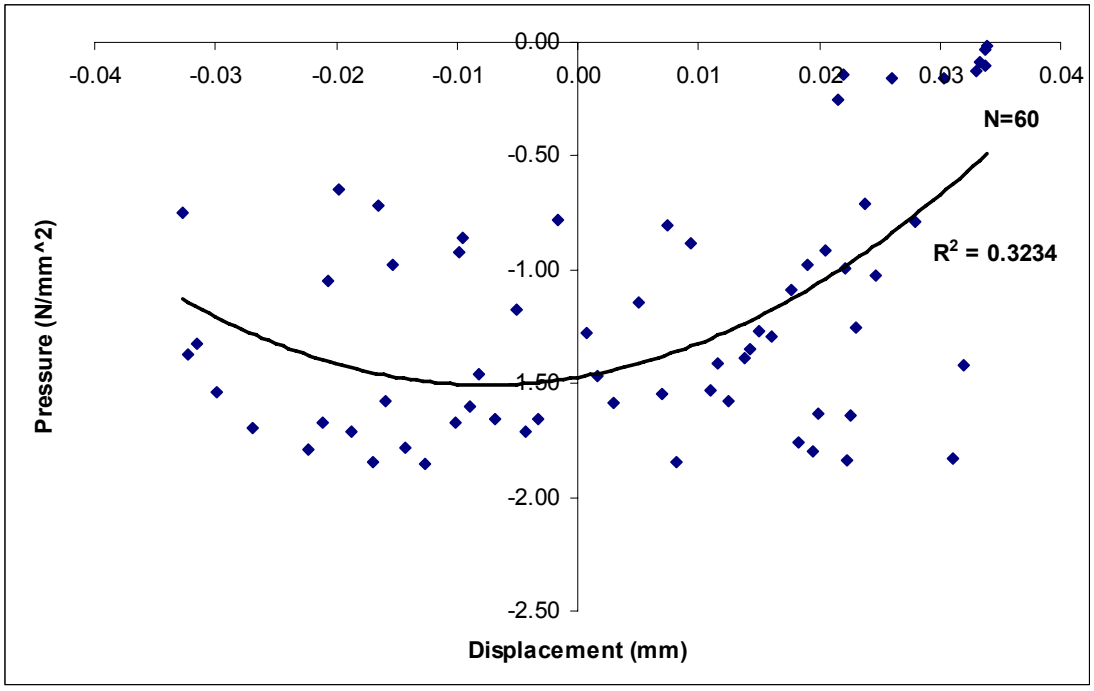

Figure 70: Contact Pressure Variation across Vibration Amplitude with Wear Evolution due to Fretting Cycles

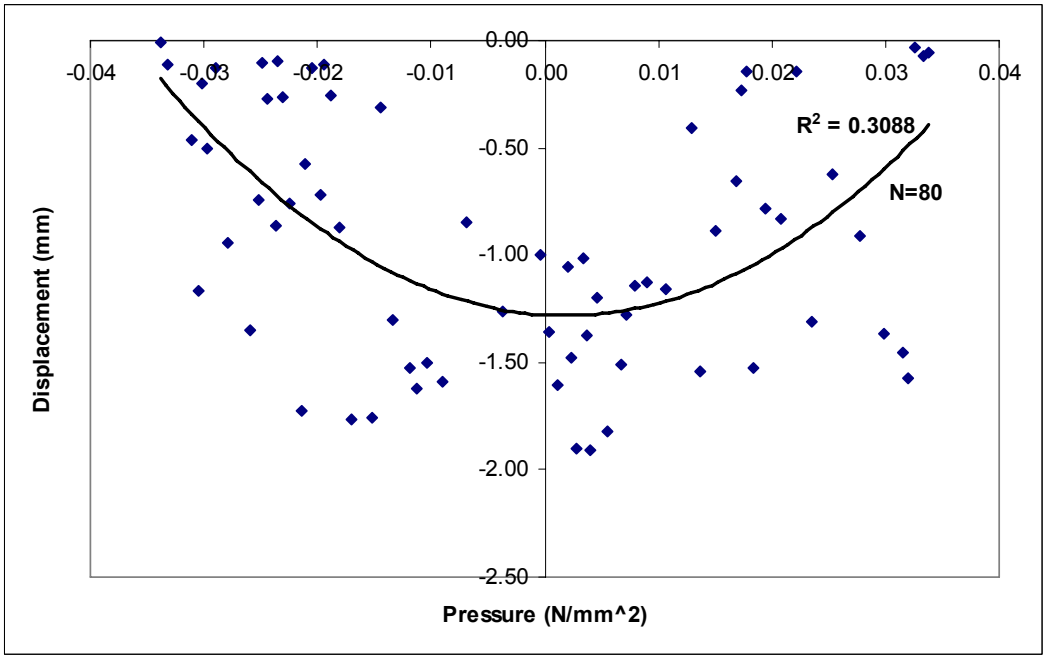

Figure 71: Contact Pressure Variation across Vibration Amplitude with Wear Evolution due to Fretting Cycles

6.2 Model Validation

The model was validated by comparing the wear rate for a particular contact system with the wear rate obtained from experimental results for the same contact system. The experimental contact system selected was steel-on-steel contact system, from Kato [1994]. Kato has used two experimental data points and used a linear fit between them which is shown in Figure 74. Steel-on-steel contact system is a common electrical contact system used in battery contacts. The wear coefficient for steel-steel contact was assigned a value of 0.0150, Rabinowicz [1995]. The hardness value of steel used was Hv 700. The wear-rate was calculated as a function of the wear coefficient, hardness, sliding velocity and contact pressure using formula,

$$\frac{h}{t} = \frac{k}{H} * \frac{s}{t} * P \qquad (25)$$

The contact pressure was continuously extracted from the model and updated, depending on the location of the node on the receptacle and the position of the upper pin. Figure 74 shows a plot of model predictions and experimental data. Wear of contact (in mm) was plotted on the Y axis and the sliding distance (in mm) was plotted on the X axis. The experimental wear-rate was found by calculating the slope of this plot. Simulation results were extracted from the model and plotted on the same x and y axis. Simulation plots were plotted for several nodes on the top face of the receptacle. The slopes, which indicate wear rates, were compared for the experimental plot and the simulation plots. Similar wear rates were found, indicating the model has been validated

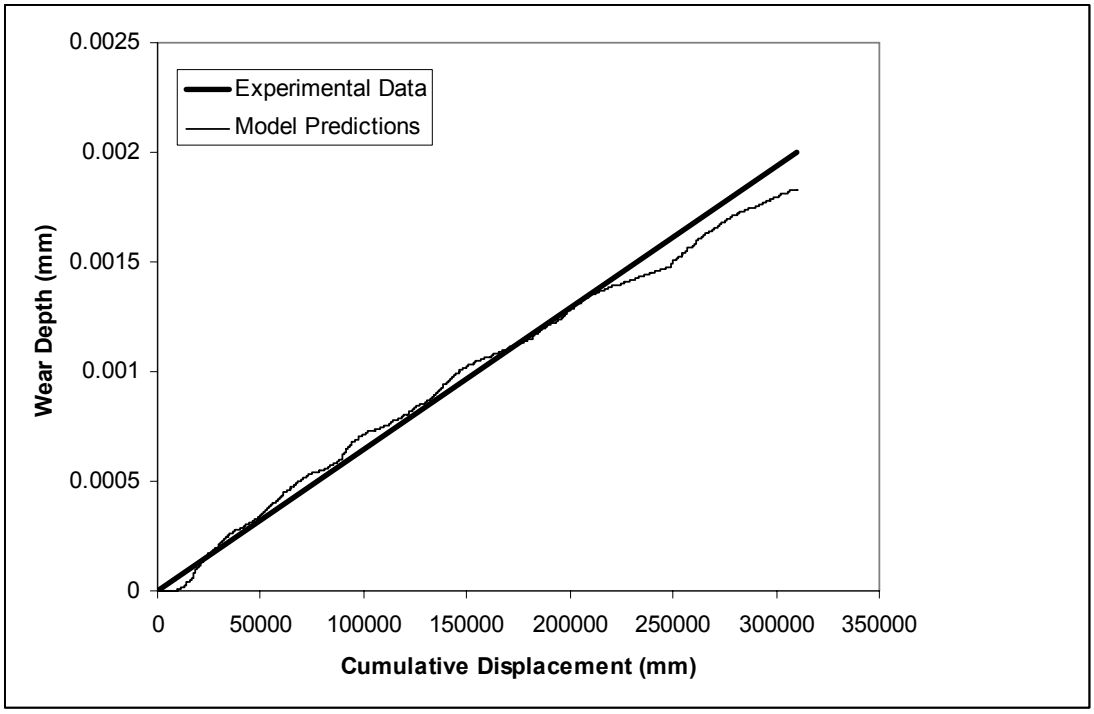

Figure72: Comparison of Predicted Wear Rates Versus Experimental Results

The model was also validated for a copper-on-copper contact system. The model was validated by comparing the wear rate for a copper-on-copper contact system with the wear rate obtained from Archard's wear law for the same contact system. Copper on copper contact system is a very common electrical contact system used in electrical contacts. A 10MPa pressure load was applied on the top face of a slider as shown in Figure 21. This copper slider reciprocated against a copper receptacle. The wear coefficient for copper-copper contact was assigned a value of 0.0110, Rabinowicz [1995]. The hardness value of copper used was Hv 130. A clean and dry contact surface was assumed with a coefficient of friction equal to 1.21. The contact pressure was continuously extracted from the model and updated, depending on the location of the node on the receptacle and the position of the upper pin. The analytical data was calculated from Archard's law using the formula,

$$h = \frac{K}{H} * s * P \qquad (26)$$

Upon substituting the values, this relation was found to be, h = 0.00025761*s. The Archard's law plot was plotted using this relation. Wear depth of the slider (in mm) was plotted on the Y axis and the cumulative sliding distance (in mm) was plotted on the X axis. Simulation results were extracted from the model and plotted on the same x and y axis. Simulation plots were plotted for several nodes on the top face of the receptacle. The slopes, which indicate wear rates, were compared for the theoretical Archard's Law plot and the simulation plot as shown in Figure 75. Similar wear rates were found, indicating that the model had been validated.

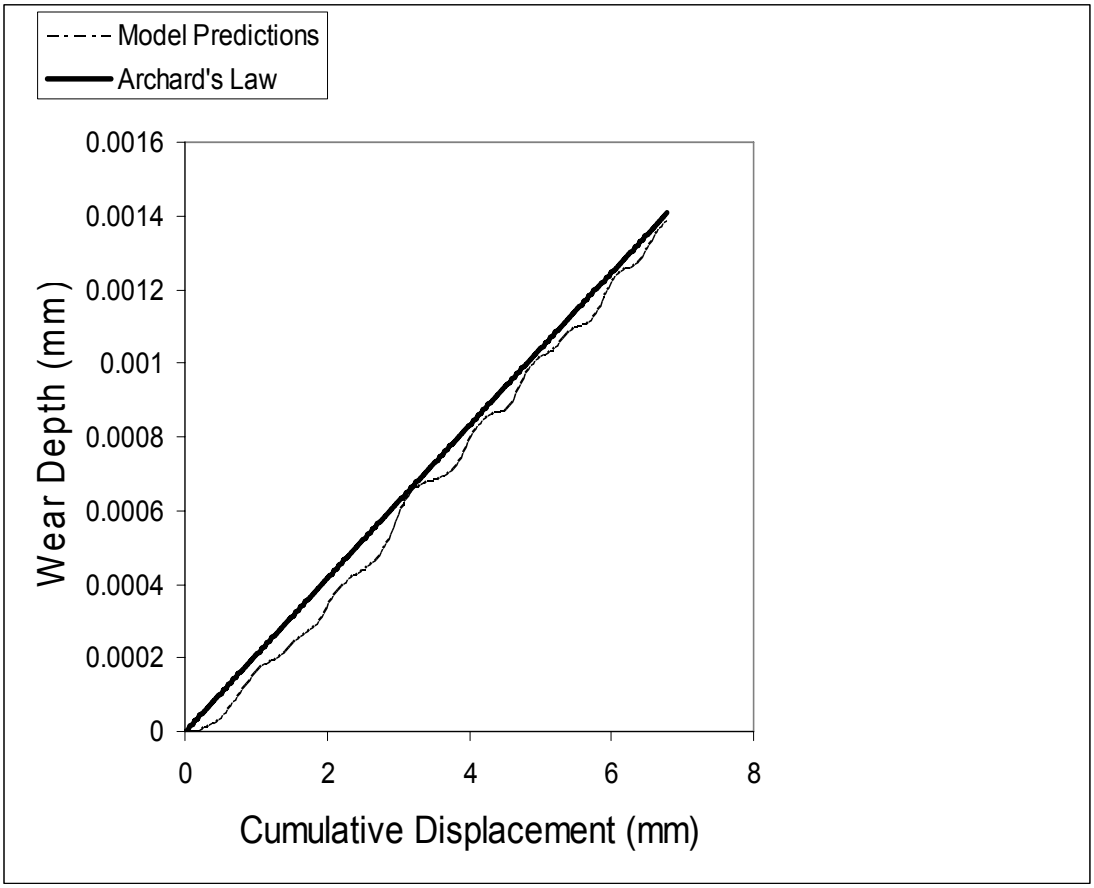

Figure73: Comparison of Predicted Wear Rates versus Theoretical Results

CHAPTER 7

SUMMARY AND FUTURE SCOPE FOR WORK

7.1 Summary

In this work, a methodology for simulation of fretting wear in electrical contacts has been presented. Electrical contacts are subjected to relative motion due to vibrations or thermo-mechanical loads during operation. The finite element model developed in this paper targets a variety of end applications including RAM memory sockets, SD-card sockets, micro-processor ZIF sockets and fuzz button pressure contacts. In RAM memory sockets relative motion may be experienced due to vibration or thermo-mechanical loads during operation. This results in edge connector pads wear causing an increase in contact resistance and electrical failure. In SD-card sockets repetitive sliding contact may be encountered due to shock, drop, thermo-mechanical loads, key-pad actuation, battery insertion and removal, or during removal of the memory cards for data transfer. In micro-processor ZIF sockets, relative motion may be caused due to vibrations resulting from internal sources like cooling systems. It is critical to simulate the wear in these electrical contacts to predict product life. The model has been constructed in Hypermesh. Wear is calculated using Archard's Wear Law. This wear is applied to the surface of the wearing

surface in the form of nodal displacements. The nodes are moved in the direction of wear by a magnitude, calculated using Archard's Law. This nodal movement causes the mesh elements to distort severely. To ensure, continuation of the wear simulation for a large number of cycles, the wearing surface is remeshed using Adaptive Meshing. Arbitrary lagrangian-eulerian (ALE) formulation with adaptive meshing has been used to simulate wear in this model. ALE has been used to combine the advantages of the Lagrangian and Eulerian descriptions. The use of ALE in this model, allows a topologically similar mesh throughout the analysis, without creating or destroying elements, allowing the mesh to move independently of the material. The nodes of the computational mesh may be moved with the continuum in lagrangian fashion, or held fixed in eulerian manner, or may be moved in an arbitrary way. This freedom of moving the computational mesh allows greater distortions of the continuum to be handled than would be allowed by a purely lagrangian method, with more resolution than the eulerian method. ALE adaptive meshing enables the maintenance of a high quality mesh throughout an analysis, even when the contact surface gets worn out, by allowing the contact surface mesh to move independently of the material. The topology and connectivity of the elements is not altered. The simulation has been run for over 2000 fretting cycles. Wear accrues on the contact-surface of the connector with increase in the fretting cycles. The wear rate is uneven because of the changes in the surface profile, contact pressure and the instantaneous relative velocity with the evolution of the wear process. The model was validated by comparing the wear rate for a steel-on-steel contact system with the wear rate obtained from experimental results for the same contact system. The contact pressure was continuously extracted from the model and updated, depending on the location of the

node on the receptacle and the position of the upper pin. Wear of contact (in mm) was plotted on the Y axis and the sliding distance(in mm) was plotted on the X axis. The experimental wear-rate was found by calculating the slope of this plot. Simulation results were extracted from the model and plotted on the same x and y axis. Simulation plots were plotted for several nodes on the top face of the receptacle. The slopes, which indicate wear rates, were compared for the experimental plot and the simulation plot. Similar wear rates were found, indicating that the model had been validated. The model was also validated by comparing the wear rate for a copper-on-copper contact system with the wear rate obtained from Archard's Law for the same contact system.

7.2 Scope for future work

The wear model can be validated for several other contact systems like gold-on-gold, steel-on-copper, and gold-on-copper. More complex 2D and 3D models can be constructed depending on the specific contact being simulated. An experimental setup can be created to simulate fretting wear for various contact systems. A Bruel and Kjaer vibration system can be used to generate vibrations in the slider.

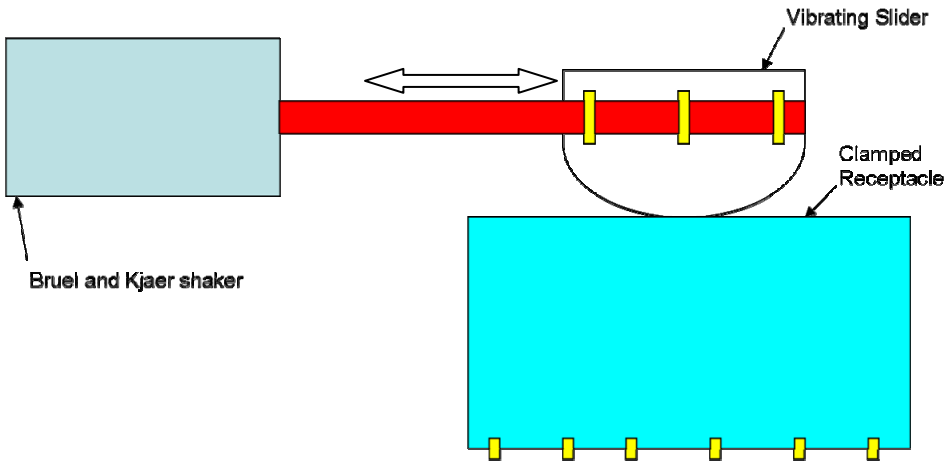

Figure74: A typical vibration experimental setup

A vibration setup typically consists of a shaker, fixture with clamps to fix the specimen, generator of input signal that excites shaker software and hardware that may be used to control vibrations and take measurements [Przemysław 2005].

The receptacle would be clamped down and the slider would be connected to a shaker as shown in Figure 76. When the shaker is excited, the slider will oscillate on the receptacle resulting in fretting wear. A profilometer can be used to measure the wear depth at regular intervals. A plot of wear depth versus the sliding distance can be plotted. The slope of this plot will predict the wear rate. This experimental wear rate can than be compared to the wear rate predicted by this model. By changing the material of the slider and the receptacle various contact systems can be tested using this experimental setup.

BIBLIOGRAPHY

Antoniou R. And Subramanian C., Wear Mechanism Map For Aluminum Alloys, Scripta Metall., Vol. 22, pp. 809-814, 1988

Agelet De Saracibar C., M. Chiumenti, On The Numerical Modeling Of Frictional Wear Phenomena, Comput. Methods Apl. Mech. Engineering, Vol.177, pp.401-426, 1999

Archard J. F., Contact And Rubbing Of Flat Surfaces, J. Apl. Phys., Vol. 24, No. 8, pp. 981-8, 1953

Archard J. F., Single Contacts And Multiple Encounters, J. Apl. Phys., Vol. 32, No. 8, pp. 1420-5, 1961.

Armero F And Love E, An Arbitrary Lagrangian-Eulerian Finite Element Method For Finite Strain Plasticity, Int. J. Numer. Methods Eng, Vol. 57, pp. 471–508, 2003

Ashby M.F. And Lim. S.C., Wear Mechanism Maps, Scripta Metall., Vol.24, pp.805-810, 1990

Barwell F.T., Wear Of Machine Elements, In: N.P. Suh, N. Saka (Eds.)., Fundamentals Of Tribology, The Mit Press, pp. 401–441, 1978

Bayer R.G., Mechanical Wear Prediction And Prevention, Marcel Dekker, 1994

Bowden F. P. And D Tabor,Friction, Lubrication And Wear: A Survey Of Work During The Last Decade, Br. J. Appl. Phys., Vol. 17, pp. 1521-1544, 1966

Burwell Jt, Strang Cd, On The Empirical Law Of Adhesive Wear, Journal Of Applied Physics, Vol. 23, pp.18–28, 1952

Cantizano A, A. Carnicero A, G. Zavarise, Numerical Simulation Of Wear-Mechanism Maps, Computational Materials Science, Vol. 25, pp. 54–60, 2002

Challen J.M. And P.L.B. Oxley, An Explanation Of The Different Regions Of Friction And Wear Using Asperity Deformation Models, Wear, Vol.53, pp.229-243, 1979

Chen H. & Alpas A. T., Sliding Wear Map For The Magnesium Alloy Mg-9al-0.9 Zn (Az91), Wear, Vol. 246, pp.106- 116, 2000

Childs T.H.C., The Sliding Wear Mechanisms Of Metals, Mainly Steels, Tribology International, Vol. 13, pp. 285-293, 1980

Childs T.H.C., The Mapping Of Metallic Sliding Wear, Proc. I. Mech. E., Vol. 202, pp. 379-395, 1988

Cocks M., Interaction Of Sliding Metal Surface, J. Appl. Phys., Vol. 33, pp. 2152-2101, 1962.

Dickrell D. J. And Sawyer W. G., Evolution Of Wear In A Two-Dimensional Bushing, Tribology Transactions, Vol.47, pp.257-262, 2004

Ding, J., Leen S.B., And Mccoll, I., The Effect Of Slip Regime On Fretting Wear-Induced Stress Evolution, International Journal Of Fatigue, Vol. 26, pp.521-531, 2004

Donea J., Antonio Huerta, J.-Ph. Ponthot And A. Rodrıguez-Ferran, Arbitrary Lagrangian–Eulerian Methods, Encyclopedia Of Computational Mechanics. Volume 1:Fundamentals, 2004

Eden E.M., W.N. Rose And F.L. Cunningham, The Endurance Of Metals, *Inst. Mech. Eng.*, pp. 875, 1911

Franklin, F. J., Widiyarta, I., Kapoor, A.,Computer Simulation Of Wear And Rolling Contact Fatigue, Wear, Vol. 251, pp. 949_955, 2001

Gonzalez C., Martin A., Garrido M. A., Gomez M. T., Rico A., And Rodriguez J., Numerical Analysis Of Pin On Disc Tests On Al-Li/Sic Composites, Wear, Vol. 259, pp. 609-612, 2005

Hamed A,, W Tabakoff, Rb Rivir, K Das, P Arora, Turbine Blade Surface Deterioration By Erosion, Journal Of Turbomachinery, Vol. 127, Issue 3, pp. 445-452, July 2005

Hegadekatte V., N Huber, And O Kraft, Finite Element Based Simulation Of Dry Sliding Wear, Modelling Simul. Mater. Sci. Eng., Vol. 13, pp. 57–75, 2005

Hirst W., Wear Of Unlubricated Metals, Proc. Conf. Lubr. Wear, Ime, London Pp.674–681, 1957

Hoffmann. H., Hwang C., And Ersoy K. Advanced Wear Simulation In Sheet Metal Forming, Annals Of The Cirp, Vol. 54, pp. 217-220, 2005

Holm R., Electric Contacts. Berlin: Springer-Verlag. 1946.

Hsu, S. M., Shen, M. C., & Ru_, A. W., Wear Prediction For Metals, Tribology International, Vol. 30, pp.377-383, 1997

Jiang J. And Arnell R. D., On The Running-In Behaviour Of Diamond-Like Carbon Coatings Under The Ball-On-Disk Contact Geometry, Wear, Vol. 217, pp.190-199, 1998

Kalin M. & Vizintin, J.,Use Of Equations For Wear Volume Determination In Fretting Experiments. Wear, Vol. 237, pp. 39_48, 2000

Kapoor, A. And Franklin, F. J., Tribological Layers And The Wear Of Ductile Materials, Wear, Vol. 245, pp. 204-215, 2000

Kapoor, A., Williams, J. A., And Johnson, K. L., The Steady State Sliding Of Rough Surfaces, Wear, Vol. 175, pp. 81-92, 1994

Kim N.H., Won D., Burris D., Holtkamp B., Gessel G., Swanson P., And Sawyer, W. G., Finite Element Analysis And Experiments Of Metal/Metal Wear In Oscillatory Contacts, Wear, Vol. 258, pp.1787-1793, 2005

Kato H., T.S. Eyre And B. Ralph, Wear Mechanism Map Of Nitrided Steel Acta Metal. Mater., Vol. 42, No. 5, pp. 1703-1713, 1994

Kato K. And Hokkirigawa K., Abrasive Wear Diagram, Proc. Eurotrib, Vol. 4, Section 5.3, pp. 1-5, Elsevier, Amsterdam, 1985

Kónya L., Váradi K., And Friedrich, K., Finite Element Modeling Of Wear Process Of A Peek-Steel Sliding Pair At Elevated Temperature, Periodica Polytechnica, Mechanical Engineering, Vol. 49, pp. 25-38, 2005

Ko, D. C., Kim, D. H., And Kim, B. M., Finite Element Analysis For The Wear Of Ti-N Coated Punch In The Piercing Process, Wear, Vol.252, pp.859-869, 2002

Lancaster, J, The Formation Of Surface Films At The Transition Between Mild And Severe Metallic Wear, Proc. Roy. Soc. A, Vol. 273 pp.466-83, 1963

Laursen T.A. And J.C. Simo, A Continuum-Based Finite Element Formulation For The Implicit Solution Of Multi-Body, Large Deformation Frictional Contact Problems, Int. J. Numer. Methods Engg. Vol. 36, pp. 3451–3485, 1993

Lim S.C. And M.F. Ashby, Wear Mechanism Maps, *Acta Metal.* Vol.**35**, Pp. 1–24, 1987

Lim S.C., M.F. Ashby And Brunton J.H., Wear-Rate Transitions And Their Relationship To Wear Mechanisms, Acta. Metall., Vol. 35, pp.1343-1348, 1987

Liu Y., Asthana R. And Rohatgi P., A Map For Wear Mechanisms In Aluminum Alloys, J. Mater. Sci., Vol. 26, pp. 99-102, 1991

Mccoll, I. R., Ding, J., And Leen, S., Finite Element Simulation And Experimental Validation Of Fretting Wear, Wear, Vol. 256, pp.1114-1127, 2004

Molinari J.F., M. Ortiz, R. Radovitzky And E.A. Repetto, Finite-Element Modeling Of Dry Sliding Wear In Metal, Engineering Computations, Vol. 18 No. 3/4, pp. 592-609, 2001

Nazem M. And D. Sheng, Arbitrary Lagrangian-Eulerian Method For Consolidation Problems In Geomechanics, International Conference On Computational Plasticity, Vol. 8, 2005

Öquist M., Numerical Simulations Of Mild Wear Using Updated Geometry With Different Step Size Approaches, Wear, Vol. 249, pp. 6-11, 2001

Podra Priit, Soren Andersson, Simulating Sliding Wear With Finite Element Method, Tribology International, Vol. 32, pp.71-81, 1999

Rabinowicz, Friction And Wear Of Materials, Edition 2, Table 6.2, pp. 159, 1995

Rhee S. K., L. Halberstadt, J. A. Mansfield, Wear Of Materials, Asme, pp. 560 – 568, 1977

Rigney, D. A., The Role Of Hardness In The Sliding Behavior Of Materials, Wear, Vol.175, pp. 63-69, 1994

Rigney, D. A., Comments On The Sliding Wear Of Metals, Tribology International, Vol. 30, pp.361-367, 1997

Slade P., Electrical Contacts: Principles And Applications, New York Marcel Dekker, Inc., 1999.

Suh N. P., The Delamination Theory Of Wear, Wear, Vol. 25, pp.111-124, 1973.

Sui H., Pohl H., Schomburg U., Upper G., And Heine, S., Wear And Friction Of Ptfe Seals, Wear, Vol. 224, pp.175-182, 1999

Sandisk Secure Digital Card, Product Manual, Version 1.9, 2003

Sarkar A.D., Friction And Wear, Academic Press, 1980

Sarkar A.D., Wear Of Metals, Pergamon Press, International Series On Materials Science And Technology, Vol.18, 1977

Scott D, Treatise On Materials Science And Technology, Wear, Vol.13, Academic Press, 1979

Strömberg N., Finite Element Treatment Of Two-Dimensional Thermoelastic Wear Problems, Computational Methods For Applied Mechanical Engineering, Vol. **177,** pp. 441–455, 1998

Thompson J.M. And Thompson M.K.,A Proposal For The Calculation Of Wear. Proceedings Of The 2006 International Ansys Users Conference & Exhibition, Pittsburgh, Pa., 2006

Tomlinson A. Philos. Mag. **7**, pp. 905–911, 1927

Yan W., O'dowd N. P., And Busso E. P., Numerical Study Of Sliding Wear Caused By A Loaded Pin On A Rotating Disc, J. Mech. Phys. Sol., Vol. 50, pp.449-470, 2002